Generation and Characterisation of an HRP-3-deficient Mouse Model

Dissertation

zur
Erlangung des Doktorgrades (Dr. rer. nat.)
der
Mathematisch-Naturwissenschaftlichen Fakultät
der
Rheinischen Friedrich-Wilhelms-Universität Bonn

vorgelegt von

Katharina M. Klein

aus

Duisburg

Bonn, März 2013

Angefertigt mit Genehmigung der Mathematisch-Naturwissenschaftlichen Fakultät
der Rheinischen Friedrich-Wilhelms-Universität Bonn

1. Gutachter: Prof. Dr. Volkmar Gieselmann

2. Gutachter: Prof. Dr. Dieter Fürst

Tag der Promotion: 24. Juli 2013

Erscheinungsjahr: 2013

Tho' much is taken, much abides; and tho'
We are not now that strength which in old days
Moved earth and heaven, that which we are, we are;
One equal temper of heroic hearts,
Made weak by time and fate, but strong in will
To strive, to seek, to find, and not to yield.

Alfred Lord Tennyson

Contents

List of Figures

List of Tables

Acronyms

AD Alzheimer's Disease
APC Adenomatous polyposis coli
APP Amyloid precursor protein
APS Ammonium persulphate
ARMS Ankyrin repeat-rich membrane spanning adaptor protein

BAC Bacterial artificial chromosome
BCP 1-bromo-3-chloropropane
bFGF Basic fibroblast growth factor
Bp Basepairs
BSA Bovine serum albumine

cAMP Cyclic adenosine monophosphate
CNTF Ciliary neurotrophic factor

DAB 3,3'-Diaminobenzidine tetrahydrochloride
DAPI 4',6-diamidino-2-phenylindole
DMSO Dimethyl sulphoxide
DNA Deoxyribonucleic acid
DNTP Deoxynucleoside-triphosphate
DT-A Diphtheria toxin fragment A

E Extinction
EDTA Ethylene diamine tetra acetic acid
EEF2 Eukaryotic elongation factor 2
EGFP Enhanced green fluorescent protein
EGF Epidermal growth factor
EGFR Epidermal growth factor receptor
ES Embryonic stem cells
EST Expressed sequence tag

FCS Fetal calf serum

GDNF Glial-cell-line-derived neurotrophic factor
GFAP Glial fibrillary acidic protein
GSK-3-β Glycogen synthase kinase 3 beta
GST Glutathione S-transferase

HAT Hypoxanthin aminopterin thymidine, supplement

HATH Homologue to the amino terminus of HDGF
HB-EGF Heparin-binding EGF-like growth factor
HDGF Hepatoma-derived growth factor
HPRT Hypoxanthine phosphoribosyltransferase
HRP-3 Hepatoma-derived growth factor-related protein-3
HZ Heterozygous

IGLE Intraganglionic laminar endings
IHC Immunohistochemistry
ILK Integrin-linked kinase

Kb Kilo base pairs
KDa Kilo Dalton
KO Knockout

LEDGF Lens epithelial-derived growth factor
Lif Leukemia inhibitory factor
LoxP Locus of X-over P1

Map-2 Microtubuli-associated protein-2
MAPK Mitogen-activated protein kinase
MEF Mouse embryonic fibroblasts
mRNA Messenger RNA

NBM Neurobasal medium
NT-3 Neurotrophin-3
NT-4/5 Neurotrophin-4/5
NT-6 Neurotrophin-6

p75^{NTR} P75 neurotrophin receptor
PAGE Polyacrylamide gel electrophoresis
PBS Phosphate buffered saline
PCR Polymerase chain reaction
PD Parkinson's Disease
PDGF Platelet-derived growth factor
PFA Paraformaldehyde
PI3 Phosphatidyl inositol-3

RT-PCR Reverse transcription Polymerase chain reaction
RNA Ribonucleic acid

SecaB Secondary antibody control
SDS Sodium dodecyl sulfate

TBS Tris-buffered saline
TGF-α Transforming growth factor alpha
Trk Tropomyosine-related kinase
Tyr Tyrosinase

V Volt

WT Wild type

1 Introduction

1.1 Neurotrophic Factors

A pioneer of neurobiology, Rita Levi-Montalcini, died recently on 30 December 2012. Together with her colleague Stanley Cohen, she was a recipient of the Nobel Prize for Physiology or Medicine in 1986 for "their discovery of growth factors", namely the first neurotrophic factor: nerve growth factor (NGF). By implanting mouse sarcomas intra- and extra-embryonically into chicken embryos, she was able to prove the existence of a neurite outgrowth promoting agent which lead to hyperplasia in the whole sympathetic system of the embryo (Levi-Montalcini [1952] Watts [2013]).

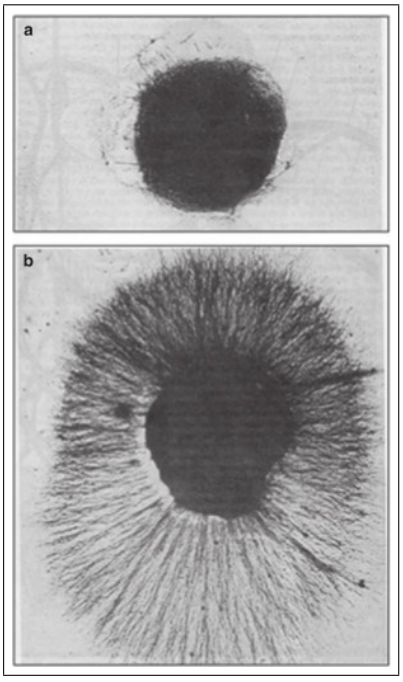

Figure 1.1 – **NGF-induced neuritogenesis.** Chicken sensory ganglia from eight-day-old chickens were isolated and cultivated without (a) and with (b) NGF. With this experiment Levi-Montalcini and Calissano [1979] were able to show the outgrowth promoting ability of NGF (Calissano et al. [2010]).

A modern definition states "neurotrophic factors are secreted molecules that play a crucial role in the development, function, maintenance, and plasticity of the nervous system" (Alsina et al. [2012]). But Levi-Montalcini's results were not fully accepted until almost twenty years after the discovery, when NGF was further studied and isolated for the first time (Bocchini and Angeletti [1969]). Since then, more members of the same protein family, which were named neurotrophins, have been identified. These are the the brain-derived neurotrophic factor (BDNF), neurotrophin-3 (NT-3), neurotrophin-4/5 (NT-4/5) and neurotrophin-6 (NT-6, only in fish). NT-4/5 was first discovered in *Xenopus laevis*, named NT-4, while a human neurotrophin was

identified and named NT-5, before it was shown that the factors were homologous and thus named NT-4/5 (Dawbarn and Allen [2003]). In addition, other proteins with neurotrophic activity, belonging to different growth factor families, are known today. Amongst others, these are glial-cell-line-derived neurotrophic factor (GDNF), transforming growth factor alpha (TGF-α), platelet-derived growth factor (PDGF) or ciliary neurotrophic factor (CNTF). Today, the list is still growing (Yuen et al. [1996]).

Levi-Montalcini's work was a foundation for the neurotrophic theory which hypothesises that after the innervation of the target tissue is completed, neurons compete for neurotrophic factors, probably by perfecting access to these factors (e.g. via axonal branching or formation of synapses) and not due to a limited supply of them. Neurons without access to neurotrophic factors undergo apoptosis in order to establish a quantitative equilibrium between neurons and target tissue (Oppenheim [1989]). This theory was adapted and further extended: it is now known that trophic factors are not only provided via secretion by the target cells, but also via autocrine signalling from the neuron itself and via paracrine signalling from other non-neuronal cell types. Furthermore, one neuronal population can be supplied not only by one, but by multiple trophic factors, whereas one trophic factor can supply more than one population of neurons (Yuen et al. [1996]). Neurons from the central and peripheral nervous system differ even more in their behaviour towards neurotrophic factors than subpopulations of neurons. Meyer-Franke et al. [1995] revealed that, in contrast to cells from the peripheral nervous system (dorsal root ganglia, sensory or sympathetic neurons), postnatal rat retinal ganglion cells from the central nervous system do not respond to BDNF treatment alone. Unlike NGF in dorsal root ganglia, BDNF will not keep a high percentage of these cells alive for a longer period of time. But increasing the intracellular cyclic adenosine monophosphate (cAMP) levels, e.g. by adding forskolin, or stimulating the electrical activity by adding KCl, greatly promoted the survival effect of the trophic factors. The authors discussed that cAMP might increase the number of receptors for trophic factors on the cell surface, which makes the cell more sensitive towards them.

The neurotrophic theory also provides a foundation for the understanding of neuronal death during embryonic brain development. It has been known for many years that - depending on the specific brain region - between 20 % and 80 % of the differentiated neurons undergo apoptosis during neurogenesis (Oppenheim [1991]).

Brain development is absolutely dependent on programmed cell death of neuronal precursor cells; this was shown in several knockout mice deficient of regulatory elements of apoptosis. For example, caspase-3- and caspase-9-deficient mice exhibit a dramatical excess of neurons in the central nervous system, forming highly disorganised structures (Kuida et al. [1996], Kuida et al. [1998]). The limited amount of neurotrophins protects selected cells, while others undergo apoptosis (de la Rosa and de Pablo [2000]). That ensures that the density of the surviving cells matches the needs of the target tissue.
However, not only during brain development, but also in the adult nervous system, neurotrophic factors play an important role in mediating neuronal viability, differentiation and morphology (Reichardt [2006]).

1.2 Receptors and Signalling Pathways

1.2.1 The Tropomyosine-related Kinase Receptor Family

The family members of the neurotrophins are small proteins of about 30 kDa that are produced as protein precursors (pro-neurotrophins). These are posttranslationally modified by proteolysis to their mature form, which has a molecular weight of approximately 13 kDa. The mature proteins form homodimers that are non-covalently linked and are secreted by the cell (Dawbarn and Allen [2003], Reichardt [2006]).
These dimers are able to activate designated receptors to induce positive signalling pathways as well as negative feedback loops which restrict their own signal transduction.
Each member of the neurotrophin family has one main receptor from the tropomyosine-related kinase (trk) receptor family. Some neurotrophins, e.g. NT-3, are also able to activate more than one receptor, but the binding to their main receptor is more stringent.
The trk family of receptors consists of three main members (trkA, trkB and trkC) and their splice forms. Their structure shows common features: they consist of an extracellular factor binding domain which is specific to the respective neurotrophin and has an immunglobuline-like structure. Intracellularly, they have a tyrosine kinase domain. When a factor is bound, the receptor dimerises and the cytosolic

domains transphosphorylate each other. Different signalling cascades are now activated, the major ones being:

- Ras leads to the activation of the mitogen-activated kinase pathway (MAPK) and ultimately to a differentiation-promoting pathway, neurite outgrowth and transcription of anti-apoptotic proteins

- Phosphatidyl inositol-3 (PI3) kinase phosphorylates phosphoinosides, which mediate an activation of the kinase Akt. Via downward cascades, Akt induces neuronal outgrowth and survival, e.g. by blocking proteins from the pro-apoptotic Bcl-2 family. Furthermore, the 3-phosphoinosides recruits proteins of the Rho-GTPases to the membrane, e.g. Cdc42, Rac and Rho. Their main task is the organisation of the actin-based cytoskeleton and thus to promote neurite outgrowth along neurotrophic gradients

- Phospholipase Cγ1 promotes synapse plasticity by activating protein kinase C-regulated pathways which, amongst others, lead to a release of Ca^{2+} and an activation of Ca^{2+}-dependent kinases.

Other signalling pathways are involved as well, though they are not fully understood yet. It may be possible that different groups of neurons also use different signalling cascades (Crowder and Freeman [1998], Reichardt [2006]).

1.2.2 The p75^{NTR} Receptor

P75^{NTR} (p75 neurotrophin receptor) was the first receptor discovered to bind NGF. It was named after its size, 75 kDa, belongs to the tumor necrosis factor superfamily, and has an intracytosolic death domain. Although it is able to bind all members of the neurotrophin receptor family, it was shown to bind the pro-neurotrophins with thousandfold higher affinity (Friedman [2010]).
Figure 1.2 summarises the different binding patterns of neurotrophins with their respective receptors. While the immature pro-neurotrophins bind strongly to p75^{NTR}, the binding of their mature proteins to the receptor is characterised by a low binding affinity. Each neurotrophin has a designated receptor, e.g. trkA is the main receptor of NGF, trkC the main receptor of NT-3, and trkB is shared by BDNF and NT-4. NT-3 is also able to activate trkA and trkB with lower affinity. The

pro-neurotrophins are not able to bind trk receptors.
Sortilin is a co-receptor for $p75^{NTR}$ and necessary for its activation. When a pro-neurotrophin is bound, the following pathways are induced (Reichardt [2006]):

- A jun kinase signalling cascade leads to downstream activation of c-jun, the pro-apoptotic factor p53 and an activation of the fas receptor. All these events induce apoptosis
- The Nfκb pathway is activated and thus promotes neuronal survival
- Without neurotrophin binding, $p75^{NTR}$ activates RhoA, a small Rho-GTPase, which further leads to the induction of neuronal outgrowth. When a pro-neurotrophin is bound, this activation is blocked and outgrowth is inhibited. This is supported by diminished neuronal outgrowth, shown in a mouse model with a mutation in the $p75^{NTF}$ gene. While the inactivation of Rho, on the other hand, increased neuronal outgrowth in primary neuronal cell cultures (Yamashita et al. [1999]).

An overview of the described signalling cascades is also depicted in figure 1.3. Depending on which receptor is activated, several pathways are induced, leading to the expression of pro- or anti-apoptotic genes.
In a nutshell, neurotrophic factors are able to induce different cell signalling pathways, leading to either survival or death of the cell. The outcome depends on the binding factor (pro-neurotrophin or neurotrophin) and on the receptor (trk or $p75^{NTR}$). An equilibrium of a neurotrophic factor and its immature protein is thus necessary in the cell to maintain its status quo. That is the reason why antibody-mediated depletion of NGF in cell culture may actually result in better survival of the cells (D. Sanes, A. Thomas [2006]).

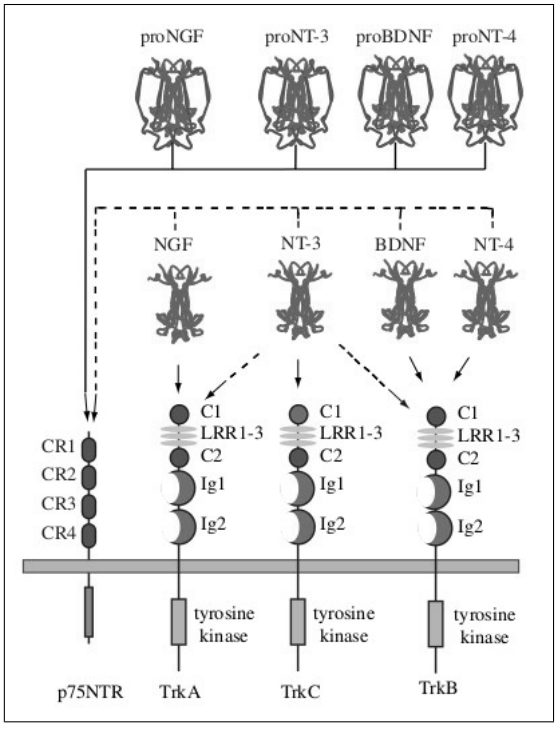

Figure 1.2 – Neurotrophins and their receptors. Different binding patterns of neurotrophin family members with their respective receptors (figure from Reichardt [2006]).

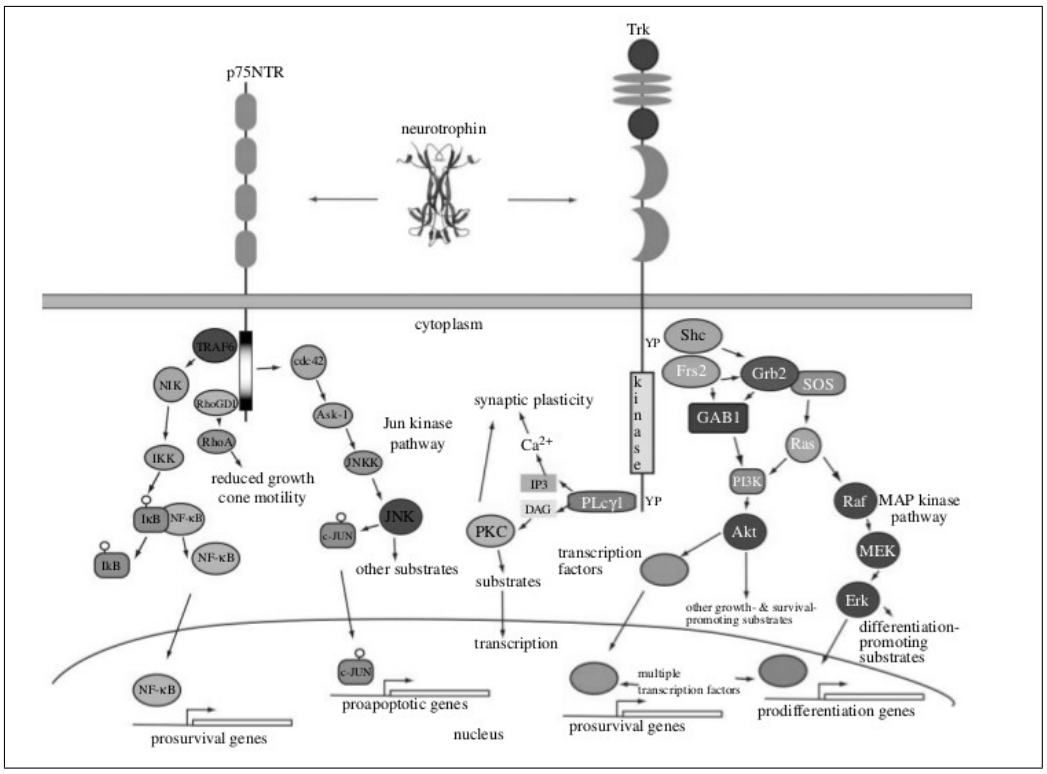

Figure 1.3 – Signalling pathways of neurotrophic factors. Overview of the signalling pathways that can be induced by the binding of neurotrophic factors to their respective receptors. Both receptors, trk and $p75^{NTR}$ are able to bind a factor and activate a downstream cascade. Trk receptors activate downstream events, as MAP kinase pathway and induction of Akt, which induce the expression of anti-apoptotic factors. $p75^{NTR}$ can induce the expression of pro-apoptotic factors (c-jun) as well anti-apoptotic factors (Nfκb), dependent on regulatory mechanisms, which are further described in the next chapter (figure from Reichardt [2006]).

1.3 Regulation

The neurotrophic receptors $p75^{NTR}$ and tropomyosine-related kinase (trk) trigger completely opposing cellular pathways, which decide between life or death of a neuron. The cellular events leading to this decision are not fully understood yet, but different mechanisms for the regulations of signal cascades have been described.
The amount and the concentration of a neurotrophin (expression level) is one regulatory mechanism for the cell. Additionally, the expression levels of the receptors decide their frequency on the cellular surface. The more receptors are available for activation, the lower is the amount of neurotrophins needed for the same outcome.

Only a few molecules are necessary for the activation and once the downward cascade is started, it amplifies itself. Furthermore, negative feedback loops are activated after the signalling cascade starts, which allows for their own regulation (Yuen et al. [1996]).
Therefore, expression of neurotrophins and their respective receptors is the first method of regulation. Additionally, many external factors, such as cytokines, steroids and TGFβ are able to influence the expression levels of neurotrophins, too (Reichardt [2006]).
Posttranslational modifications allow for further regulation. An important step is the endoproteolytic processing of the pro-neurotrophins into their mature form, which can be controlled by the expression levels of proteases and is thus probably tissue-dependent. Neurotrophins can be cleaved by several proteases, intracellularly as well as extracellularly (Lee et al. [2001]). Different factors are cleaved and secreted within the same cell type. In hippocampal neurons, NGF is cleaved in the trans-Golgi network, and secreted via the constitutive pathway, so that it is always available to the cell. In the same cell type, BDNF is not cleaved in the trans-Golgi network, but packed from there into secretory granules and secreted via the regulated secretory pathway. Proteolytic processing takes place within the granules, which are released upon specific signalling (Farhadi et al. [2000]).
Surprisingly, both neurotrophic receptor types (trk or $p75^{NTR}$) are located in the same multiprotein complexes on the surface of the cell and even influence each other. This mechanism allows the activation of one receptor type, while at the same time suppressing the other. Reichardt [2006] describes three proteins and complexes that have been shown to interact with both receptors simultaneously, namely the ankyrin repeat-rich membrane spanning adaptor protein (ARMS), caveolin and the complex p62-Traf6-IRAK. When trk is bound by a factor, ARMS is phosphorylated and induces prolonged activation of Ras and Erk (figure 1.3), supporting the trk-activated downstream events. Caveolin and p62-Traf6-IRAK also allow for the interaction of trk and $p75^{NTR}$ and possibly suppress pro-apoptotic signalling to support trk-mediated anti-apoptotic signalling.

1.4 Influence of Neurotrophic Factors on the Cytoskeleton

The cytoskeleton is a structural scaffold that supports the stability of eukaryotic cells. Besides stabilisation, it allows the cell to move, is a scaffold for cell organelles and allows transport within the cell. It consists of three different filaments: microfilaments (actin), intermediate filaments and microtubules. They differ by their composition, size, associated proteins and functions (Fletcher and Mullins [2010]).
Each microtubule consists of 13 protofilaments, linear heterodimeric structures of aligned α- and β-tubulin. Microtubules are the most complex of the filaments and are characterised by a phenomenon called "dynamic instability", a sequence of rapid growth and subsequent destabilisation, which are termed "rescue" and "catastrophe", respectively. This phenomenon is a quick response mechanism to changes in the environment (Conde and Cáceres [2009]).
Many associated proteins help to stabilise or destabilise microtubules, mediate movement (motor proteins), or to sever them. Neurons are highly polarised cells; the subcellular localisation of their microtubule-stabilising proteins is also clearly polarised. E.g. map2 is a stabilising factor in dendrites, but not in axons. Tau on the other hand, is a microtubule-stabilising protein only in axons (Conde and Cáceres [2009]).
The polarity of the neuron is established early in development. The cells start with the outgrowth of several neurites with the same characteristics, before one of the neurites turns into an axon, while the others become dendrites. They differ in their polarisation of microtubules: in axons they are organised with the plus end towards the outer end of the cell, whereas the orientation in dendrites is mixed. The axon is the signal-transmitting end of the cell while dendrites are the receiving ends. For further outgrowth, the axon develops a growth cone, a structure with filopodia that reaches towards the target (D. Sanes, A. Thomas [2006]).
On the tip of the growth cone, tyrosinated tubulin is concentrated. In contrast to its acetylated form, it is dynamic and has a half-life of only about five minutes. Acetylated tubulin on the other hand, is stable and has a half-life of about thirty minutes. The dynamic tubulin allows fast reactions to the environment (compare figure 1.4).
Neurotrophic factors induce neuronal outgrowth by influencing the cytoskeleton of

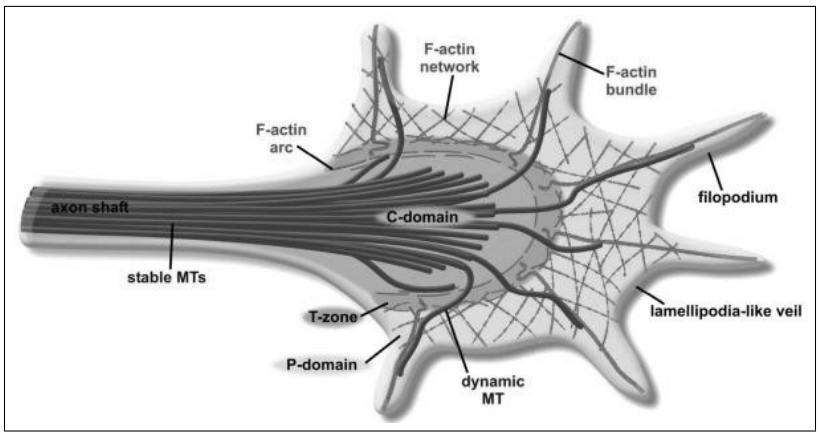

Figure 1.4 – Cytoskeletal characteristics of a neuronal growth cone. Microtubules (MT) and actin interact to form a structure which gets more stable towards the cell body, but is able to react to changes in the environment quickly at the tip of the growth cone. Three different regions can be identified: the peripheral (P)-domain (comprised of actin filaments), the central (C)-domain (stable microtubules) and the transition (T) domain (Lowery and Van Vactor [2009]).

the target cell. To elucidate this process, double knockout mice of NGF and Bax are a suitable model (Markus et al. [2002]). Bax is a pro-apoptotic member of the Bcl-2 family. When Bax is missing, apoptosis is reduced, thus, the neuronal death induced by the NGF-deficiency is diminished. This allows to study the influence of NGF on neuronal outgrowth in vivo. In this mouse model, neurons from dorsal root ganglia survived without NGF and sent neurites out into the spinal cord. Surprisingly, only peripheral cutaneous axons were missing at the time of birth. It can be concluded from these results that only axonal outgrowth over long distances is NGF-dependent. Other factors might serve as intermediate targets over short distances (Markus et al. [2002]).

A theory on how NGF induction of neuronal outgrowth works, was published by Zhou et al. [2004] (figure 1.5). As was described earlier, NGF activates phosphatidylinositol-3 (PI-3) kinase at the growth cone. This leads to the downstream activation of the small GTPases Cdc42, Rac and Rho, which organise the actin-based cytoskeleton. The activation of PI-3 kinase furthermore leads to the activation of integrin-linked kinase (ILK) and thus to the inactivation of glycogen synthase kinase 3 β (GSK-3β). This kinase phosphorylates adenomatous polyposis coli (APC). When APC is not phosphorylated, it binds microtubules, stabilises them and thus induces microtubule polymerisation. Together with actin polymerisation this leads to the outgrowth of

the axon.

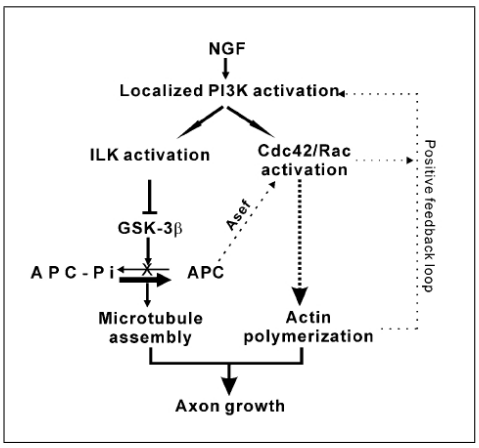

Figure 1.5 – Induction of neuronal outgrowth by NGF. NGF induces neuronal outgrowth by activation of actin polymerisation and microtubule assembly at the same time by activation of phosphatidylinositol-3 kinase. Figure from Zhou et al. [2004].

Cytoskeletal deficits go hand in hand with many neurodegenerative diseases, for example Alzheimer's disease (AD), Parkinson's disease (PD) or the motor neuron disease amyotrophic lateral sklerosis. Defective transport of proteins along the axon leads to an accumulation of cytoskeletal structures in these diseases (McMurray [2000], Brandt [2001]).

1.5 Neurodegenerative Diseases

Neurodegeneration is a hallmark of many diseases, defined by a structural loss of neurons in the central nervous system leading to cognitive deficits of various kinds. Well known examples include Alzheimer's disease, Parkinson's disease, Huntington disease, Pick's disease, Prion diseases, and others. Most of these diseases exhibit an aggregation of misfolded proteins resulting in amyloid plaques. Amyloids are defined as insoluble aggregations of proteins that are soluble under normal physiological conditions. These aggregations appear filamentous, as for example the so-called tau-tangles, misfolded tau that aggregates intracellularly and is a feature of Alzheimer's disease. Several different proteins are prone to form amyloid plaques by misfolding, and even though they share no structural similarity, the principal characteristics of their aggregations resemble each other.

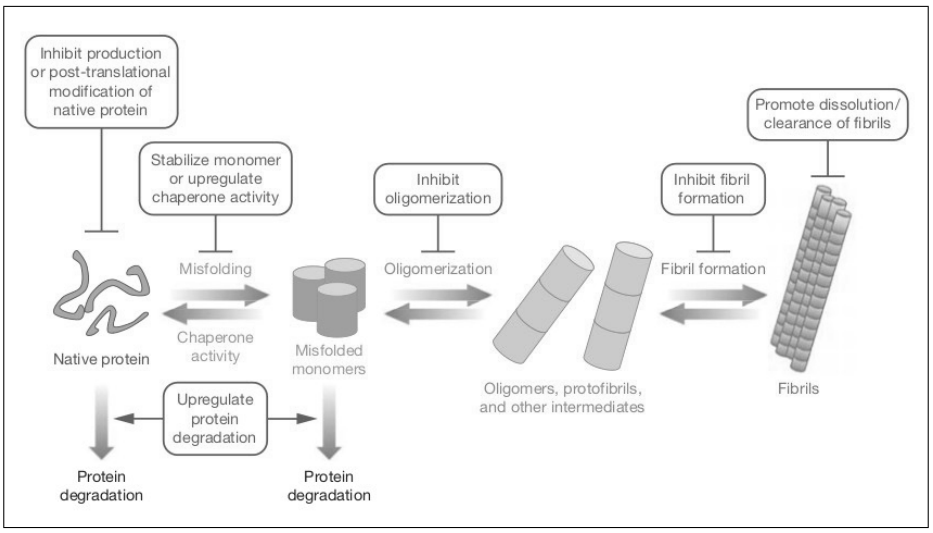

Figure 1.6 – Model for the formation of amyloid plaques. This figure presents a model for the formation of fibrils that form amyloid plaques. These plaques are a hallmark of neurodegenerative diseases and can arise from several different soluble proteins. The boxes describe several steps, e.g. the misfolding itself or the oligomerisation that could be used as therapeutic targets (figure from Skovronsky et al. [2006]).

Neurodegenerative diseases can be characterised by the protein forming the amyloid plaques and the localisation of these plaques within the brain. It is not clear though, whether these aggregates themselves or their precursors, namely oligomeres and protofibrils, are the cause or a side-effect of neurodegeneration. Nevertheless, they present us with therapeutic opportunities and potential targets. As described by Skovronsky et al. [2006], it is indicated that the amyloid plaques correlate and may be linked with incorrect axonal transport, inhibition of protein degradation and apoptosis. Figure 1.6 illustrates the process of fibril aggregation from the native protein, through the misfolded protein, to oligomers and complete fibrils. It also presents potential targets for drug design, as for example the upregulation of the protein degradation machinery as well as the inhibition of fibril formation, and others (Skovronsky et al. [2006]).

1.5.1 Neurotrophic Factors in Neurodegenerative Diseases

Neurotrophic factors were shown to be survival-promoting on a number of degenerating neurons in neurodegenerative diseases. Some examples are described in the

following, where an imbalance of neurotrophic factors is either a causing agent or a consequence in the development of the disease. Moreover, studies were performed with a focus on neurotrophic factors as a therapeutic option.
Alzheimer's disease (AD) is characterised by a loss of cholinergic neurons in the basal forebrain, cerebral cortex, and the hippocampus, leading to a defective cholinergic function and thus arousing dementia and cognitive deficits.
Different hypotheses regarding the reason for this cell loss exist (Hardy and Selkoe [2002], Dawbarn and Allen [2003]) . The amyloid hypothesis states that the plaques itself are the causing agents. In contrast, the tau hypothesis makes hyperphosphorylated tau accountable for the development of Alzheimer's disease. Alzheimer's disease belongs to the group of tauopathies due to its intracellular accumulation of hyperphosphorylated tau, in so-called tau-tangles or neurofibrillary tangles. Tau is a microtubule-associated protein that binds and stabilises microtubules. The tangles form inside the cell, thus disturbing the microtubule cytoskeleton integrity and the transport mechanism of the neuron (Skovronsky et al. [2006]).
The cholinergic hypothesis regards a decreased production of acetylcholine as a main reason for Alzheimer's disease. The loss of cholinergic neurons leads to reduced cholinergic activity, even though the overall cognitive deficits are actually worse than the loss of neurons alone accounts for (Dawbarn and Allen [2003]).
It could be presumed that neurotrophic factors are reduced in Alzheimer's disease and thus neurons degenerate, but this is not the case. On the contrary, despite no reduction of mature NGF, there is a two-fold increase of immature pro-NGF in the parietal cortex of brains affected by Alzheimer's disease (Fahnestock et al. [2001]). An imbalance of mature NGF and its precursor protein might lead to neuronal death by activation of $p75^{NTF}$, possibly due to a dysfunction of NGF retrograde transport. Additionally, knockout mouse models of NGF or its receptor trkA show a decrease in cholinergic activity and a loss of cholinergic neurons in the hippocampus, cortex and the basal forebrain (Dawbarn and Allen [2003]). Cooper et al. [2001] showed in a mouse model of Down syndrome (due to the extra copy of the amyloid precursor protein - *APP* - gene, patients with Down syndrome do develop Alzheimers disease as well) that retrograde transport of NGF is diminished and that NGF in the basal forebrain is thus decreased, as it is the case in AD patients. Additionally, it was possible to rescue cholinergic neurons of the basal forebrain in vitro and in vivo by supplementing NGF to the medium or via intracerebroventricular injections, respec-

tively. In rat models of the disease, intracerebroventricular injections were shown to enhance cognitive deficits (Dawbarn and Allen [2003]).
Intracerebroventricular injections of NGF in a clinical trial with three patients did partially confirm results from animal models. Cognitive deficits were improving, but a severe side-effect reported by all patients, was pain, which stopped after the injections. It was discussed that the pain was due to a hyperplasia of $p75^{NTF}$ positive, trkA negative Schwann cells at the medulla and the spinal cord, which was found to be nonmalignant and reversible in rat models (Dawbarn and Allen [2003]).
Nonetheless, other forms of treatment with NGF are under examination, including the injection of retrovirally infected fibroblasts, overexpressing NGF, or the nasal administration of NGF. Both show histological improvements in the basal forebrain of rats and rhesus monkeys (Dawbarn and Allen [2003]).
Another example for a neurotrophic disease in which an imbalance of neurotrophic factors occurs is Parkinson's disease (PD). It is characterised by a loss of dopaminergic neurons within the substantia nigra, a structure in the ventral midbrain, for unknown reasons. A consequence of this is the reduced production of the neurotransmitter dopamine which leads to an imbalance of neurotransmitters, neuronal loss and the common symptoms of PD (tremor, rigidity, slower movement, and postural instability). Until now, treatment is confined to symptomatic approaches and the attempt to treat the loss of dopamine with its precursor form L-3,4-dihydroxyphenylalanine, or L-dopa. L-dopa is able to cross the blood-brain barrier and increases the dopamine levels, but does not protect neurons from degeneration (Gill et al. [2003]).
Histologically, inclusions can be detected in moribund neurons, the so-called Lewy bodies. They consist of accumulated α-synuclein and ubiquitin. That associates Parkinson's disease with the group of synucleopathies. The amount and localisation of Lewy bodies varies from patient to patient and is a hallmark of the spontaneous form of PD (Dawbarn and Allen [2003]).
Glial-derived neurotrophic factor (GDNF) plays an important role in the development of dopaminergic neurons and offers the potential ability to protect motor neurons and dopaminergic neurons, as was shown in animal models of the disease. Axonal outgrowth and improved motor functions were detected after intracerebroventricular injection or the direct injection of GDNF into the substantia nigra (Gill et al. [2003]). In contrast to the results in animal models, intracerebroventricular injections into human patients of PD did not lead to an improvement of the disease.

It was hypothesised that the increased amount of tissue did not allow GDNF to penetrate into the correct regions of the brain and thus other means of delivery had to be found (Gill et al. [2003]).
A clinical trial study phase 1 with five patients and without a control group therefore injected GDNF directly into the putamen for the period of one year. The putamen is the area in the brain with the most drastic reduction of dopamine in PD patients. Gill et al. [2003] were able to show via positron emission tomography (PET) scan that the dopamine storage increased in these patients and their score of disease decreased significantly with only little side effects.
These are two examples for neurodegenerative diseases where neurotrophic factors are involved. The question whether these factors are a cause of the disease (and if they are, if this is the sole cause) or a by-product of neuronal loss, is not solved yet. But interestingly, rodent models of the diseases can at least be partially rescued with the administration of neurotrophic factors. Further research on known and yet unknown neurotrophic factors is necessary to enhance our fundamental knowledge and might thus offer the possibility to improve neurodegenerative diseases.

1.6 Hepatoma-Derived Growth Factor-Related Protein-3 (HRP-3)

Hepatoma-derived growth factor-related protein-3, in short HRP-3, is a 23 kDa sized protein with mitogenic activity that was first cloned by Ikegame et al. [1999] in a screening of expressed sequence tag (EST) databases.
It is one of five proteins established as family members of the name-giving Hepatoma-derived growth factor (HDGF), which was discovered in the supernatant of HuH-7 cells (Nakamura et al. [1994]). The other family members are: HDGF-related proteins 1, 2 and 4, and the lens epithelial-derived growth factor (LEDGF). They all share a N-terminal homologous domain (homologous to the amino terminus of HDGF, in short: HATH), while they are differing in their C-termini. Human HRP-3 and HDGF share an identity of 81.4 % in their HATH domain, while their non-HATH regions differ completely.
A common feature of HDGF family members is the bipartite nuclear localisation signal (NLS), which is localised in the conserved HATH region and the non-HATH

region and allows HRP-3 to translocate to the nucleus, as shown in the immunfluorescence in figure 1.7.

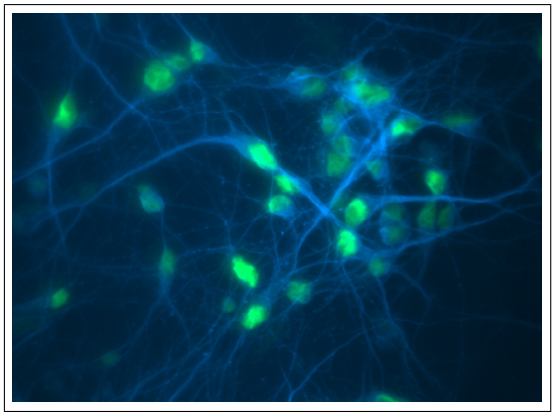

Figure 1.7 – Immuncytochemistry of primary cortical neurons. β-III-tubulin stains a neuron-specific tubulin isoform and thus indicates the outward appearance of the cell (in blue). The green staining is derived by an HRP-3-specific antibody and detects a strong nuclear signal which is common for postmitotic neurons.

Although HDGF is currently the best described protein of the family, its function is still unknown. It has mitogenic effects on fibroblasts, hepatocytes, endothelial cells and others (Everett et al. [2000], Nakamura et al. [1994], Oliver and Al-Awqati [1998]) and is presumed to play a role in angiogenesis, organogenesis and cancer development. It can be used as a prognostic marker for various cancer types and many publications show ample evidence that HDGF expression in tumours is correlated with a bad prognosis for patients, as in hepatocellular carcinoma (Hu et al. [2003]), non-small cell lung cancer (Iwasaki et al. [2005]), gliomas (Hsu et al. [2011]), breast cancer (Chen et al. [2012]) and others. Even though HDGF is overexpressed in melanomas (Bernard et al. [2003]), no formation of melanomas was detected in a transgenic mouse model by Sedlmaier et al. [2011]. In this study, transgenic mice, overexpressing HDGF in melanocytes and with a heterozygous deficiency of the tumour suppressor gene Ink4a, were exposed neonatally to UV light. Mice did not develop melanomas, thus, it was concluded that HDGF does not have oncogenic activity itself, but is a factor for non-oncogenic addiction. This concept describes the need of a cancerous cell for certain factors to keep its malignancy (Weinstein [2002]).

Whereas an overexpression of HRP-3 in mantle cell lymphomas has already been described before (Miller et al. [2000]), a more recent publication indicates a relationship between HRP-3 and tumorigenesis that is similar to HDGF. It was not only shown that HRP-3 is necessary for anchorage-independent growth in liver carcinomas but also that knockdown via siRNA in hepatocyte carcinoma cells greatly reduced the resistance against chemotherapeutics (Xiao et al. [2012]).

HDGF is strongly expressed in many organs, as for example the brain, heart, lung,

liver, spleen and muscle. In contrast, the literature differs as far as the expression of HRP-3 is concerned. Ikegame et al. [1999] display human HRP-3 mRNA via Northern blot analysis in the heart, brain, testis and kidney, Xiao et al. [2012] additionally show very weak signals for the lung, liver and pancreas, also via Northern blot analysis.
On the other hand, Abouzied et al. [2004], describe a restricted protein expression of mouse HRP-3 in the brain via immunoblotting, more specifically its neurons, with only small amount of protein in testis. Whether HRP-3 shows different expressions in humans and mice, or whether the level of expression in other organs beside the brain are too weak to detect in immunoblotting, remains to be elucidated.

1.7 Neurotrophic Activity of HRP-3

Despite the differences in the literature regarding its expression, HRP-3 is strongly expressed in neurons, but not in non-neuronal cells (except to a very small amount in oligodendrocytes). It is highly regulated during embryonic brain development and shows varying expression levels at different stages of development. The expression increases from embryonic day 15 to a very strong expression around birth, decreases strongly afterwards and is again very high in the adult mouse brain (Abouzied et al. [2004]).
Additionally, the subcellular localisation of HRP-3 changes during brain development and in cell culture. In a primary culture of cortical neurons from E14.5 mouse brains, a strong signal in neurites (axons and dendrites) is detectable in immunocytochemistry. After 10 days in culture, a translocation into the nucleus is taking place. In mature neurons, HRP-3 exhibits a strong nuclear expression with no protein detectable extranuclearly (El-Tahir et al. [2009]). The reason for the translocation is not known, although Xiao et al. [2012] discuss that MAP/Erk signalling might play a role. They transfected human hepatocyte carcinoma cells with myc-HRP-3 and report a translocation from the nucleus into the cytoplasma after stimulation with EGF.
HRP-3 is secreted by cells, although it lacks a classic signal peptide. It might thus be secreted via non-classical secretory pathways. A study on HDGF has shown that the first ten amino acids of HDGF act as a secretion signal that is also able to release a reporter gene (eGFP and SNAP) into the supernatant (Thakar et al. [2010]). The

phosphorylation of Serin 165 is inevitable for this secretion mechanism in HDGF. The conservation of the HATH domain suggests that HRP-3 is secreted similarly to HDGF.

HRP-3 has neurotrophic activity when offered as an extracellular supplement, as shown by Abouzied et al. [2010]. It promoted neurite outgrowth in a cell culture of primary cortical neurons and was able to keep the cells alive as sole supplement in the culture medium. The effects of 100 ng/ml HRP-3 resembled similar trophic effects as 5 % fetal calf serum (FCS) in the medium. An antibody-mediated inhibition of HRP-3 diminished this effect. Furthermore, coating of cell culture plates with HRP-3 recombinant protein, led to an enhanced neuronal outgrowth compared with HDGF or β-galactosidase as a control. This effect was comparable to laminin as an extracellular matrix.

HRP-3 is interacting with microtubules, promoting their stability and thus leading to neurite outgrowth. It was shown in vitro and in vivo via transfection of a cytoplasmically-located NLS mutant of HRP-3 that the amount of acetylated tubulin increases. That is a sign for the stabilisation of microtubules. HRP-3-mediated neurite outgrowth and inhibition of this outgrowth after knockdown of HRP-3 is manifested by its ability to promote microtubule polymerisation (El-Tahir et al. [2009]).

The neurotrophic and neurite-outgrowth promoting ability of HRP-3 is an effect that is performed by extracellular HRP-3 (via secretion or the addition of recombinant protein in cell culture). This is in contrast to the intracellular effects on the cytoskeleton, more specifically the stabilisation of microtubules. The uptake of HRP-3 by the cell has not been proven yet, nor is it known how an extracellular administration of HRP-3 would modulate the cytoskeleton.

1.8 Expectations and Objectives

Hepatoma-derived growth factor-related protein-3 (HRP-3) is a secreted neurotrophic factor that is most dominantly expressed in neurons. It has the ability to stabilise microtubules and thus is able to promote neurite outgrowth. Furthermore, as a sole medium supplement, it can keep neurons alive and is highly regulated during brain development. Not only the amount of expressed protein, but also the intracellular localisation, changes during development. Regardless of this, the precise function of HRP-3 is still unknown and demands further elucidation.

Via manipulation of embryonic stem cells, an HRP-3-deficient mouse line will be created using a targeting vector for homologous recombination. Exon II of the *Hrp-3* gene will be targeted and replaced with the genomic information for enhanced green fluorescent protein (eGFP) as a reporter gene that is driven under the endogenous promoter. Further features of the targeting vector include a hypoxanthine phosphoribosyltransferase (HPRT) cassette for positive selection and a diphteria toxin fragment A cassette for negative selection reducing the number of cells which have not undergone a homologous recombination event.

The introduction of a reporter gene will give further insights into the expression of HRP-3 and will help to answer the question whether HRP-3 expression in mice is restricted to brain and testis.

Knockdown of HRP-3 in primary cortical neurons leads to a reduced neurite length. The same cultures prepared from HRP-3-deficient mice will give further insight on HRP-3-related neuritogenesis.

A loss of function of HRP-3 might result in a drastic phenotype, because of its strongly regulated expression in brain development. As a result, embryonic lethality might be expected, as well as neurodegenerative phenotypes.

Other congenital defects can be expected, as well. Wat et al. [2010] identified microdeletions of the chromosomal region 15q25.2, where - amongst others - HRP-3 is located. These microdeletions are associated with a higher risk for congenital diaphragmatic hernia and the authors state that the loss of HRP-3 might lead to the patient's cognitive deficits.

Hence, the aim of this thesis is to describe the generation of an HRP-3-deficient mouse model to investigate HRP-3 expression more closely and establish a prerequisite for future functional analysis.

2 Materials

2.1 Chemicals

Unless stated otherwise, chemicals were obtained from Merck, Sigma Aldrich, Roth and Fluka. Restriction enzymes were bought from Fermentas. $[\alpha^{32}P]$-dCTP was acquired from Hartmann Analytic. All chemicals specific for embryonic stem (ES) cell cultures are described in table 2.4.

2.2 Kits

Ready-to-use kits that were used in this work are described in the following table.

Table 2.1 – Kits

Name	Manufacturer	Cat. no.
DC Protein Assay	BioRad	# 500-0111
ECL Western Blotting Substrate	Pierce	# 32106
Prime-it II Random Primer Labelling Kit	Stratagene	# 300385
QIAGEN Plasmid Mini Kit	Qiagen	# 12123
QIAGEN Plasmid Midi Kit	Qiagen	# 12143
QIAGEN EndoFree Plasmid Maxi Kit	Qiagen	# 12362
QIAquick Gel Extraction Kit	Qiagen	# 28704
QuantiTect Reverse Transcription Kit	Qiagen	# 205311
SuperSignal West Pico Chemiluminescent Substrate	Pierce	# 34080
Super Sensitive Link-Label IHC Detection System	BioGenex	# QP900-L
Vectastain ABC Kit	Vectastain Laboratories	# PK-4000

2.3 Plastic Ware and Consumables

If not stated otherwise, all general consumables were obtained from Sarstedt, Falcon and Greiner. Sterile plastic ware for cell culture was bought from Falcon and Sarstedt. Consumables that do not fit in these categories are listed in the following table.

Table 2.2 – Consumables

Name	Manufacturer	Cat. no.
Blotting paper	Albet-Hahnemuehle	# BP005 5860
Cryogenic vials	Nalgene	# V5007-500EA
Electroporation cuvettes, 4 mm gap	Molecular Bio Products	# 5540
Fuji Medical X-Ray film	Fuji	# 47410 08389
Hybond-XL blotting membrane	GE-Healthcare	# RPN2020S
Illustra MicroSpin G-50 Columns	GE-Healthcare	# 27-5330-01
Microscope cover glasses, 24 x 60 mm	Labomedic	# LAME110071
Microscope slides	Engelbrecht	# 11101
Protran Nitrocellulose Hybridization Transfer Membrane	Schleicher & Schuell	# NBA083C001EA
Sterile filters 0,2 µm, 0,1 µm	Millipore	# 83.1826
SuperFrost Plus microscope slides	Thermo Scientific	# 4951PLUS

2.4 Lab Equipment

Non-standard lab equipment is described in the following table.

Table 2.3 – Lab Equipment

Name	Manufacturer
Agarose gel electrophoresis chambers	Peqlab
Bacterial incubator	Heraeus
Binocular SMZ1500	Nikon
Cooling centrifuge Z233 MK	Hermle

Table 2.3 – Lab Equipment

Name	Manufacturer
Cooling centrifuge F34-6-38	Eppendorf
Electrophoresis chamber Mini Protean 3	Bio-Rad
Electroporator Gene pulser 2	Bio-Rad
Film developer Agfa Curix C60	Agfa Health Care
Fluorescence microscope Zeiss Axiovert 100M	Carl Zeiss
Fujifilm FLA5100 Fluorescent Image Analyser	Fuji
Incubator CO_2 Water Jacketed Incubator	Forma Scientific
Microtom RM 2155	Leica
Microplate reader	Tecan
Microwave Vacuum Histoprocessor RHS-1	Milestone
Nanodrop 2000	Peqlab
Odyssey Infrared Imager	Li-Cor
PCR Cycler T3 Thermocycler	Biometra
Phosphoimager BAS-1800II	Fujifilm
Power supply PAC 200	Bio-Rad
Power supply PAC 300	Bio-Rad
Semi-dry Western Blot	Peqlab
Scintillation counter Beckmann LS-6500	Beckmann
Sonication bath	Branic Branson
Table centrifuge 54 15 D	Eppendorf
Tissue-Tek VIP	Sakura
Tissue-Tek TEC	Sakura
Ultraturrax T25	Janke & Kunkel
UV-Transilluminator BioDoc Analyze	Biometra
Water bath for paraffin slides HI 2110	Leica

2.5 Chemicals and Supplements for ES Cell Culture

Chemicals and cell culture media, as well as supplements for embryonic stem cells are listed in the following table. All supplements are either autoclaved or filter-sterilised if not bought sterile.

Table 2.4 – ES Cell Culture

Name	Manufacturer	Cat. no.
Cell culture grade water	Gibco	# 15230
B27 supplement	Gibco	# 0080085SA
Bovine serum albumin (BSA)	Sigma Aldrich	# A9318
Dimethyl sulfoxide (DMSO) Hybri-Max	Sigma Aldrich	# D2650
Fetal calf serum (FCS, embryonic stem cell qualified)	PromoCell	# C-37387
Gelatin from porcine skin	Sigma Aldrich	# G2500
Glasgow-MEM, BHK-21	Gibco	# 21710-082
GlutaMAX	Gibco	# 35050038
HAT-supplement	Sigma Aldrich	# H0262
L-Glutamine 200 mM solution	Gibco	# 25030081
Lif	in-house production	
ß-Mercaptoethanol	Sigma Aldrich	# M3148
Monothioglycerol	Sigma Aldrich	# M6145
Neurobasal medium (NBM)	Gibco	# 21103049
Sodium pyruvate	Gibco	# S8636
Non essential amino acids	Gibco	# M7145
Phosphate buffered saline (PBS) 1 x	Gibco	# 14190
Penicillin-Streptomycin (Pen/Strep), 100 x	Gibco	# 10378016
Trypsin	Gibco	# 15090046
Trypsin inhibitor	Gibco	# R-007-100

2.6 Chemicals and Polymerases

Non-standard chemicals, as well as polymerases are listed in the following table.

Table 2.5 – Chemicals and Solutions

Name	Manufacturer	Cat. no.
Colchicine	Sigma Aldrich	# C9754
3,3'-Diaminobenzidine tetrahydrochloride hydrate (DAB)	Sigma Aldrich	# D5637
Dimethyl sulfoxide (DMSO)	Sigma Aldrich	# D2650
LongAmp Taq DNA Polymerase	New England Biolabs	# M0323S
Phenol-Chloroform isoamyl alcohol	Roth	# A156.3
Mitomycin C	Sigma Aldrich	# M4287
REDtaq ReadyMix	Sigma Aldrich	# R2523
TRIzol Reagent	Invitrogen	# 15596-026

2.7 Buffers and Solutions

The buffers and solutions that were used in this thesis are described in the following table. All buffers were prepared with double distilled water (ddH_2O) and stored at room temperature if not stated otherwise.

Table 2.6 – Buffers and Solutions

Name	Constituents	Production
Ampicillin stock solution	100 mg/ml	Storage at -20 °C, final concentration 100 µg/ml

Table 2.6 – Buffers and Solutions

Name	Constituents	Production
Blotting buffer (Western blot)	48 mM Tris pH 9.2 39 mM Glycine 20 % Methanol (v/v) 0.038 % SDS (w/v)	
Church hybridisation buffer	0.25 M NaPi (500 ml 10x NaPi, see below) 7 % SDS (w/v) 1 mM EDTA	Ad 1 l H_2O
Church washing buffer	0.02 M NaPi (80 ml 10x NaPi, see below) 1 % SDS (w/v)	Ad 2 l H_2O
DAPI	5 mg/ml	Treat in ultrasonic bath to solve. Final concentration: 1:25,000
Denaturation solution	0.5 M NaOH (20 g/l) 1.5 M NaCl (87.7 g/l)	
Depurination solution	0.25 M HCl (19 ml/l)	
DNA loading buffer 6x	10 mM Tris-HCl (pH 7.6) 0.03 % Bromophenol blue 0.03 % Xylene cyanol FF 60 % Glycerol 60 mM EDTA	
Ethidiumbromide solution	5 mg/ml	3 µl per 100 ml agarose gel
2 x HBS	280 mM NaCl 50 mM HEPES 1.5 mM Na3PO4	pH 7.13
Kanamycin stock solution	50 mg/ml	Storage at -20 °C, final concentration 100 µg/ml

Table 2.6 – Buffers and Solutions

Name	Constituents	Production
Lysis buffer (proteins)	100 mM Tris-HCl pH 7.4 150 mM NaCl 1 mM EDTA 1 mM $MgCl_2$ 1 % Triton X-100 1 µg/ml Leupeptin 1 µg/ml Pepstatin 10 µg/ml Phosphatase inhibitors 2.5 mM DTT	
Laird lysis buffer	100 mM Tris/HCl pH 8.0 5 mM EDTA 0.2 M NaCl 0.5 % SDS (w/v) 300 µg/ml Proteinase K	Add Proteinase K immediately before use
LB medium	10 g Bacto tryptone 5 g Bacto yeast extract 10 g NaCl	Solve in 1 l H_2O, adjust to pH 7.5 with NaOH, autoclave
LB plates	1.5 % Agar (w/v) in LB medium	Autoclave; after cooling down to 50 °C, pour into plates
Mowiol	Solution 1: 20 mg Mowiol 4-88 (Calbiochem) 80 ml PBS (pH 7.3) 40 ml Glycerol (87 %) 2 mM NaN_3 Solution 2: 2.5 mg n-Propylgallate 50 ml PBS (pH 7.3) 50 ml Glycerol	Working solution: 7.5 ml solution 1 + 2.5 ml solution 2

Table 2.6 – Buffers and Solutions

Name	Constituents	Production
NaPi 10 x (0.5 M)	0.5 M $Na_2HPO_4x2H_2O$ (89 g) 3-4 ml H_3PO_4	Adjust to pH 7.2 with H_3PO_4
Phosphate buffered saline (PBS) 10x	1.36 M NaCl 53 mM KCl 202 mM $Na_2HPO_4x2H_2O$ 19 mM KH_2PO_4	Ad 1 l H_2O pH adjusted to 6.75
Paraformaldehyde 8 % (PFA)	40 g Paraformaldehyd 325 µl 1 M NaOH ad 450 ml H_20 50 ml 10 x PBS	Heat PFA / H_20 / NaOH to dissolve. Adjust pH to 8.0, then add 10 x PBS.
Saline-sodium citrate buffer (SSC) 20x	175.3 g NaCl 88.2 g Sodium citrate	pH adjusted to 7.0, 1 l H_2O.
SDS-gel running buffer 10x	30.3 g Tris base 144 g Glycerol 10 g SDS	Ad 1 l H_2O
Separating gel buffer	1.5 M Tris-HCl pH 8.8	
Stacking gel buffer	0.5 M Tris/HCl pH 6.8	
SSPE 20x	3.6 M NaCl (174 g/l H_2O) 0.2 M Na_2HPO_4 (27.6 g/l H_2O) 0.02 M EDTA (7.4 g/l H_2O)	pH 7.7, ad 1 l H_2O
Tris-acetate-EDTA (TAE) 50x	2 M Tris (242.28 g) 7.85 mM EDTA (37.2 g) 57.1 ml Glacial acetic acid	Adjust to pH 8.3, ad 1 l H_2O
Tris-buffered saline (TBS) 10x	100 mM Tris-base (12.11 g) 1.5 M NaCl (87.6 g)	Adjust pH to 6.95, ad 1 l H_2O
TBS/Tween	1 x TBS 0.5 % Tween 20 (v/v)	
Transfer buffer (Southern Blot)	0.4 N NaOH (16 g/l H_2O)	

2.8 Eukaryotic Cell Cultures

2.8.1 Buffers and Solutions for Eukaryotic Cell Cultures

If not bought sterile, all buffers and solutions for ES cell cultures were either autoclaved or filter-sterilised. They were stored at 4 °C, if not stated otherwise.

Table 2.7 – Buffers and Solutions for Cell Cultures

Name	Constituents	Production
Complete neurobasal medium (NBM)	50 ml neurobasal medium 2 % B27 1 mM GlutaMAX 1 x Pen/Strep	
Freezing medium for ES cells	50 % Culture medium for ES cells 30 % FCS 20 % DMSO	2 x Stock solution, store at -20 °C
Freezing medium for mouse embryonic fibroblasts (MEF)	60 % Culture medium for MEFs 20 % FCS 20 % DMSO	2 x Stock solution, store at -20 °C
Gelatine (for coating)	1 % Gelatine in H_2O (w/v)	Autoclave two times
Growth medium	DMEM with GlutaMAX 5 % FCS 1 x Pen/Strep	
Growth medium for ES cells	Glasgow-MEM, BHK-21 15 % FCS 1 mM Sodium pyruvate 2 mM L-Glutamine 1 % Non essential amino acids 0.1 % Leukemia inhibitory factor 0.15 mM Monothioglycerol	
Growth medium for mouse embryonic fibroblasts (MEF)	DMEM 10 % FCS	

Table 2.7 – Buffers and Solutions for Cell Cultures

Name	Constituents	Production
	1 mM β-Mercaptoethanol 2 mM L-Glutamine 1 x Pen/Strep	
Hepes-buffered-saline (HBS) for electroporation 10x	10 g HEPES 16 g NaCl 0.25 g $Na_2HPO_4x2H_2O$ 0.74 g KCl 2 g D-Glucose	Adjust to pH 7.2, ad 200 ml H_2O. Filter sterilise with a 0.1 µm filter, store at -20 °C
Selection medium	Cell culture medium for ES cells add one vial HAT-Supplement	
ES-Trypsin	400 ml PBS (1x) 100 ml EDTA (1.85 g/l) 5 ml 2.5 % Trypsin	Store at -20 °C

Table 2.8 – Plasmids

Number	Name	Description
-	pLif	For the production of lif (Smith et al. [1988]), kindly provided by Dr. C.Völker.
-	Exon2KO-HSV	Generated by Rainer Gallitzendoerfer (unpublished).
-	pDTA	Kindly provided by Joachim Degen.
P9	pcDNA3.1	Expression vector (Invitrogen). Contains the Cytomegalovirus enhancer-promoter.
P11	pHWloxP	Cloning vector, contains a floxed HPRT-Minigene (Magin et al. [1992]).
P18	pBluescript (pBSK)	Cloning vector (Stratagene).
607	HRP3-Exon2KO6.1	HRP-3 targeting vector, cloned in this work.
610	Probe2	Probe for HRP-3 Southern blots, cloned in this work.

2.9 DNA Ladders

Table 2.9 – DNA Ladders

Name	Company	Fragments [*bp*]
λ/HindIII	Fermentas (# SM0102)	23,130, 9416, 6557, 4361, 2322, 2027, 564
λ DNA EcoRI + HindIII	Fermentas (# SM0192)	21,226, 5148, 4973, 4286, 3530, 2027, 1904, 1584, 1375, 947, 831, 564
50 bp ladder	Fermentas (# SM0371)	1000, 900, 800, 700, 600, 500, 400, 300, 250, 200, 150, 100, 50
1 kb plus ladder	Fermentas (# SM1334)	10,000, 8000, 6000, 5000, 4000, 3000, 2000, 1500, 1000, 500

2.10 Bacterial Strains

Table 2.10 – Bacterial Strains

Name	Genotype
XL-1 Blue	supE44 hsdR17 recA1 endA1 gyrA46 thi relA1 lac F'[$proAB^{+}, lacl^{q}, lacZ\Delta M15, Tn10\,(tet^{r})$]
JM-110	rpsL (Str^{r}) thr leu thi-1 lacY galK galT ara tonA tsx dam dcm supE44 $\Delta\,(lac - proAB)$ [$F, traD36, proAB, lacI^{q}Z\Delta M15$]

2.11 Eukaryotic Cell Lines

All cell lines were regularly tested for mycoplasma.

Table 2.11 – Cell Lines

Name	Origin	Notes
HM-1	mouse embryonic stem cells from 120/ola mice	Magin et al. [1992], HPRT-deficient. Cell line was a gift from Dr. Joachim Degen
COS-7	monkey	Production of leukemia inhibitory factor (lif) for ES cells
MEF	mouse embryonic fibroblasts	Isolated from NMRI mice, described in 3.3.1

2.12 Primers

Table 2.14 describes the primers that were used in this thesis to either generate constructs or genotype mice.

2.13 Plasmids

Table 2.8 contains plasmids that were used either for the cloning of the targeting construct or other purposes. Maps of all plasmids are listed in the supplemental materials.

2.14 Antibodies

Primary and secondary antibodies that were used in this thesis are described in table 2.12 and 2.13.

Table 2.12 – Antibodies

Name	Origin	Company	WB	ICC	IHC	AR
alpha-tubulin	mouse	DSHB (clone 12G10)	1:10,000	-	-	-
beta-III-tubulin	mouse	Dianova (T-1315)	1:1500	1:100	1:100	10 mM Sodium citrate, pH 6
GFP	mouse	hybridoma supernatant from Prof. Magin	1:1000	1:100	-	-
GFP	mouse	Roche	-	-	1:500	10 mM Sodium citrate, pH 6
GFP	rabbit	Abcam (# ab6556)	1:5000	1:500	-	-
C-terminal ms HRP-3	rabbit	Abouzied et al. [2004]	1:1000	1:100	1:100	2 mM EDTA
HDGF	rabbit	Abouzied et al. [2004]	1:1000	1:100	-	-
Human HRP-3	mouse	Santa Cruz, clone A10 (# sc-376558)	1:1000	1:100	1:100	2 mM EDTA

Table 2.13 – Secondary antibodies

Origin	coupled	Company	WB	ICC	IHC
goat α mouse	alexa 568	Molecular Probes (# A-11061)	-	1:600	1:600
goat α rabbit	alexa 488	Molecular Probes (# A-11008)	-	1:600	1:600
goat α rabbit	Cy-2	Dianova (# 111-225-003)	-	1:600	1:600
goat α mouse	Cy-2	Dianova (# 111-225-164)	-	1:600	1:600
goat α rabbit	Cy-3	Dianova (# 111-165-144)	-	1:600	1:600

goat α mouse	peroxidase	Dianova (# 115-035-044)	1:5000	-	-
goat α rabbit	peroxidase	Dianova (# 115-035-003)	1:5000	-	-
goat α rabbit	biotinylated	Jackson Laboratories (# 111-065-144)	-	1:600	1:600

Table 2.14 – Primer

Number	Name	Sequence	Usage
1181	BNP 500	AGCCTACCCTCTGGTAGATTG	Genotyping of mice, knockout
1482	GFPsense	GACAACCACTACCTGAGCAC	Genotyping of mice, knockout
1588	HRP-3exon2sense	CTATGCCTACGTCTGTTCCTGTT	Genotyping of mice, wild type
2004	HRP3Ex4SondeAS	TCTCCCCTCTCCTTTTCCAT	Sequencing
2476	Eef-2 sense	ATCCTCACCGACATCACCAAG	RT-PCR
2477	Eef-2 antisense	CTGCTCTGGACACTGGATCTC	RT-PCR
2742	HRP3-KO-HPRT-as	CACAGAGGGCCACAATG	Sequencing
2841	HDGFqPCRs	GACCTGGTGTTTGCGAAGAT	RT-PCR
2842	HDGFqPCRas	GCTTGCCAAACTTCTCCTTG	RT-PCR
2857	HRP-3 sense	GCAATGACACGAGAAACACGAC	RT-PCR
2858	HRP-3 antisense	GACAACAAAGACCGTTGGTTCA	RT-PCR
SF04	HRP3ex2kosense	ATCGATGTTAATCATAGCAGGGCAGGCAT	Cloning of the long homologous arm of HRP-3-exon2-KO6.1
SF05	HRP3ex2koanti	ATCGATGGATGTTGAGGAAGGTTAACCTGAG	Cloning of the long homologous arm of HRP-3-exon2-KO6.1

Table 2.14 – Primer

Number	Name	Sequence	Usage
SF18	HRP3Ex2KOas	CTATGCCTACGTCTGTTCCTGTT	Genotyping of mice, wild type
SF42	Southern2s	AAAAGTCCTCCACAGTCAATCC	Genotyping, Southern blot probe
SF70	HRP3KOscras	GCTGAACTTGTGGCCGTT	Genotyping
SF194	eGFPs	CAGCCACAACGTCTATATCATG	RT-PCR
SF195	eGFPas	GAACTCCAGCAGGACCATG	RT-PCR
	pEGFP-C2-RP	GATCACATGGTCCTGCTG	Sequencing
	EGFP-N	CCGTCCAGCTCGACCAG	Sequencing

2.15 Software

Determination of neurite lengths was performed with the ImageJ plugin NeuronJ (Meijering et al. [2004]). Clone Manager Version 9 from Sci-Ed was used to generate plasmid maps and plan constructs. This thesis was written in Texmaker 3.5. Image processing was performed with the Axiovert software (Zeiss), the GNU Image Manipulation Program (GIMP) 2.8.4 and Inkscape 0.48.

2.16 Trademarks

3 Methods

3.1 Techniques for the Isolation and Quantification of Nucleic Acids

3.1.1 Isolation of Plasmid DNA

Isolation of plasmid DNA was performed using the principle of alkaline lysis (Birnboim and Doly [1979]). This method allows the separation and isolation of plasmid DNA from bacterial chromosomal DNA due to different behaviour to denaturing agents.
For small volumes up to 2 ml of bacterial cultures, a mini preparation was performed using the Qiagen Plasmid Mini Kit according to the manufacturer's protocol. For medium cultures up to 50 ml a midi preparation was performed using the Qiagen Plasmid Midi Kit. For the purification of DNA suitable to transfect embryonic stem cells, the Qiagen EndoFree Plasmid Maxi Kit was used.

3.1.2 Isolation of Genomic DNA from ES Cell Clones

For fast genotyping of ES cell clones, DNA from 96-well plates was isolated. After aspiration of the growth medium, cells were washed once with 200 µl pre-warmed PBS. Afterwards, cells were incubated overnight with 50 µl Laird buffer containing 80 µg/ml proteinase K. Plate were placed in a plastic box padded with wet tissues and incubated at 55 °C. The following day, plates were allowed to cool down to room temperature for one hour, before gently adding 100 µl of 100 % ethanol per well. After one hour of incubation, the plates were then quickly inverted on tissue paper to dump the ethanol without disturbing the DNA at the bottom of the plates. The DNA was washed three times with 100 µl 70 % ethanol, each time dumping the ethanol as described. The plates were left to dry at room temperature for one hour,

before the DNA was solved in 80 µl water, transferred to a microcentrifuge tube and used for PCR analysis.

3.1.3 Isolation of Genomic DNA from Mouse Tail Biopsies

Genomic DNA for genotyping was extracted from mouse tail biopsies. About 0.2 mm of tail were cut and 500 µl Laird buffer containing 300 µg/ml Proteinase K were added. The tails were incubated overnight in a shaking water bath at 55 °C. The following day, a phenol-chloroform extraction was carried out (described in 3.1.4).

3.1.4 Phenol-Chloroform Extraction

Phenol-chloroform extraction was carried out to extract genomic DNA for PCR genotyping or Southern blotting. 1/2 volume phenol-chloroform isoamyl alcohol was added to the lysate and shaken vigorously. After five minutes of centrifugation at 15,000 x g, the upper phase, which contains the nucleic acids, was transferred to a fresh microcentrifuge tube. Following this, one volume of chloroform was added. The mixture was shaken again, and centrifuged as described. The upper phase was transferred to a fresh tube. The DNA was precipitated by adding one volume of isopropyl alcohol. This was shaken and then centrifuged for 10 minutes at 18,000 x g. The supernatant was discarded, and 300 µl 70 % ethanol were used to wash the DNA pellet. After another centrifugation step, the supernatant was discarded and the pellet left to dry. 50 - 200 µl of water were used to dissolve the DNA which was then used for PCR or Southern blot analysis.

3.1.5 Sodium Acetate Precipitation

Sodium acetate was used for the precipitation of small amounts of DNA. The following was added to the solution: $1/10^{\text{th}}$ of sodium acetate (pH 4.6) and an amount of 100 % ethanol equal to 2.5 times the volume of the original solution. After 10 minutes of incubation on ice, the solution was subsequently centrifuged and the supernatant discarded. The DNA pellet was washed once with 250 µl 70 % ethanol, dried, and dissolved in an appropriate amount of water.

3.1.6 Isolation of Total RNA from Mouse Tissues

TRIzol reagent was used for the isolation of total RNA from mouse tissues. TRIzol is a monophasic solution of phenol and guanidine isothiocyanate that allows the disruption of cells and tissues while protecting RNA from degradation through RNases (Chomczynski and Sacchi [1987]).
1 ml of TRIzol per 100 mg of tissue was used for the homogenisation in a glass-Teflon tissue grinder. Homogenates were centrifuged for ten minutes at 12,000 x g, 4 °C and the clear supernatant was transferred to a new 15 ml reaction tube. Homogenates were incubated for five minutes at room temperature to allow dissociation of nucleoprotein complexes. Subsequently, 0.1 ml of 1-bromo-3-chloropropane (BCP) per ml TRIzol were added. After 15 seconds of shaking and incubation for three minutes at room temperature, the mixture was centrifuged for 15 minutes at 12,000 x g and 4 °C. The clear, colourless upper phase contains the RNA and was transferred into a fresh tube. 500 µl of isopropanol per ml TRIzol were used to precipitate RNA for ten minutes at room temperature. After centrifugation for ten minutes at 12,000 x g, a RNA pellet was visible. After washing with 1 ml 70 % ethanol per ml TRIzol, and centrifugation at 7,500 x g for five minutes at 4 °C, the RNA was left to dry for ten minutes. The pellet was then dissolved in an appropriate amount of RNase-free water by incubating at 55 °C for ten minutes.

3.1.7 Estimation of Nucleic Acid Concentration

A Thermo Scientific NanoDrop 2000 spectrophotometer was used to measure nucleic acid concentration. 50 µg/ml double-stranded DNA, or 40 µg/ml RNA respectively, have an extinction of 1 at 260 nm. Proteins have their maximum extinction at 280 nm, thus the quotient E260/280 provides indications about the purity of the nucleic acid. For DNA, the quotient should lie between 1.8 and 2.0. For RNA, between 1.9 and 2.2, whereas lower values indicate contamination with proteins or phenol.

3.1.8 Separation of Nucleic Acids by Agarose Gel Electrophoresis

To visually estimate DNA concentration, separation by agarose gel electrophoresis was performed. Agarose forms a polymer and due to their negative charge, nucleic acids migrate through the agarose, depending on their size and conformation. Different concentrations of agarose were used for different sizes of DNA: 1 % for sizes between 1 and 10 kb and 2 % gels for smaller fragments between 0.2 and 1 kb. Ethidium bromide was used to visualise the DNA. 6 x loading dye was added to the samples (see 2.6). A voltage of 3 - 4 V/cm^2 was used for nucleic acid electrophoresis.

3.2 Modification of Nucleic Acids

3.2.1 Restriction Digests

Restriction enzymes from Fermentas were used for digestion of DNA according to the manufacturer's instructions. For cloning experiments, 1-3 µg DNA were digested in a volume of 20 µl for varying time spans ranging from one hour up to twelve hours at 37 °C.

3.2.2 Extraction of Linearised DNA from Agarose Gel

To isolate the requested fragment after a restriction digest, the desired band was cut from the gel with the help of an UV hand lamp. DNA was extracted using the QIAquick Gel Extraction Kit (Qiagen) according to the manufacturer's instructions. DNA was eluted in 30 µl ultrapure water and the concentration estimated via agarose gel electrophoresis, see 3.1.8.

3.2.3 Dephosphorylation of Linearised Vectors

To keep linearised vectors from religating, the FastAP thermosensitive alkaline phosphatase from Fermentas was used according to the manufacturer's instructions.

3.2.4 T4 Polymerase

For the integration of unphosphorylated PCR products in dephosporylated vectors, the insert had to be phosphorylated first. The T4 Polynucleotid Kinase (T4 PNK) from Fermentas was used according to the manufacturer's instructions.

3.2.5 Ligation

To link vector and insert covalently, T4 DNA Ligase (Fermentas) was used. It uses ATP to form the phosphodiester bond for blunt or cohesive ends respectively. The molar proportion of vector-to-insert is 1:5. 20 ng vector were incubated with the appropriate amount of insert for one hour at room temperature, this was followed by heat shock transformation.

3.2.6 Heat Shock Transformation

Competent XL-1 blue were stored at -80°C in 90 µl aliquots. For heat shock transformation, the bacterial solution was placed on ice for 5-10 minutes. 10 µl of the ligation mixture or 10 ng of purified plasmid DNA (re-transformation) were added to the bacteria (a maximum of $1/10^{\text{th}}$ of the bacterial solution). After a 20 minute incubation on ice, the heat shock was performed for one minute at 42 °C. Bacteria were left for two minutes on ice to cool down, before 900 µl of LB-medium were added. The suspension was placed in a shaking incubator for one hour at 37 °C, before plating on the appropriate LB-plates.

3.3 Embryonic Cell Culture

HM-1 cells are an embryonic stem cell line derived from 129/ola mice (Magin et al. [1992]). They are deficient for hypoxanthine phosphoribosyltransferase (HPRT), which allows using the HRPT-minigene as a positive selection cassette.
The HM-1 cells were a gift from Dr. Joachim Degen. Those were cultivated in a Thermo Forma Incubator at 5 % CO_2 and 37 °C. All work was performed using the sterile bench HERA Safe (Thermo Scientific).
HM-1 cells were cultivated in lif-containing medium (see 2.7, production of lif see 3.3.2) on a layer of mitotic inactive mouse embryonic fibroblasts (MEF or "feeder

cells", see 3.3.1).
Cell culture flasks were coated with gelatine, using a 0.1 % working solution (see table 2.6). The bottom of the plate was completely covered, and the solution incubated for ten minutes at room temperature, before aspirating.
For thawing of cells, cryo vials were taken from liquid nitrogen, unfreezed in a 37 °C waterbath and quickly transferred into a 15 ml reaction tube containing 10 ml of culture medium. Cells were pelleted by centrifuging five minutes at 800 x g and the supernatant was aspirated. After resuspending in culture medium, cells were then transferred to the gelatine coated culture dish.
For the feeder cell layer, MEFs were added in a density of 5 x 10^4 cells per cm^2. They were allowed to settle down for 30 minutes up to one day, before adding the ES cells to the same flask.
Culture medium was changed daily and embryonic stem cells were subcultured in a 1:3 to 1:6 ratio every two to three days. For subculturing, medium was aspirated and cells were washed twice with 5 ml warm PBS per T25 plate before trypsin was added (1 ml per T25 flask). Dishes were placed in the incubator for 1-5 minutes until cells formed a single cell suspension. This process was accelerated by careful tapping on the side of the dish every few minutes. After all cells were detached, they were resuspended in fresh culture medium and placed on fresh gelatine-coated dishes. For each subculture, the passage number was increased by one.
To freeze cells, a culture in their logarithmic growth phase was trypsinised as described above. Cells were collected in 10 ml of medium and pelleted by centrifugation. The pellet was resuspended in 500 µl culture medium and distributed into cryo vials. Each vial contained about 5 x 10^6 to 8 x 10^6 cells. 500 µl freezing medium (2.7) were added dropwise. Vials were closed and quickly transferred into a Nalgene freezing container which was then stored at -80 °C. After 24 to 48 hours, the vials were transferred to liquid nitrogen.

3.3.1 Culture of Mouse Embryonic Fibroblasts (MEF)

Isolation

Embryonic fibroblasts were used as "feeder" cells for embryonic stem cells. They produce and secrete growth factors which help to keep the cells in an undifferentiated state. HM-1 cells are able to grow MEF-independent, but especially when the cell

number was low (e.g. for selection) working with the addition of MEFs was preferred due to the healthier state of the HM-1 cultures.
For the isolation of MEFs, a 13.5 days pregnant C56Bl/6N mouse, was anaesthetised with chloroform and euthanised by cervical dislocation. The uterus containing the embryos was taken out and placed into a dish with sterile PBS. All extraembryonic tissues were removed and the heads cut off. The embryos were dissected using a scalpel and everything except the liver was transferred into a 15 ml reaction tube. 1 ml trypsin per embryo was added and incubated for ten minutes in a shaking waterbath at 37 °C. Using a syringe, the suspension was pressed through a 18 gauge needle until completely homogenised. Cells were taken up in feeder cell medium (see table 2.7) and plated on two T75 plates per embryo. MEFs were subcultured up to a maximum of four passages at a ratio of 1:3 every two or three days.

Inactivation and Cryopreservation

For mitotic inactivation 10 µg/ml mitomycin C were added to the confluent culture. Cells were incubated for three hours at 37 °C, before they were washed five times with warm PBS. MEFs were subsequently trypsinised with 2 ml per T75 flask, taken up in 10 ml and pelleted by centrifuging for five minutes at 800 x g. Three vials of cells were frozen from a T75 plate. Cell pellets were taken up in MEF freezing medium (see table 2.7) and distributed to the appropriate amount of cryo vials. Vials were placed in a Nalgene freezing container at -80 °C and transferred to liquid nitrogen two days later.

3.3.2 Production of Leukemia Inhibitory Factor (lif)

Leukemia inhibitory factor (lif) is a growth factor which keeps embryonic stem cells in an undifferentiated state. Cos-7 cells were used for lif production.
Cells were expanded in ES cell medium without lif, β-mercaptoethanol and antibiotics until 15 T75 plates were confluent. Three plates at a time were washed with PBS twice, trypsinised and taken up in 10 ml medium. Cells were centrifuged for five minutes at 800 x g. The supernatant was discarded and the cell pellet was taken up in 1.6 ml 1 x HBS electroporation buffer (see table 2.6). 800 µl cell suspension were electroporated with 120 µg pLif at 0.8 V and 3 µF. This was repeated once. Cells were taken up in fresh culture medium and plated on a 15 cm dish.

After 24 hours, the culture medium was replaced. 25 ml fresh medium were added, left on the plates for 72 hours and harvested. An additional 25 ml were added and left on the cells for 42 hours before harvesting. Both batches were combined, and filtered first through a 0.45 µm sterile filter, and then through a 0.1 µm filter.
The lif-containing medium was aliquoted and tested for its effectivity. For this, two 24-well plates were plated with ES cells without lif and feeder cells, one with 1,000 cells per well, and one with 500. The freshly produced lif was added in different concentrations ranging from 1:100 to 1:5,000. As a control, one well is grown without any lif and one with the previously produced batch. Cells were cultivated for seven days with daily medium replacement and then rated for their differentiation. The optimal concentration of lif leads to less than 5 % differentiated cells.

3.3.3 Gene Targeting of Embryonic Stem Cells

Transfection of ES cells via Electroporation

HRP-3Exon2KO6.1 was used as a targeting vector for the stable transfection of HM-1 cells. DNA was prepared using the QIAGEN EndoFree Plasmid Midi Kit, quantified, and 250 µg were digested overnight using PmeI in a total volume of 200 µl. 1 µl was separated using agarose gel electrophoresis to assess the quality of the digestion. If the plasmid was successfully linearised, a phenol-chloroform extraction (see 3.1.4) was performed, following a subsequent sodium acetate precipitation (see 3.1.5). The DNA pellet was taken up in 100 µl sterile cell culture grade water.
A healthy culture of HM-1 in logarithmic growth phase on a T75 plate was used for the targeting experiment. Cells were trypsinised as described above, taken up, and pelleted by centrifuging for five minutes at 800 x g. Supernatant was discarded and the pellet was washed in 10 ml warm PBS and centrifuged again. After aspiration of the supernatant, the cell pellet was resuspended in 800 µl 1 x HBS for electroporation and DNA was added. After pipetting up and down for two times, the cell-DNA-suspension was transferred without air bubbles to the electroporation cuvette. Electroporation was performed immediately using the Gene Pulser 2 (Biorad) at 3 µF and 0.8 V. The cuvette was left in place for ten minutes, before cells were placed in 50 ml prewarmed ES cell culture medium and plated on fifteen 10 cm dishes.

Selection of ES Cells and Cultivation of Clones

Aminopterin leads to the blockage of *de novo* DNA synthesis by inhibiting the dihydrofolate reductase. Adding hypoxanthine and thymidine gives the cell the possibility to utilise the salvage pathway, if the hypoxanthine phosphoribosyltransferase (HPRT) is available. Since HM-1 cells are HPRT-deficient, only cells which have successfully taken up the targeting vector, are able to survive the selection.
Selection was started 24 hours after electroporation by adding HAT-supplement to the culture medium (see 2.7). The medium was renewed every 48 hours, every 24 hours after cells started dying. On days 8-12 of the selection, cell clones were picked with a 200 µl pipette tip under a microscope, and transferred into a 96-well plate on feeder cells.
Medium in the 96-well plates was renewed daily. After two to six days, the medium turned yellow within one day, indicating that the cells were crowded enough to be subcultured. Therefore the medium was aspirated and cells were washed twice with 200 µl prewarmed PBS using a multichannel pipette. 50 µl trypsin were added to each well and the plates were incubated for five to ten minutes at 37 °C until all cells were detached. 150 µl culture medium were added and cells were resuspended using the multichannel pipette. Cells were then subcultured on four fresh 96-well plates; two were used for DNA extraction (see 3.1.2) and two for freezing.

Freezing and Thawing of 96-Well Plates

Freezing of 96-well plates allows easy storage of a high number of ES cell clones. An indicator for the cells being crowded enough is when the medium of most wells turns yellow within 24 hours. At this point the medium was then aspirated, cells were washed twice with 200 µl prewarmed PBS, and 50 µl trypsin were added per well. Cells were left in the incubator for five to ten minutes with occasional tapping of the side of the plate, until they were completely detached. 50 µl of freezing medium were added and cells were resuspended using the multichannel pipette. Plates were wrapped with Parafilm, placed in a few layers of paper towel and surrounded with aluminium foil. They were stored at -80 °C.
For thawing, plates were placed in the incubator for 24 hours until the cells were adherent again. Only then was the culture medium renewed. Positive clones and those surrounding them were then subcultured as soon as possible on 48-well plates.

Genotyping of ES Cell Clones

DNA from 96-well plates was isolated as described in section 3.1.2. 5 µl of DNA solution were used for the genotyping PCR. The expected PCR product has a size of 2,368 bp.

Table 3.1 – Genotyping PCR for ES Cell Clones

(a) Reaction Mix

Amount	Components
2 µl	Primer SF42 (5 pmol)
2 µl	Primer SF70 (5 pmol)
3.75 µl	2 mM dNTPs
5 µl	5 x PCR buffer
1 µl	DNA
0.5 µl	longAmp Polymerase
ad 25 µl	H_2O

(b) PCR Program

Step	Temp.	Time	
1	94 °C	180 sec	
2	94 °C	30 sec	
3	58 °C	45 sec	
4	65 °C	140 sec	to step 2, 34 cycles
5	65 °C	600 sec	
6	4 °C	∞	

Karyotype Analysis

To exclude chromosomal aberrations, the number of chromosomes had to be determined. Mice have a set of 40 acrocentric chromosomes.
Medium on a confluent 6 cm dish was replaced by colchicine-containing medium in a concentration of 0.1 mg/ml. Colchicine stabilises microtubules and therefore prevents the successful completion of mitosis. After one hour of incubation at 37 °C, cells were harvested with trypsin, taken up in 1 ml of culture medium and centrifuged for five minutes at 500 x g. The supernatant was discarded and the pellet taken up in

4 ml 0.56 % potassium chloride solution. After eight minutes of incubation at room temperature, which leads to the destruction of the cells and nuclei, the solution was centrifuged under the same conditions and taken up in 2 ml fixative (methanol to glacial acetic acid in a ratio 1:3). This was incubated for five minutes before centrifugation and fixation were repeated twice. Finally, the chromosomes were taken up in 0.5 ml fixative and dripped dropwise onto a glass slide from one meter height. Slides were stained for ten minutes with 200 µl DAPI before they were washed in water and embedded in Mowiol. Microscopic pictures were taken under 1,000 x magnification and chromosomes were counted.

3.3.4 Isolation of Primary Cortical Neurons

Neuronal cultures were isolated as described in El-Tahir et al. [2009]. A E14.5 days pregnant mouse was euthanised and the uterus removed. Embryos were dissected and the heads cut off. Using fine forceps, the skull was opened and the brain taken out with a spoon-like instrument. Under a binocular microscope cerebral cortices were isolated and the meninges removed with forceps. The cortices were placed in 50 ml ice-cold PBS and allowed to settle down. Then these were incubated for ten to twelve minutes in a shaking 37 °C waterbath with 1 ml 0.5 % trypsin-EDTA (see table 2.4) per brain.
A mixture of trypsin inhibitor and 100 mg/ml BSA in H_2O (7.5 ml trypsin inhibitor + 2.5 ml BSA) was used to inhibit trypsin. The mixture was allowed to settle for a few minutes at room temperature, it was then homogenised with a 10 ml pipette in complete NBM medium (1 ml per brain, see table 2.4). Cells were counted and plated on poly-l-lysine-coated glass cover slips with 40,000 cells per cm^2 and incubated for 48 hours at 37 °C, 5 % CO_2.

3.4 Analysis of Mice

Mice were kept under standard housing conditions in a 12 hour light-dark cycle with food and water *ad libitum*. All experiments were carried out in accordance with local and state regulations concerning animal research.
DNA from mouse tail clippings (see 3.1.3) was used for the genotyping of mice via PCR.

3.4.1 PCR for Mouse Genotyping

Table 3.2 – PCR for mice genotyping

(a) Reaction Mix

Amount	Components
2 µl	Primer 1181 (5 pmol)
2 µl	Primer 1482 (5 pmol)
2 µl	Primer 1588 (5 pmol)
2 µl	Primer SF18 (5 pmol)
50 ng	DNA
ad 10 µl	H_2O
10 µl	Redtaq ReadyMix

(b) PCR Program

Step	Temp.	Time	
1	95 °C	180 sec	
2	95 °C	30 sec	
3	58 °C	45 sec	
4	72 °C	60 sec	to step 2, 34 cycles
5	72 °C	300 sec	
6	4 °C	∞	

3.4.2 Southern Blotting Using Church Buffer

Southern blotting allows the detection of a DNA sequence within complete genomic DNA. Therefore, DNA is restriction digested, separated via agarose gel electrophoresis, and blotted on a membrane. Radioactive probes are hybridised with the membrane and can be made visible with a X-ray film.

20 µg DNA from mouse tail clippings were digested overnight using 3 µl EcoRI in a total volume of 60 µl. On the next morning, 0.5 µl were added and again incubated for two hours at 37 °C. The DNA was then separated on a 0.8 % agarose gel without ethidiumbromide at 60 V. A control gel containing ethidiumbromide was run with 1/10th of the digested DNA to control successful digestion.

When the DNA was sufficiently separated, as was evaluated by the running distance

of bromophenol blue, electrophoresis was stopped. The gel was placed in acidic depurination (see table 2.6) solution. Incubation was performed two times for seven minutes under slight shaking. After rinsing the gel in ddH_2O for a minute, it was placed in denaturation solution three times for ten minutes each. For equilibration, the gel was then placed in 0.4 N NaOH (transfer buffer) for five minutes, afterwards the Southern blot was assembled as shown in figure 3.1. A vessel containing transfer buffer was bridged with a plastic tray, on which a piece of Whatman paper connected both sides of the transfer buffer. The agarose gel was then placed upside down on the Whatman paper, with the Hybond XL membrane on top. Three layers of Whatman paper with the same size as the gel were placed on top. An about 15 cm pile of paper towel was stacked, finished with a weight of 250 - 500 g on top. Blotting was performed overnight.

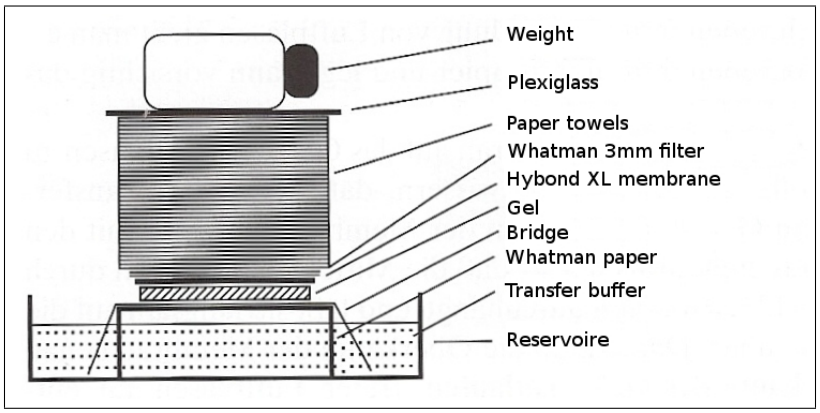

Figure 3.1 – Assembly of a capillary blot. This picture illustrates the assembly of a capillary blot. Image modified from "'Nucleinsäure-Blotting"', Darling, D.C., Brickell, P.M., Spektrum, Akad. Verlag, 1996, Page 67.

On the next day, the blot was disassembled. The pockets of the agarose gel were marked on the membrane using a needle. Then the membrane was equilibrated ten minutes in 1 x NaPi (table 2.6) and subsequently left to dry for 30 minutes at room temperature on a piece of Whatman paper. To fix the DNA on the membrane, it was then baked for two hours at 80 °C.

The membrane was prehybridised for two hours at 65 °C in Church hybridisation solution (table 2.6).

The radioactive probe was prepared by digesting plasmid no. 610 with the FastDigest enzymes XhoI and XbaI. After gelextraction and quantification, 50 ng of DNA

were labelled using the Stratagene Primer it II labelling kit according to the manufacturer's instructions.
Illustra MicroSpin G-50 Columns (GE Healthcare) were used to purify the probe from unincorporated nucleotides according to the manufacturer's instructions. 15 µl radioactive probe were denatured, adding 15 µl 2 M NaOH and incubated for ten minutes. Afterwards, the radioactive probe was added to the prehybridised membrane and hybridised overnight at 65 °C.
The membrane was placed in a plastic container and rinsed two times in prewarmed 65 °C Church washing buffer. The buffer was discarded and fresh washing buffer was added. The plastic container was then placed in a shaking water bath at 65 °C. Every five to ten minutes, the radioactivity of the membrane was measured using a handheld Geiger counter. This was performed until radioactivity reached approximately 0.5 to 1 Bq/cm^2. Afterwards, the membrane was sealed into a plastic bag. Autoradiography was performed using an intensifying screen (Kodak).

3.4.3 RT-PCR

Total RNA from mice was prepared as described in 3.1.6. 0.5 µg RNA was reverse-transcribed using the Qiagen QuantiTect kit according to the manufacturer's instructions. 1 µl of the mix was used to perform a PCR.

Table 3.3 – Reverse Transcription PCR

(a) Reaction Mix

Amount	Components
2 µl	Primer (5 pmol)
2 µl	Primer (5 pmol)
1 µl	cDNA
ad 10 µl	H_2O
10 µl	Redtaq ReadyMix

(b) PCR Program

Step	Temp.	Time	
1	95 °C	180 sec	
2	95 °C	30 sec	
3	56 °C	30 sec	
4	72 °C	60 sec	to step 2, 34 cycles
5	72 °C	300 sec	
6	4 °C	∞	

3.5 Protein Biochemistry

3.5.1 Preparation of Protein Lysates

Either primary tissues or cells were used to produce homogenates for the detection of proteins via Western blotting. Cells were washed with 37 °C prewarmed PBS once. They were then scraped from the surface of the plate with a cell scraper in 1 ml of PBS. The suspension was transferred to a 1.5 ml reaction tube and centrifuged for five minutes at 500 x g. The supernatant was discarded and the cell pellet was lysed using protein lysis buffer (see table 2.6). For this, 250 µl lysis buffer were added to the pellet and the mixture was suspended. This was then incubated on ice for 30 minutes. The homogenate was then sonificated three times for 15 seconds each. Between the sonification steps the samples were incubated on ice for 30 seconds. The samples were then centrifuged for 30 minutes at 18,000 x g and 4 °C, to separate insoluble cell parts. The protein-containing supernatant was then transferred to a fresh reaction tube and used for protein estimation. Lysates were stored at -20 °C. To generate lysates from mouse tissue, immediately after preparation, the tissues were shock frozen in liquid nitrogen and stored at -80 °C until further processing. Tissues were weighted and 500 to 1000 µl per 100 mg lysis buffer was used for homogenisation. The frozen tissue was transferred to a glass-Teflon homogeniser, the lysis buffer was added and the tissue was homogenised on ice. Homogenates were then incubated on ice for 20 minutes and further treatment took place as described above for cell lysates.

3.5.2 Protein Estimation

For the estimation of protein amounts in cell and tissue homogenates, the BioRad DC Protein Assay was used (principle see Lowry et al. [1951]) according to the manufacturer's instructions. A BSA concentration series ranging from 0.0625 mg/ml to 2 mg/ml BSA in PBS or lysis buffer was used to determine the concentration of the sample. The extinction was measured at 750 nm using a Tekan microplate reader.

3.5.3 SDS-PAGE

For immunoblot detection, protein lysates were separated on a sodium dodecyl sulfate polyacrylamide gel electrophoresis (SDS-Page), blotted on a membrane and incubated with specific antibodies. Detection took place with enhanced chemiluminescence.
If not stated otherwise, 12.5 % SDS- PAGE gels were used in this thesis, since they allow optimal separation of proteins between 12 and 60 kDa.
See table 3.4 for the composition of a 12.5 % SDS-PAGE gel. Gels with a thickness of either 0.75 mm or 1 mm were used.
For sample preparation 4 x Laemmli buffer was added to 50 µg protein in the appropriate amount to dilute to 1 x buffer. The samples were then placed in a heating block for five minutes at 95 °C. After cooling down on ice, samples were applied to the gel. 100 V were applied to the gel until the samples reached the separating gel. Then the potential was raised to 200 V until the bromophenol blue in the loading buffer ran out of the gel.

Table 3.4 – Components of a SDS-PAGE gel

Components	1 ml Stacking gel (5 %)	5 ml Separating gel (12.5 %)
Water	604 µl	2,100 µl
40 % Acrylamid	125 µl	1,560 µl
Tris HCl(*)	250 µl	1,250 µl
10 % SDS	10 µl	50 µl
10 % APS	10 µl	50 µl
Temed	1 µl	5 µl

(*)Tris HCl pH 6.8 for stacking gel and pH 8.8 for separation gel.

3.5.4 Western Blotting (Semi-Dry)

Western blotting is a technique that allows the transfer of proteins from an SDS-PAGE gel to a membrane in order to allow detection of specific proteins with antibodies. In this thesis nitrocellulose membranes were used.
When the SDS-PAGE was finished, the gel was subsequently placed in blotting buffer (see table 2.6) while the blot was set up. Whatman paper and nitrocellu-

lose membrane were cut to the size of the gel and pre soaked in blotting buffer. From anode to cathode, three layers of Whatman paper were stacked up, followed by the membrane, the gel, and another three layers of Whatman paper. The setup was checked to be free of bubbles, before blotting was performed for 45 minutes at $3\,mA/cm^2$.
After successful blotting, the membrane was blocked in 5 % skim milk/TBS for one hour at room temperature. All incubations were performed on a shaker. Incubation with the first antibody (see table 2.12 for dilutions) was performed for one hour at room temperature, or overnight at 4 °C in 0.5 % skim milk/TBS-T. The membrane was subsequently washed with TBS-T three times, for five minutes each. Incubation with the secondary antibody was performed for one hour at room temperature in 0.5 % skim milk/TBS-T. Again the blot was washed three times with TBS-T, followed by a last five minute washing step in TBS. The Pierce ECL western blotting substrate was used for the detection of the peroxidase-coupled secondary antibody, according to the manufacturer's instructions.
The Odyssey infrared imager allows the detection of two proteins at the same time using secondary antibodies coupled to fluorophores. The protocol is performed as for the enhanced chemiluminescence method, but no substrate is required. Membranes are scanned wet using the Odyssey imager.

3.6 Histology

3.6.1 Immunocytochemistry (ICC)

Immunocytochemistry (ICC) allows the visual detection of proteins inside the cell. Cells were cultured on glass cover slips in 24-well plates under normal culturing conditions. For fixing, they were washed once with PBS. Subsequently, 500 µl 4 % PFA were added and incubated for ten minutes at room temperature. The PFA was discarded and the cover slips were washed with PBS two times. Cells were permeabilised using 0.2 % triton-x-100/PBS for seven minutes. Following this, cover slips were placed upside down on a piece of Parafilm, on which 30 µl blocking solution (3 % bovine serum albumin (BSA) in PBS) have been dripped. For primary antibody incubation, the antibody (see table 2.12 for instructions) was diluted in 1 % BSA/PBS and incubated for one hour as described above. Cover slips were

then washed three times by slewing them in PBS, before placing them on a drop containing the secondary antibody in 1 % BSA/PBS. Again the cover slips were washed, adding a final washing step in water, drying them on tissue paper, before embedding them in Mowiol on a glass slide. After drying for 24 hours, the slides were microscopically analysed.

3.6.2 Immunohistochemistry (IHC)

Immunohistochemistry (IHC) enables the visual detection of specific proteins in tissues with antibodies. Paraformaldehyde (PFA)-fixed tissue is embedded in paraffin and cut with a microtome.

Tissue Preparation and Paraffin Embedding

For tissue preparation, mice were euthanised with chloroform and the tissues of interest were removed. They were placed in 4 % PFA for fixing for 12-24 hours at room temperature. After washing in PBS for three times to remove the PFA, the tissues were dehydrated using the Tissue-Tek VIP machine. It performed the following dehydration series: 2 x 70 % ethanol, 2 x 96 % ethanol, 3 x 100 % ethanol, 2 x xylene; each step taking one hour. This was followed by four paraffin steps, 45 minutes each.
When the dehydration was complete, the tissues were embedded in paraffin using metallic forms. Forms were kept cool for 30 minutes at -8 °C on a cooling plate, before the paraffin block was taken out and stored at 4 °C until sectioning.

Paraffin Sectioning

Paraffin blocks were pre-cooled to -8 °C on a cooling plate before they were sectioned using an RM 2155 microtome (Leica). Usually 4 µm thin sections were cut, these were transferred with a brush to a 42 °C water bath. The sections were placed on a SuperFrost plus microscope slide, which are positively charged and thus allow better adherence of the tissue. The sections were kept overnight in a 37 °C incubator, which allows vaporisation of residual water, and were then stored at 4 °C for further processing.

Staining of Paraffin Sections

Deparaffinisation was the first step in staining of paraffin sections. Glass slides were placed in a rack and washed using the following series: 2 x ten minutes xylene, 2 x ten minutes 100 % ethanol, 2 x five minute 96 % ethanol, 1 x five minutes 70 % ethanol, 1 x 50 % ethanol, tap water. Slides were then stored in tap water until antigen retrieval was performed. Antigen retrieval was undertaken in a microwave vacuum histoprocessor RHS-1 for 20 minutes at 95 °C. The type of antigen retrieval is depended on the antibody, see table 2.12 for details. Slides were placed in a beaker glass and completely covered in the buffer of choice (e.g. 2 mM EDTA pH 8 for HRP-3 staining).
Antigen retrieval was followed by cooling down the slides to room temperature by applying water from the outside of the beaker glass for 30 minutes.
Slides were washed in TBS once, before permeabilising for seven minutes in 0.2 % Triton-X-100/TBS, followed by three more washes in TBS. Glass slides were placed in a wet chamber and blocked with 30-150 µl 3 % BSA/TBS for one hour at room temperature. The first antibody was diluted in 1 % BSA/TBS and incubated overnight at 4 °C. Glass slides were washed three times in TBS. Following this, they were incubated for one hour at room temperature in a solution of fluorescent secondary antibody and DAPI diluted in 1 % BSA/TBS. Slides were embedded in Mowiol and left to dry for 24 hours and stored at room temperature.

Chromogenic Immunohistochemistry

For chromogenic staining, sections were treated as described in 3.6.2. After antigen retrieval, slides were washed three times in TBS. To block endogenous peroxidases, the sections were incubated for ten minutes in 3 % H_2O_2 in H_2O. Slides were again washed three times in TBS, then they were permeabilised for seven minutes in 0.2 % Triton-X-100/TBS, followed by three more washes in TBS. Sections were blocked and incubated with the primary antibody as described above. For the HRP-3 staining, a biotinylated goat anti rabbit secondary antibody, diluted 1:200 in 1 % BSA/TBS, was used. Incubation took place for one hour at room temperature. Then, the solutions from the Vectastain ABC kit were prepared according to the manufacturer's instructions, given dropwise onto the sections and incubated for one hour at room temperature. Slides were again washed for three times in TBS,

before development took place. A 0.05 % solution of 3,3'-Diaminobenzidine tetrahydrochloride (DAB) with 0.03 % H_2O_2, was given onto the sections until a satisfying signal was reached. Sections were subsequently washed in water and dehydrated for embedding in the following way: 1 x 30 seconds in 70 % ethanol, 2 x 30 seconds in 96 % ethanol, 2 x 30 seconds 100 % ethanol and 1 x 30 sec xylene. Slides were then embedded in DPX mounting medium.
For immunohistochemistry of GFP, slides were treated as described above, up to the incubation with the primary antibody. The mouse anti GFP antibody (Roche) was diluted 1:500 in 3 % BSA/TBS and incubated overnight at 4 °C on the slides. Slides were washed for three times in TBS, then the Super Sensitive link-label-IHC detection system (BioGenex) was used. This system uses the biotin-streptavidin amplified (B-SA) instead of the avidin-biotin complex (ABC) method. Instead of 20 minutes, as described by the manufacturer, the solutions were incubated for one hour each. The slides were washed three times for five minutes in TBS, between and after the incubation with link and label solution. Development was performed with DAB as described above, but a longer time (up to ten minutes) was needed to gain signals.

3.6.3 Whole Mount Staining

Whole mount embryo staining was performed using a slightly modified protocol, derived from www.abcam.com/technical. An E11.5 pregnant mouse was euthanised, cut open and embryos were transferred into ice-cold PBS. All extraembryonic tissues were carefully removed and the embryo was fixed in 4 % PFA overnight at 4 °C.
On the next day, embryos were transferred to a 12-well plate. Three washes with 1 % Triton-X-100/PBS, 30 minutes each, were performed. Embryos were blocked twice for one hour at room temperature in 1 ml 5 % normal goat serum (NGS) + 1 % bovine serum albumine (BSA) in PBS. To inhibit endogenous peroxidases, embryos were placed in block solution with 0.1 % H_2O_2 overnight at 4 °C.
The next day, embryos were washed twice for ten minutes in block solution and then placed in block solution containing c-terminal HRP-3 antibody (1:100), as well as 0.1 % sodium azide. Incubation took place for four days at 4 °C.
Embryos were washed three times, one hour each, in 1 %Triton/block solution and then three times, ten minutes each, in 1 %Triton/PBS to remove traces of sodium

azide. The secondary antibody, diluted in blocking buffer (goat anti rabbit biotinylated, 1:200), was added and the embryos incubated for two days at 4 °C.
On the following day, embryos were washed three times for ten minutes each in 1 %Triton/PBS. For three hours, they were incubated in Vectastain ABC-Kit which was prepared according to the manufacturer's instructions. For development, embryos were placed in a 0.05 % solution of 3,3'-Diaminobenzidine tetrahydrochloride (DAB) with 0.03 % H_2O_2. When the staining showed the desired intensity, embryos were washed in PBS and pictures were taken with a binocular microscope.

4 Results

4.1 Organisation of the Targeting Vector

The HRP-3 targeting construct is composed of two homologous regions, a 1.4 kb short arm and a 10.6 kb long arm. These regions are necessary for the homologous recombination event. The short arm allows PCR-based screening from the genomic area to the inserted targeting vector. A longer homologous region is more efficient for a successful homologous recombination event. A loxP-flanked reporter gene and a positive selection cassette are located between those homologous arms. As a reporter gene, eGFP without a promoter is employed. It uses the endogenous *Hrp-3* promoter and therefore allows visualisation of HRP-3 expression.
The hypoxanthine phosphoribosyltransferase (HPRT) minigene is used for positive selection. It is an enzyme of the salvage pathway, which adds ribose-5-phosphate to hypoxanthine and thus produces inosine monophosphate, an intermediate in the purine metabolism. HM-1 cells are HPRT-deficient (Magin et al. [1992]). Medium that contains hypoxanthine, aminopterin and thymidine (HAT-medium) is used as a selection medium. Aminopterin inhibits DNA *de novo* synthesis, thus forcing the cell into the salvage pathway for DNA synthesis. Only those cells that successfully took up the HRPT gene are able to survive in selection medium.
Additionally, a negative selection is included in the targeting vector. A diphtheria toxin fragment A (DT-A) cassette is localised upstream of the short homologous arm. In case of a random integration of the whole targeting vector, DT-A expression will kill the cells. A DT-A cassette enables a tenfold reduction in the amount of false-negative clones (Yagi et al. [1990]). To prevent cell death by transient transfection, no polyA signal was included downstream of the DT-A cassette.

4.1.1 Construction of the Targeting Vector

The targeting vector is a modified version of the plasmid Exon2KO-HSV, which did not succeed in the production of targeted ES cell clones. It was cloned by Rainer Gallitzendoerfer. In short, Exon2KO-HSV is a GFP-knockin vector that targets exon 2 of *Hrp-3*. The HPRT minigene and the GFP are flanked by two loxP sites and two homologous regions, one short 5' arm (1488 bp) and a long 3' arm (4999 bp). A thymidine kinase cassette is located antisense to the long arm. The performed modification includes three parts. The 5' arm is shortened to allow an efficient PCR-based screening. A longer 3' arm is cloned to enhance the change of a homologue recombination event. Lastly, a diphteria toxin cassette (DTA) as a negative selection is inserted on the site of the short homologous arm.

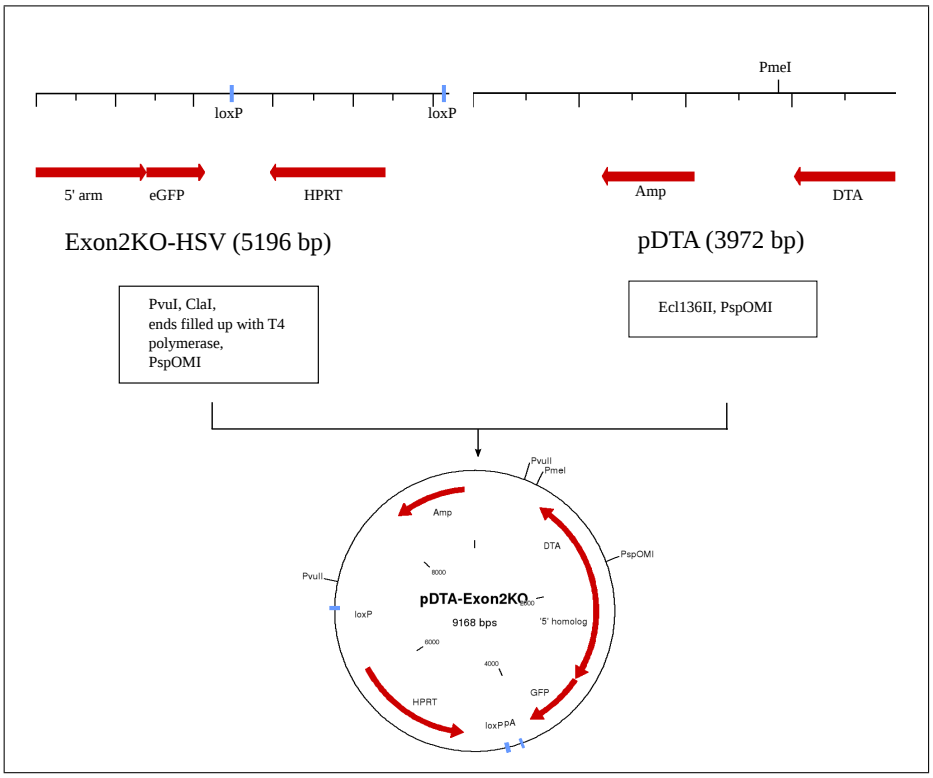

Figure 4.1 – First step of the cloning strategy for HRP-3-Exon2KO6.1. The plasmid Exon2KO-HSV was cut using PvuI and ClaI. The generated ends were blunted with T4 polymerase, then the fragment was cut with PspOMI. Subcloning into the Ecl136II/PspOMI cut pDTA vector led to the product pDTA-Exon2KO.

The first part of the cloning strategy is detailed in figure 4.1. Exon2KO-HSV was cut

using the restriction enzymes PvuI and ClaI. ClaI was necessary to cut a fragment with a similar size as the target fragment. This digestion resulted in the following products: 15,244 bp, 6946 bp, 5085 bp, 1993 bp, 1044 bp and 176 bp.
The 6946 bp fragment was gel-extracted and then blunted using T4 polymerase to fill up the PvuI-generated sticky ends. Subsequently, the fragment was cut using PspOMI, resulting in the main 5196 bp and a smaller 1752 fragment. The bigger fragment was gel-extracted and subcloned into pDTA. The target vector pDTA had been cut with Ecl136II/PspOMI. The resulting 3972 bp fragment was then separated from the 129 bp fragment by gel extraction. This resulted in a plasmid, pDTA/Exon2KO, which was control digested using PvuII. This led to the expected products of 6655 bp and 2513 bp.

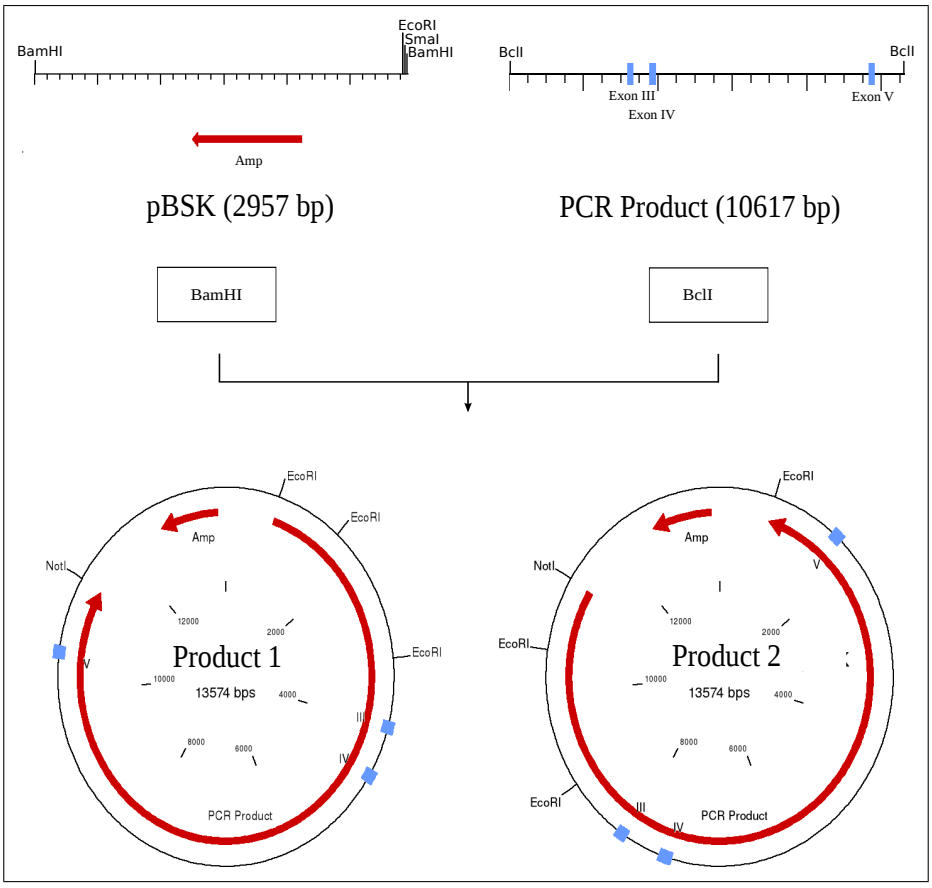

Figure 4.2 – Second step of the cloning strategy for HRP-3-Exon2KO6.1 The PCR product, generated with primers SF04 and SF05 was cut with BclI and subcloned into the BamHI-cut, dephosphorylated pBSK backbone. The two possible products were identified via EcoRI control digestion.

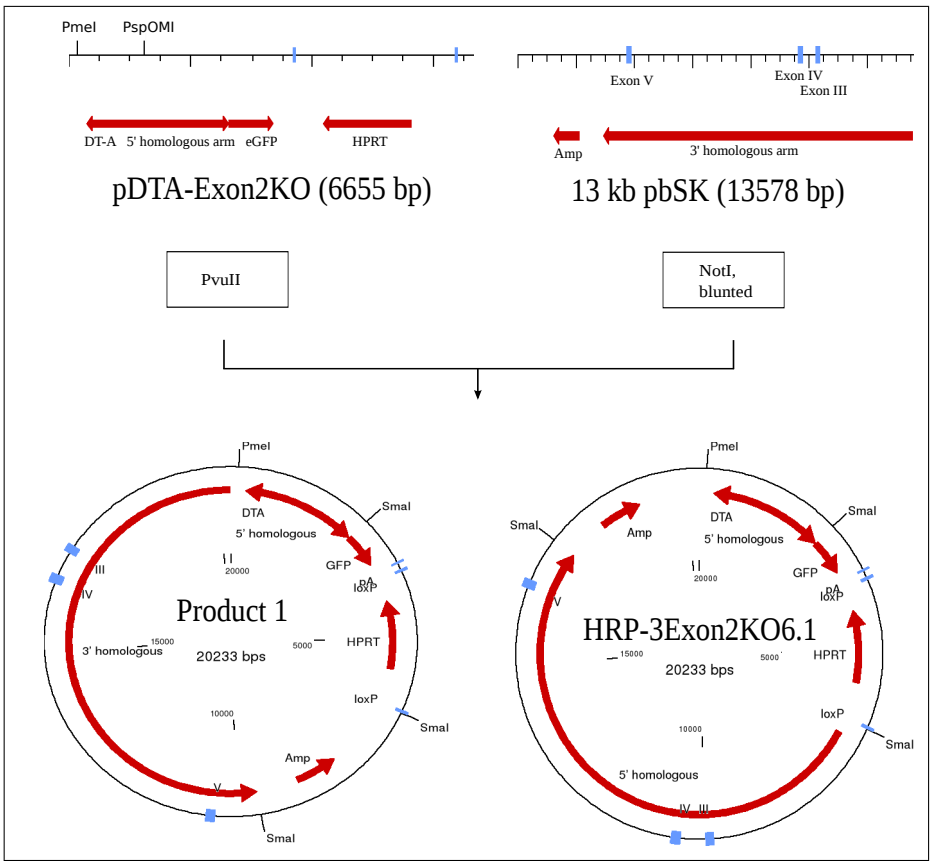

Figure 4.3 – Third step of the cloning strategy for HRP-3-Exon2KO6.1 pDTA-Exon2KO was cut with the blunt end cutter PvuII and the 6655bp fragment gel isolated. The target vector for subcloning, 13kb-pBSK was cut with the single cutter NotI, subsequently blunted, dephosphorylated and ligated with the insert. Two plasmids could have possibly been generated, they were identified with a SmaI control digestion.

Step two of the cloning strategy is pictured in figure 4.2. To clone the long homologous arm, the BAC clone bMQ440-k24 (Source BioScience, UK) was used as a PCR template. A 12,976 bp fragment, containing the region upstream of exon 2, was amplified using the primers SF04 and SF05. The PCR product was digested with BclI, which cut two times, generating three fragments: 10,617 bp, 1707 bp and 652 bp. The 10,617 bp fragment was gel-purified and subcloned into the BamHI site of the 2957 bp pBluescript II SK(-) vector (Stratagene). Since the insert can integrate in two directions, the two possible products had to be differentiated by a control digestion. A digest with EcoRI led to the following three fragments for the plasmid with the false integration: 11097 bp, 1612 bp and 865 bp. For the correct integration

(which was named 13kb-pBSK) the three resulting fragments were 8176 bp, 3784 bp and 1612 bp.
Step three is described in illustration 4.3. 13kb-pBSK was cut with the single cutter NotI and subsequently treated with T4 Polymerase to achieve blunt ends. The 13574 bp fragment was gel-extracted.
pDTA/Exon2KO was digested with PvuII, leading to fragments sized 6655 bp and 2513 bp. The bigger fragment was ligated with the NotI-cut, blunted 13kb-pBSK fragment. Thus producing the final targeting vector, HRP-3-Exon2-KO6.1. To screen for correct insertions, the plasmid was cut with SmaI. The wrong product results in fragments of 13267 bp, 3792 bp and 3174 bp. The correct plasmid leads to sizes 10884 bp, 5558 bp and 3792 bp. The result of the control digestion with SmaI is shown in figure 4.4. DNA from 15 colonies was analysed, six of them were positive for the correct integration (number 1, 2, 4, 5, 13, 14 and 15). The other colonies showed a restriction pattern resulting from either wrong insertion or the original plasmids, pDTA-Exon2KO (3792 bp and 5372 bp) or 13kb-pbSK (13,578 bp). A midi scaled DNA preparation was performed for colonies number 4 and 15 and further restriction digested were performed. Colony number 4 was sent for partial sequencing to GATC Biotech (Konstanz, Germany) and used for all further experiments. The sequencing results as well as a complete plasmid map can be found in the supplement. For the targeting experiments, HRP-3-Exon2KO6.1 was digested with PmeI for linearisation.

4.2 Gene Targeting in Embryonic Stem Cells

4.2.1 Targeting Scheme

Illustration 4.5 pictures the homologous recombination of the targeting vector with the wild type allele resulting in the mutant allele. The *Hrp-3* gene consists of six exons, with a 30 kb gap between exon 1 and exon 2. Previous experiments targeting exon 1 were not successful. Therefore the construct that is used here, targets exon 2, thus creating a fusion protein of exon 1 and eGFP.

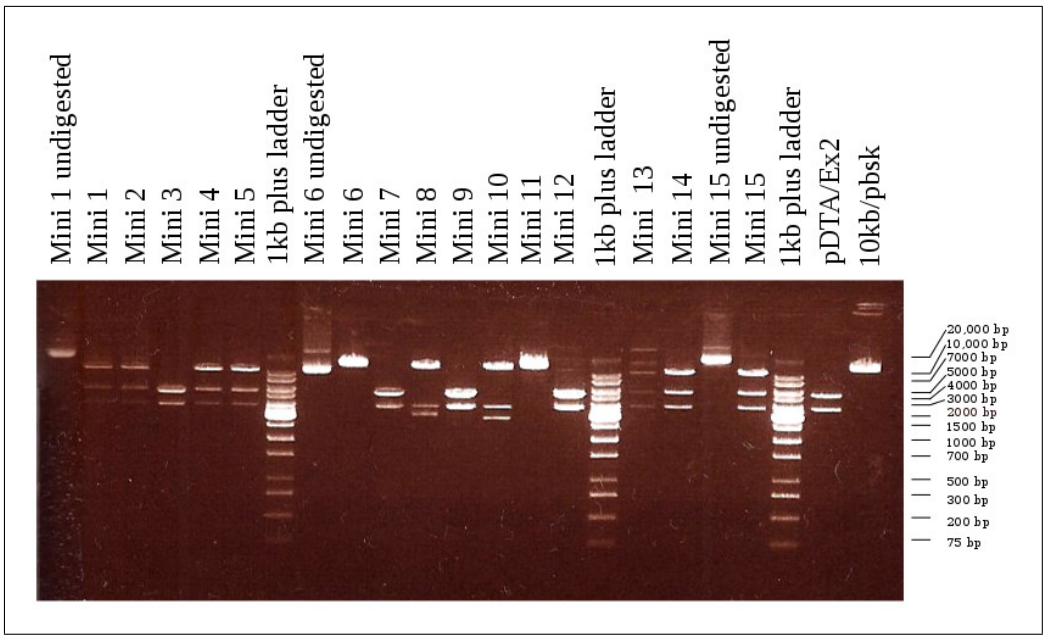

Figure 4.4 – **Control digested DNA from mini preparations.** For the last cloning step, 15 colonies were analysed by DNA preparation and subsequent DNA restriction digestion with SmaI and agarose gel electrophoresis. Undigested controls for colonies 1, 6 and 15 were used as negative controls as well as the original plasmids used for the ligation (pDTA-Exon2KO and 13kb-pbsk). Colonies number 1, 2, 4, 5, 13, 14 and 15 show a restriction pattern fitting to the expected 10884 bp, 5558 bp and 3792 bp. Other colonies show an integration into the wrong direction (8 and 9) or the pattern of the origin plasmids (3, 6, 7, 9, 11 and 12).

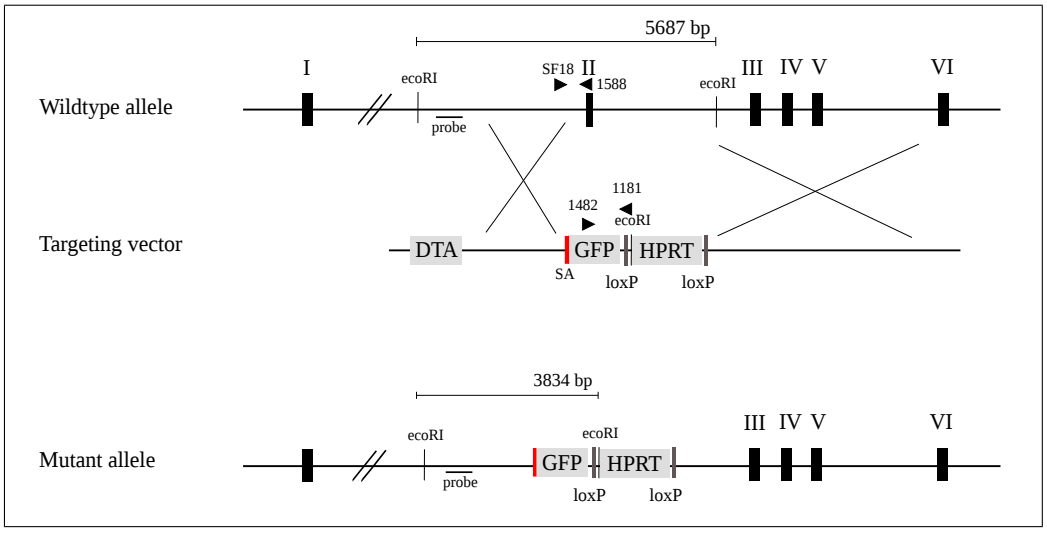

Figure 4.5 – **Targeting scheme for *Hrp-3* exon 2.** The wild type allele of *Hrp-3* consists of six exons (depicted as narrow black boxes, named I-VI), exon 2 is targeted with this plasmid. The homologous regions are marked by crossed lines. GFP is the reporter gene, HPRT the selection cassette. DTA the negative selection cassette, that is not included if a homologous recombination occurs only in case of a complete and random integration. Arrowheads designate genotyping primers. The southern blot probe, as well as the restriction enzyme cutting sites (EcoRI) and the resulting fragments are depicted as well. SA marks the splice acceptor side from exon 2. The mutant allele shows the successfully integrated reporter gene and selection cassette.

4.2.2 Targeting of Embryonic Stem cells

In the successful targeting experiment, 14 96-well plates were populated with ES cell clones. All plates were subcultured on four plates, from which two were for freezing and two for DNA extraction. Via PCR and Southern blot analysis, it was screened for clones with a successful homologous recombination of the targeting vector. Only one positive ES cell clone was detected, number 9.45, the 45^{th} clone of the 9^{th} 96-well plate.
Picture 4.6 shows the section of the Southern blot that includes clone #9.45. The 5687 bp-sized wild type band can be seen in most of the clones. If there is no band visible, the cell clone did not grow successfully or there was not enough DNA isolated. Only for clone number 45, a part of a second band is visible which fits the size of the expected 3834 bp knockout fragment.

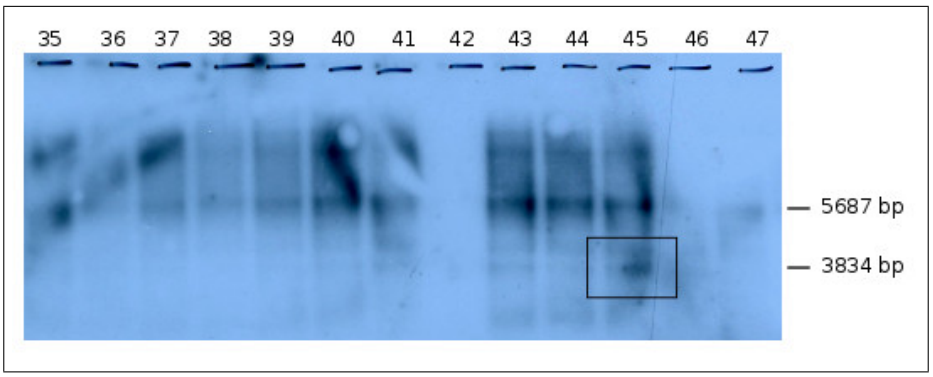

Figure 4.6 – Southern blot screening of embryonic stem cell clones Screening of embryonic stem cells was performed for each 96-well plate. The part of the autoradiograph containing clone #9.45 is pictured here. The wild type band at 5687 bp is visible in most of the clones. Only in clone #9.45 an additional band at 3834 bp is visible (framed).

Image 4.7 shows a photo of the agarose gel electrophoresis of the PCR corresponding to the first part of plate number 9. In some clones are background bands or genomic DNA visible, since the amount of template DNA was not quantified. Only for clone #9.45 a single clear band at the expected size of 2,368 bp is visible.

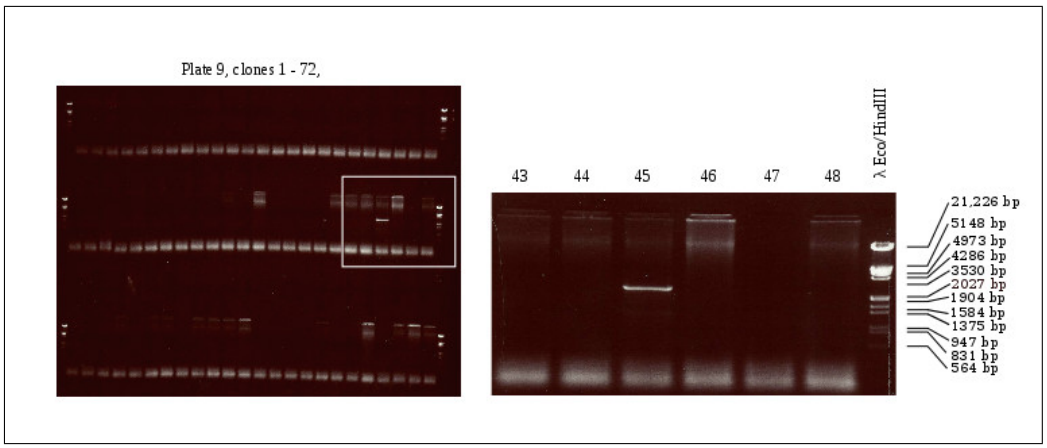

Figure 4.7 – PCR-based screening of embryonic stem cell clones #9.01 to #9.72 The electrophoresis of the ES cell genotyping PCR shows a clear band at 2,368 bp for clone #9.45.

4.3 Generation of HRP-3-deficient Mice

Clone #9.45 was expanded and its correct karyotype confirmed by karyotype analysis. Then, it was used for morula injection in C57Bl/6N morulae. The injection was performed by the Haus für experimentelle Therapie (HET) in Bonn. It resulted in the birth of two highly chimeric offspring, from which one was female and one male (see picture 4.8).
The mice were mated to C57Bl/6N wild type mice and resulting offspring was analysed for its coat colour. Brown-coloured offspring indicated successful germline competence. Black-coloured offspring originated from the C56Bl/6N morula.
While the female mouse gave birth to two brown mice, none of them heterozygous, the male fathered less then 50 % brown-coloured offspring, from which half were heterozygous and thus founded the HRP-3-deficient mouse line.

Heterozygous animals that were derived from matings of the male chimerae with C57Bl/6 females, were backcrossed with C56Bl/6 mice to breed onto a pure genetic background. Since backcrossing takes between five and 10 generations, analyses

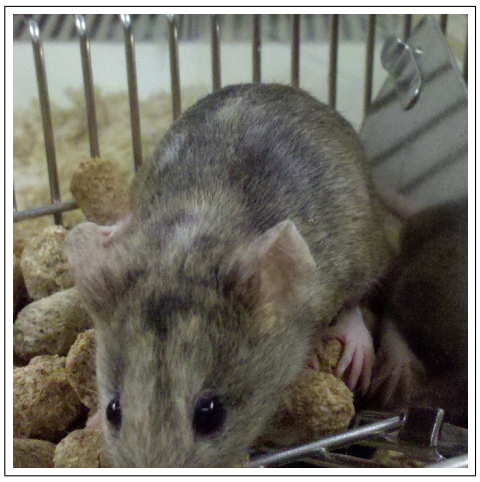

Figure 4.8 – Chimeric mouse resulting from the injection of clone #9.45. This picture shows the male chimera that resulted from the morula injection. When mated to C57Bl/6N mice, about 50 % of the litter was brown, indicating successful germline competence.

described here were carried out on a mixed background.

4.4 HRP-3-Deficient Mice are Viable and Reproductive

Litters, arisen from the breeding of heterozygous females with heterozygous males, were genotyped and showed the expected Mendelian ratio of 50 % heterozygous, 25 % wild type and 25 % knockout animals.

Homozygous knockout mice showed no conspicuous defects or deficits compared to wild types. They were viable and reproductive. The amount of litters, as well as the number of babies in the litter was comparable to wild type mice. Although some HRP-3-deficient females neglected their offspring and showed less parental care, it was not observed as a permanent condition in the breed.

Up to the age of ten months, no obvious phenotype differing from wild types was observed. It is likely that homozygous mutant mice have a normal life span, equivalent to their genetic background.

A trend was observed that knockouts were treated more aggressively by their litter mates resulting in fights and severe bites. No further fighting was seen when the knockout was removed from the cage. This trend was neither statistically analysed nor were behavioural tests performed.

4.5 HRP-3-Deficient Mice Have a White Coat Colour

HPR-3 knockout mice had mostly a white coat colour. In matings of non-white heterozygous animals, 18 of the 21 born homozygous offspring were white. Of the three non-white knockout mice, two were black and one grey, all of them fathered white as well as non-white knockout mice. No white heterozygous or wild type animal was ever born.

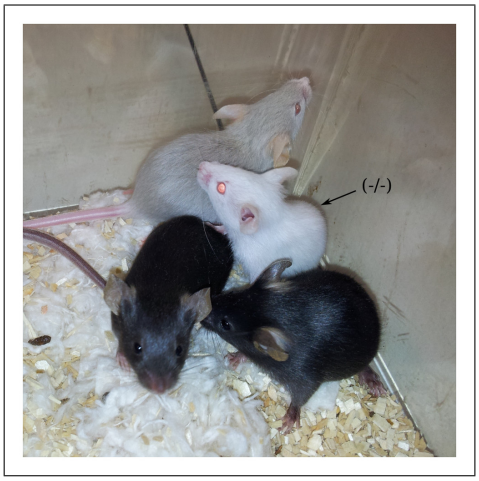

Figure 4.9 – Different coat colours in litters of the HRP-3 mouse line. This picture shows a litter derived from heterozygous parents. The white coloured mouse with red eyes is HRP-3-deficient, whereas all other coat colours indicate either an heterozygous or wild type genotype.

Image 4.9 shows a photo of a litter derived from a heterozygous mating. Mice with a variety of other coat colours were born. This included black, agouti, beige, bright grey and dark grey, showing no connection between coat colour and genotype. Only bright white animals with red eyes were shown to be HRP-3-deficient. Due to possible HRP-3-unrelated phenotypes, non-white animals were preferred for further matings.

4.6 Proof of HRP-3-Deficiency

HRP-3 expression in wild type, heterozygous and mutant mice was analysed via Western blotting at the protein level and reverse Transcription (RT)-PCR at the RNA level. HRP-3-deficient mice express an enhanced form of the green fluorescent protein (eGFP) instead of HRP-3 under the endogenous promoter. When regarding

the literature for HRP-3, the main expression is supposed to be in the brain, so this tissue was chosen for first analyses.

4.6.1 Western Blot Analysis of HRP-3, eGFP and HDGF

Western blot analysis was performed to substantiate that homozygous mice were completely deficient of HRP-3. For this, 50 µg of brain lysate of wild type, heterozygous and knockout mouse brain were loaded onto an SDS-gel. After separation, the gel was blotted on a nitrocellulose membrane and processed as described in 3.5.3. One part of the gel was incubated with anti-C-terminal HRP-3 antibody, one with an anti-eGFP antibody (ab6556) and one part with an antibody against HDGF as a loading control.

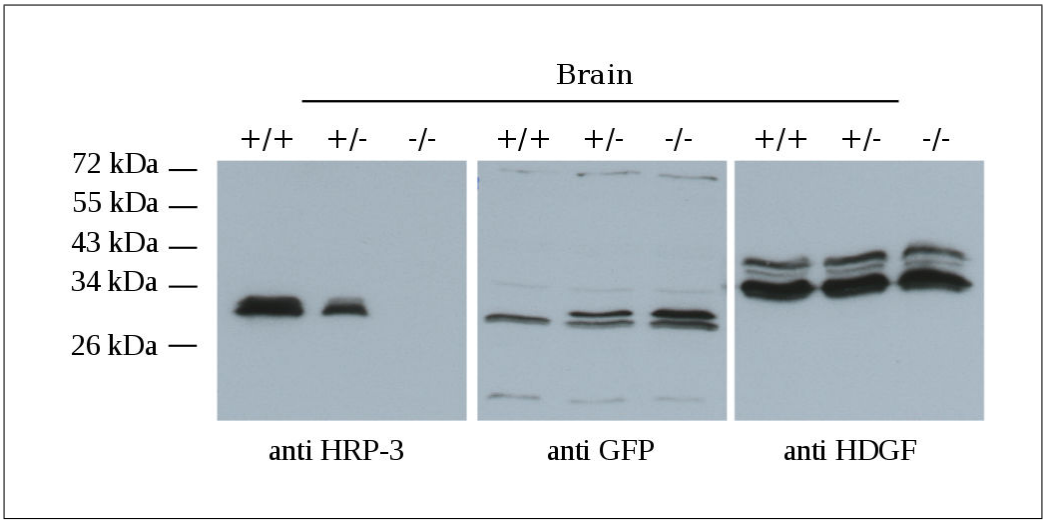

Figure 4.10 – Western blot analysis of brain lysates. Lysates of wild type, heterozygous and knockout brains were analysed regarding their HRP-3, eGFP and HDGF expression. The HRP-3 antibody detected a protein at about 30 kDa which corresponds to HRP-3. A reduced signal is detected in heterozygous mice and no signal in HRP-3 deficient mice. The GFP antibody detected a background protein band in all three genotypes at about 28 kDa and a specific protein slightly higher, which fits to the expected 31 kDa HRP-3-eGFP-fusion protein. This protein is only detected in the heterozygous and knockout brain. The HDGF antibody detected two proteins at 38 and 42 kDa, as expected, with no variation to the genotype.

Picture 4.10 shows the result of the Western blot. The HRP-3 antibody detects a protein with a size of about 30 kDa is detected. HRP-3 has a size of 23 kDa, but, due to running anomalies, runs at about 30 kDa in an SDS-gel. The signal is weaker

in the lysate of heterozygous mouse and no signal is detected in the brain lysate of the deficient animal.
Using the GFP antibody ab6556 from Abcam, a protein of about 28 kDa is visible in all lysates. Even though this antibody is affinity-purified, it shows several background bands depending on the type of tissue. Is also recognises a specific protein, which is only detected in heterozygous and knockout tissue with a size of about 30 kDa. Since the first exon of HRP-3 is still expressed, a fusion protein with a size of 31 Da is expected in mutant tissues.
The HDGF antibody detects two proteins with an apparent molecular weight of 38 kDa and 42 kDa, which do not vary in their intensity depending on the genotype.

4.6.2 Reverse Transcription PCR on Different Tissues

To evaluate whether the HRP-3-deficiency is complete, at RNA level as well as protein level, total RNA was isolated as described in 3.1.6. The following tissues were used: the brain, liver, heart and lungs, each from wild type, heterozygous and knockout animals. After reverse transcribing the RNA to cDNA, a PCR with cDNA-specific primers was performed. Wild type brain RNA was treated the same way without the reverse transcriptase, as a control for genomic DNA (-RT).
Eukaryotic elongation factor 2 (EEF2) specific primers were used to amplify an internal control gene as a reference. A product of 275 bp was expected to be amplified. As can be seen in figure 4.11, in the top panel, strong signals corresponding to the correct size were detected by agarose gel electrophoresis in all samples. The intensity of the signals are the same for every sample. Primers 2857 and 2858 were used to amplify an HRP-3 specific product of 161 bp. As evidenced in the second part of 4.11, a strong signal is detected in the brain of wild type and heterozygous mice, but not in the deficient. A very weak signal can be seen in the liver, but slightly stronger signals in heart and lungs of wild type and heterozygous mice. No signal is visible in the control without reverse transcriptase.
GFP-specific primers SF194 and SF195 amplify a 231 bp sized fragment. No signal can be seen in either the brain, liver, heart or lungs of wild type mice. Whereas a PCR product migrating at the correct size is visible in tissues of heterozygous and knockout mice. Due to different exposure times, the intensities are not comparable.

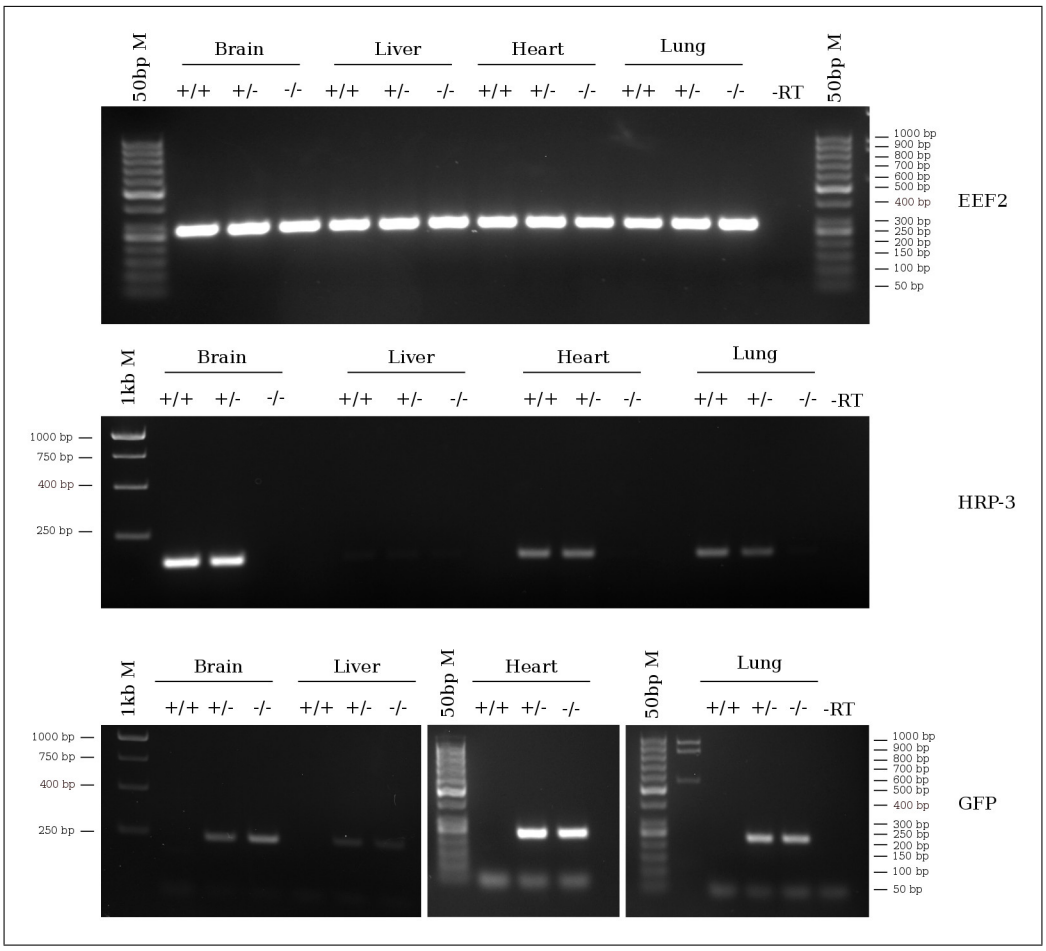

Figure 4.11 – Reverse Transcription PCR on cDNA derived from the brain, liver, heart and lungs. To analyse the HRP-3-deficiency at the RNA level, total RNA was isolated from the brain, liver, heart and lungs. After transcription in cDNA, a PCR with gene-specific primers was performed. The products were separated via agarose gel electrophoresis. PCR products of the expected sizes, 275 bp for EEF2, 161 bp for HRP-3 and 231 bp for GFP, are visible. M stands for marker, -RT designates the control without reverse transcriptase.

4.6.3 Immunohistochemistry of the Brain

Expression of HRP-3

Paraffin sections of adult HRP-3 wild type and mutant brain were stained for HRP-3 for further affirmation. As Heba El-Tahir described in her doctoral thesis (Eltahir [2009]), HRP-3 is expressed strongly in several regions of the brain. HRP-3-deficient tissue will allow a confirmation of the specificity of the staining. Four different regions of the brain were analysed: the olfactory bulb (figure 4.12), the cortex (figure 4.13), the hippocampus (figure 4.14) and the cerebellum (figure 4.15).

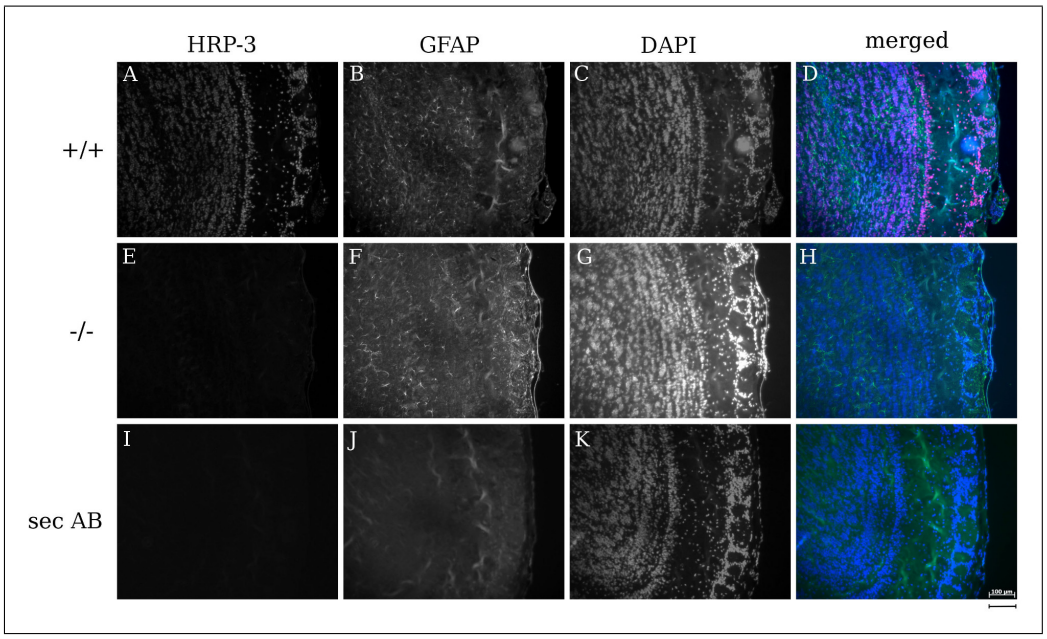

Figure 4.12 – Immunohistochemistry of the olfactory bulb. Paraffin sections of wild type (+/+) and knockout (-/-) olfactory bulbs were stained using the antibodies rabbit anti HRP-3 (A and E, red in merged pictures) and mouse anti GFAP (B and F, green in merged pictures). Nuclei were stained with DAPI (C, G, K, blue in merged pictures). Goat anti rabbit C3 and alexa 488 goat anti mouse, respectively, were used as secondary antibodies. For the secondary antibody control, paraffin sections were not incubated with a primary antibody (I and J). The scale bar designates 100 µm.

Figure 4.12 shows 4 µm thick paraffin sections that were stained for HRP-3 and glial fibrillary acidic protein (GFAP), an intermediate filament protein, expressed in astrocytes, whose up- or downregulation is a marker for neurodegeneration or astrogliosis. A nuclear staining can be detected with the HRP-3 antibody in wild type olfactory bulbs (A), but not in knockout (E) or in the secondary antibody

control (I), where only a diffuse background is visible. From the inside to the outside, expression of HRP-3 can be matched to granular cells of the olfactory bulb, the mitral cell layer that surrounds them, and cells within the glomerular layer. GFAP staining of wild type and knockout tissue did not show any differences (B, F).

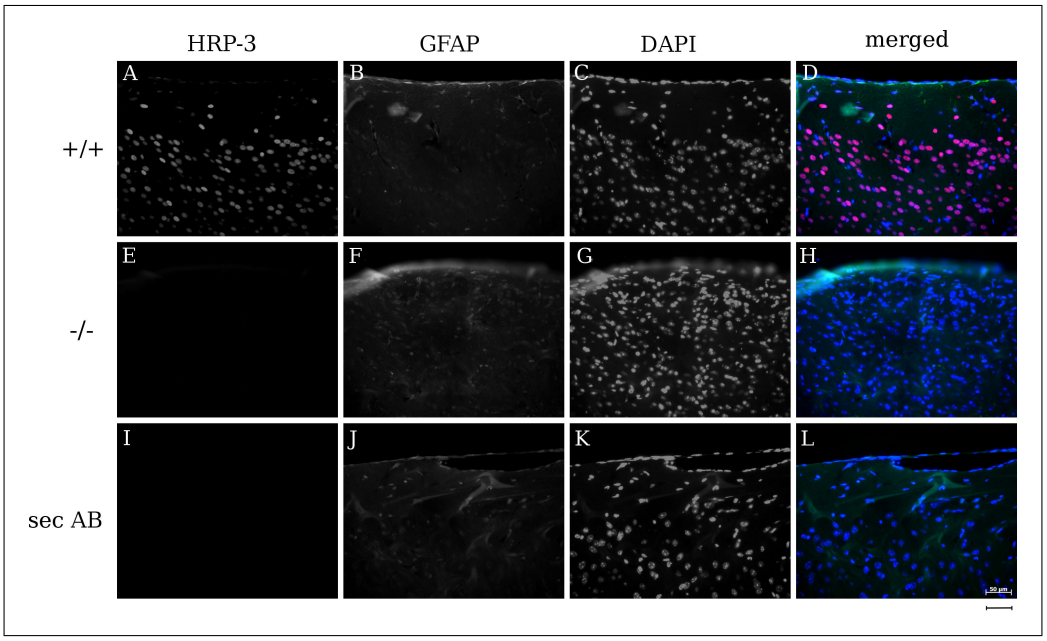

Figure 4.13 – Immunohistochemistry of the cerebral cortex. The cerebral cortex above the hippocampus of wild type and knockout mice was analysed for HRP-3 expression via immunohistochemistry. A GFAP co-staining was performed to check for astrogliosis. Images A and E show the signal detected with rabbit anti HRP-3 antibody and goat anti rabbit C3 secondary antibody. The secondary antibody control was performed without a primary antibody (I and J). Images B and F show the signal that was detected with goat anti mouse GFAP and alexa 488 goat anti mouse secondary antibody. Nuclei were stained with DAPI (C, G and K) and D, H and L show the merged results with HRP-3 in red, GFAP in green and DAPI in blue. The scale bar designates 50 µm.

Paraffin sections of the brain, more specifically the cerebral cortex, stained against HRP-3 and GFAP, are shown in figure 4.13. The antibody against HRP-3 detects nuclear signals in the cerebral cortex of wild type mice (A), but neither in knockout mice (E) nor in the secondary antibody control (I). As described in El-Tahir et al. [2006], the nuclear signal is found in to cells in layer II and III of the cerebral cortex. No abnormal GFAP staining is detectable in knockout cortices.

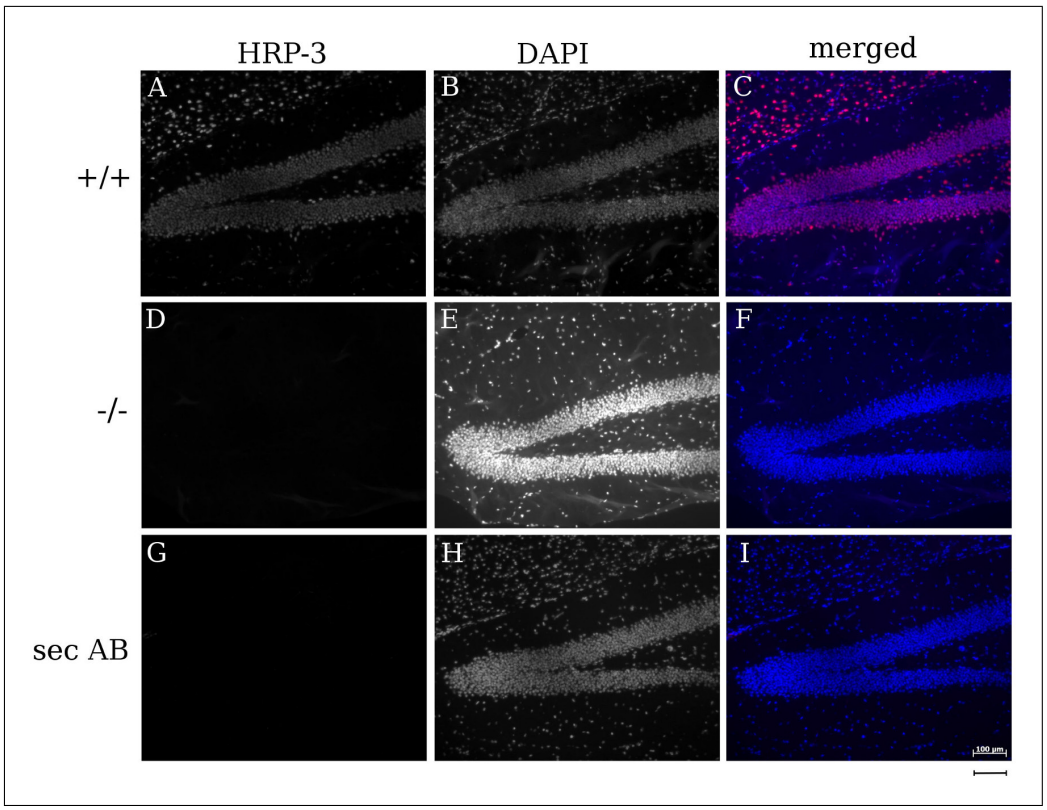

Figure 4.14 – Immunohistochemistry of the hippocampus Wild type and knockout brains were stained using an HRP-3 antibody and the hippocampi were analysed. Images A and D show the HRP-3 staining for wild type and knockout, image G the corresponding secondary antibody control without primary antibody and goat anti C3 as a secondary antibody. Nuclei are stained with DAPI (pictures B, E and H) and merged images with HRP-3 signals in red are presented in C, F and I. The scale bar designates 50 µm.

An HRP-3 antibody has been used to detect HRP-3 expression in the hippocampus. Picture 4.14 shows a dominant nuclear HRP-3 signal in the granule cells of the dentate gyrus of wild type brain. No signals were detectable in the knockout brain or the secondary antibody control.

Paraffin sections of wild type and knockout brain, more specifically the cerebellum, were stained with an HRP-3 and β-III-tubulin antibody, depicted in 4.15. HRP-3 staining in wild type cerebellum shows a strong nuclear signal in the Purkinje cells (cell bodies and neurites are positive for β-III-tubulin). Scattered cells in the molecular layer of the cerebellum also show a strong signal for HRP-3. Surprisingly, there is a weak but consistent expression of HRP-3 in granule cells of the nuclear

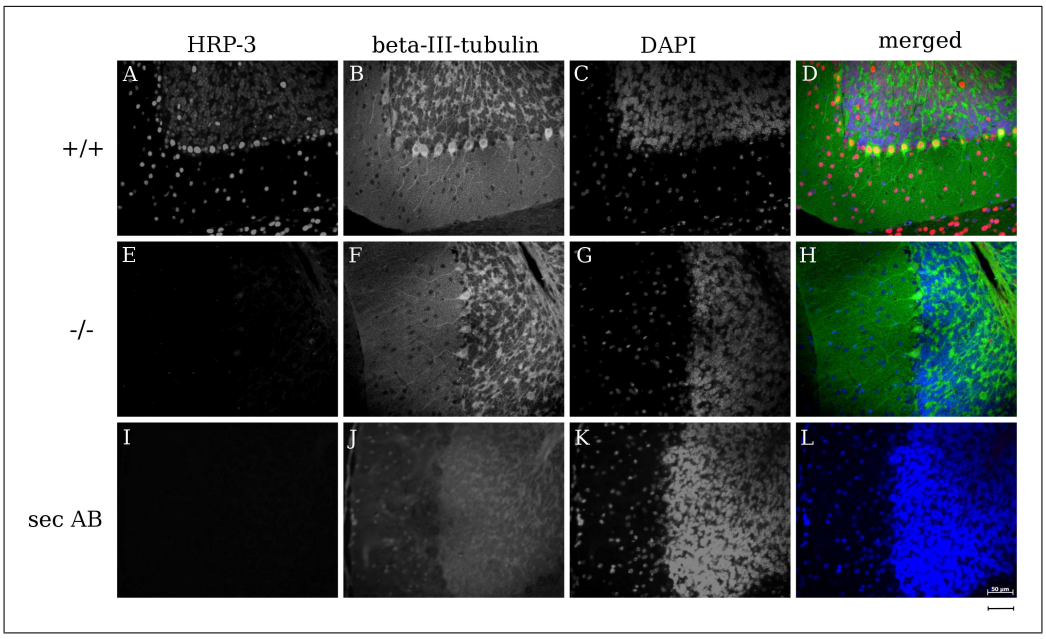

Figure 4.15 – Immunohistochemistry of the cerebellum. Goat anti rabbit HRP-3 and goat anti mouse β-III-tubulin antibodies were used to detect expression in the cerebellum of wild type and knockout mice. Goat anti rabbit C3 and alexa 488 goat anti mouse were used as secondary antibodies. Images A and E show HRP-3 expression in wild type and knockout cerebellum, images B and F show β-III-tubulin expression. Nuclei are stained with DAPI (C, G, K) and D, H and L show the merged images with HRP-3 in red and β-III-tubulin in green. The scale bar designates 50 µm.

layer. According to El-Tahir et al. [2006], granule cells of the cerebellum - in contrast to granule cells of the hippocampus and olfactory bulb - are negative for HRP-3. No signal is detectable in in granule cells of knockout mice nor in the secondary antibody control.
β-III-tubulin staining of the cerebellum does not reveal any anomalies in knockout mice. The appearance of Purkinje does not differ from wild type Purkinje cells.

Lesion in the Cerebral Cortex

Due to time constraints, only a limited supply of animals older than six months was available for the analyses that were performed here. In one individual case, a six-month-old knockout and a respective wild type mouse were analysed via immunohistochemistry and cortical lesions were detected in the knockout animal. Figure 4.16 shows paraffin sections of the cerebral cortex of wild type (A and B) and knock-

out animals (C and D) in different magnifications. The cortex is visibly thinner in HRP-3-deficient animals than in the wild type control and a loss of the distinctive lamination is detectable. Furthermore, a major proliferation of microvessels within the lesions is visible.

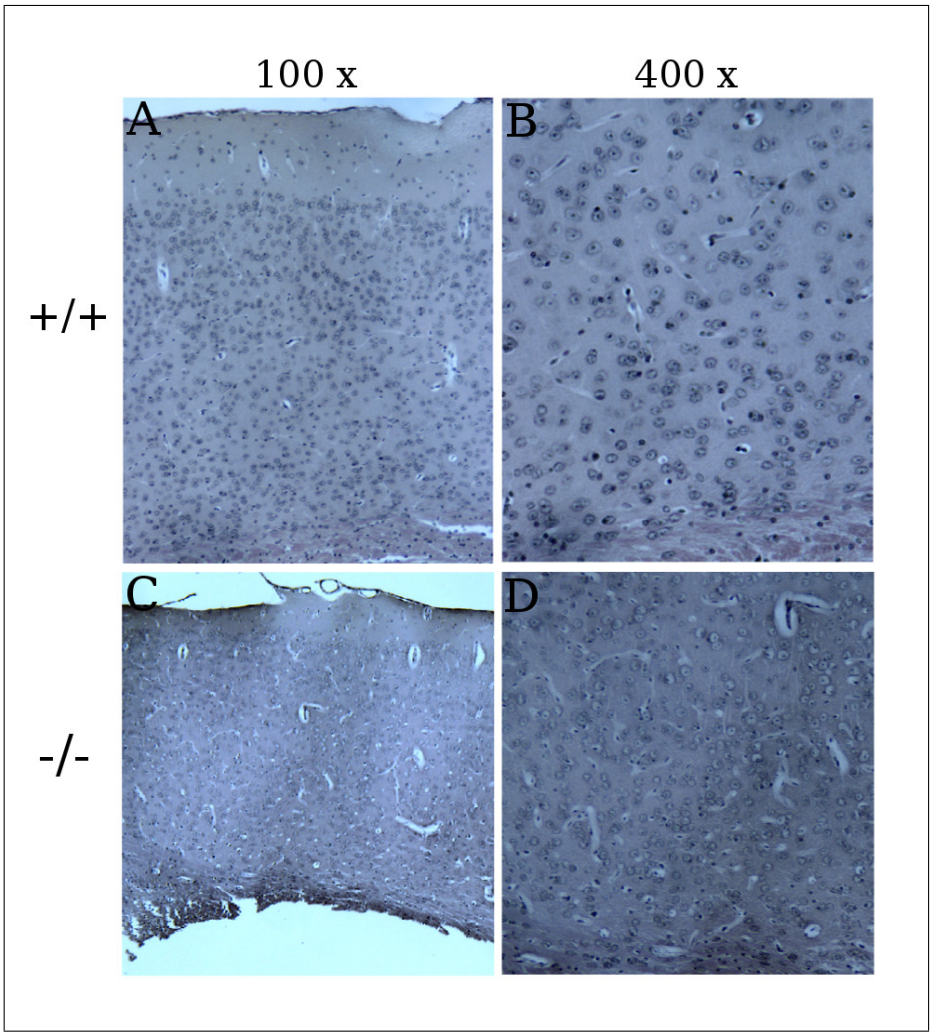

Figure 4.16 – **Lesions in the cerebral cortex** Paraffin sections of brains from wild type and knockout mice were stained for HRP-3 and nuclei counterstained with hematoxylin. Images A and B show the cerebal cortices of wild type mice in different magnifications, images C and D the cortices of knockout mice. The cortex of HRP-3-deficient brains is visibly thinner, cortical laminas are indistinct and a higher amount of microvessels is visible. Data produced by Prof. Hartmann, Institut für Anatomie, Bonn

Paraffin sections of the same area were stained for GFAP. Images of this staining are depicted in figure 4.17. Activated astrocytes indicating an astrogliosis were

detectable in the knockout but not in the wild type brain.

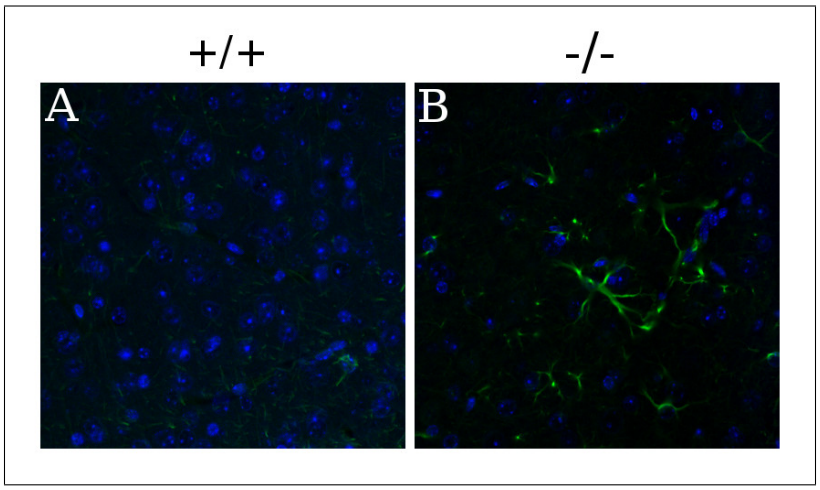

Figure 4.17 – GFAP staining of the lesion in a cerebral cortex. Paraffin sections of wild type and knockout mouse brains were stained for GFAP (green). Nuclei were counterstained with DAPI (blue). Image A depicts the staining in the cerebral cortex of a wild type mouse, image B in the knockout mouse. Activated astrocytes are clearly visible in B.

Expression of eGFP in Knockout Mice

To confirm the expression of the eGFP reporter gene in HRP-3 deficient tissue, paraffin sections of the brain were stained against eGFP. Surprisingly, although multiple GFP antibodies and antigen retrievals were tested, expression of GFP was only marginally detectable. The only partially successful method used a mouse anti GFP antibody from Roche, after antigene retrieval with 10 mM sodium citrate with prolonged incubation with the BioGenex supersensitive link-label IHC kit. This led to very weak but detectable signals. As positive control, paraffin sections of the brain of 8-days-old pax-2-deficient mice (kindly provided by Sabine Topka, Institut für Anatomie, Bonn) were used, which expressed GFP under the pax-2 promoter. While the development of pax-2-sections with 3,3'-Diaminobenzidine tetrahydrochloride hydrate (DAB) was stopped after two minutes, the development of HRP-3-sections was stopped after fifteen minutes as no further enhancement of the signal took place. This included negative controls.
Brightfield pictures of wild type and knockout brain were taken at the same time to ensure equal exposure and image processing (see picture 4.18, A). Contrast and brightness were enhanced using GNU Image Manipulation Program (GIMP). The

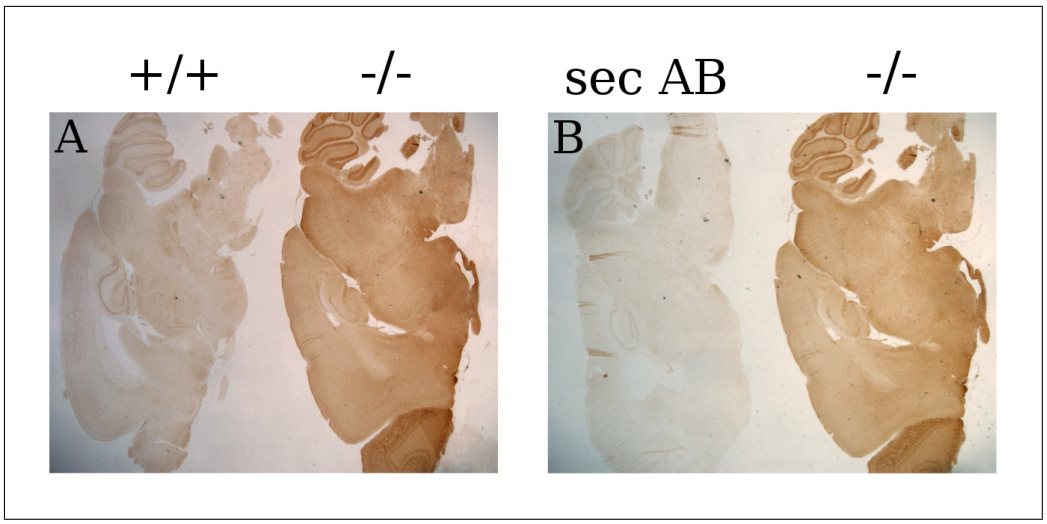

Figure 4.18 – Immunohistochemistry of the brain. Immunohistochemistry was performed on paraffin sections of wild type and knockout brains. A mouse anti GFP primary antibody was detected with the BioGenex Super Sensitive Link-Label kit and the reaction was developed with DAB for fifteen minutes. Pictures of wild type and knockout brain (A) and secondary antibody control and knock out brain (B) were taken together to ensure identical exposure time and image processing. Contrast and brightness were optimised using the GIMP software.

secondary antibody control and the knockout brain were photographed together as well (4.18, B). The wild type brain, as well as the secondary antibody control, do show a weak background staining, with many structures of the brain being clearly visible (e.g. the hippocampus, the cerebellum). In total, the knockout brain sections have a darker colour and more specific signals. Some structures of the brain, such as the olfactory bulb and the cerebellum, show a darker staining than the rest of the brain. This does fit to HRP-3 expression data in the olfactory bulb and the cerebellum.

Image 4.20 shows an overview of the complete sections and detailed photos of the cerebellum and the olfactory bulb of wild type and knockout mice in different magnifications. It is obvious that the entirety of the brain is stained much darker than the wild type control or the secondary antibody control. But when analysed microscopically, almost no clearly positive structures or single cells can be seen. Single cells are only stained weakly and a co-staining with hematoxylin makes it impossible to detect the brown signal. No stained neurites were found. The wild type and the secondary antibody control show a weak background staining of Purkinje cells

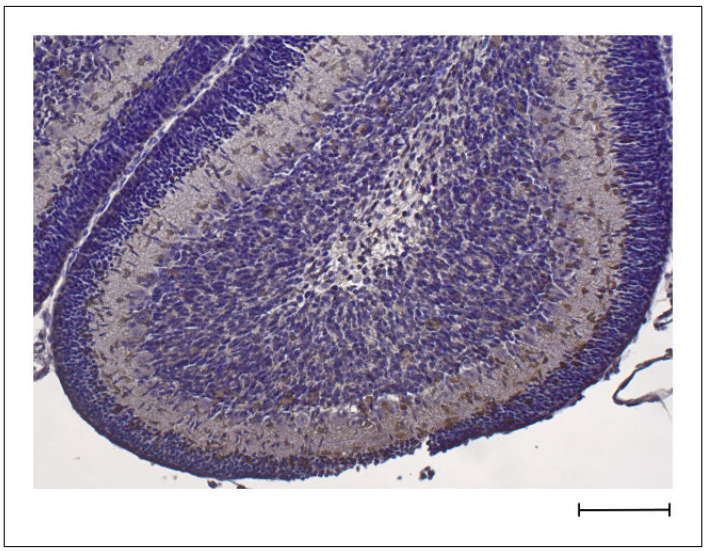

Figure 4.19 – Immunohistochemistry of the cerebellum of pax-2 mice. Paraffin sections of brains from pax-2 mice were stained together with HRP-3-deficient mice as a positive control. After 2 minutes of incubation with DAB substrate, a strong dark brown staining was visible. Sections were counterstained with hematoxylin for a better structural overview. The scale bar depicts 100 µm.

in the cerebellum (best visible in magnifications B and F). No staining of granule cells can be detected in these negative controls, but granule cells are positive for eGFP expression in knockout brain (D1 and D2). Also, in the olfactory bulb of wild type mice and the secondary antibody control, background staining can be detected (magnifications A and E). But eGFP staining of the knockout olfactory bulb shows a signal that fits to the HRP-3 staining in wild type (see image 4.12, A). The granular cells, the mitral cell layer and cells in the glomerular layer are stained darker than the respective controls.

Overall, the signal is very weak and seems to be diffuse. Magnifications of the cortex and the hippocampus are not shown due to the bad signal-to-noise ratio in the magnifications.

On the other hand, the GFP positive control (picture 4.19) shows a strong dark brown signal in the developing P8 cerebellum which relates to pax-2 positive interneurons. The GFP staining protocol can therefore be declared as successful. However, the question, why GFP expression in HRP-3-deficient mice is so weak, remains.

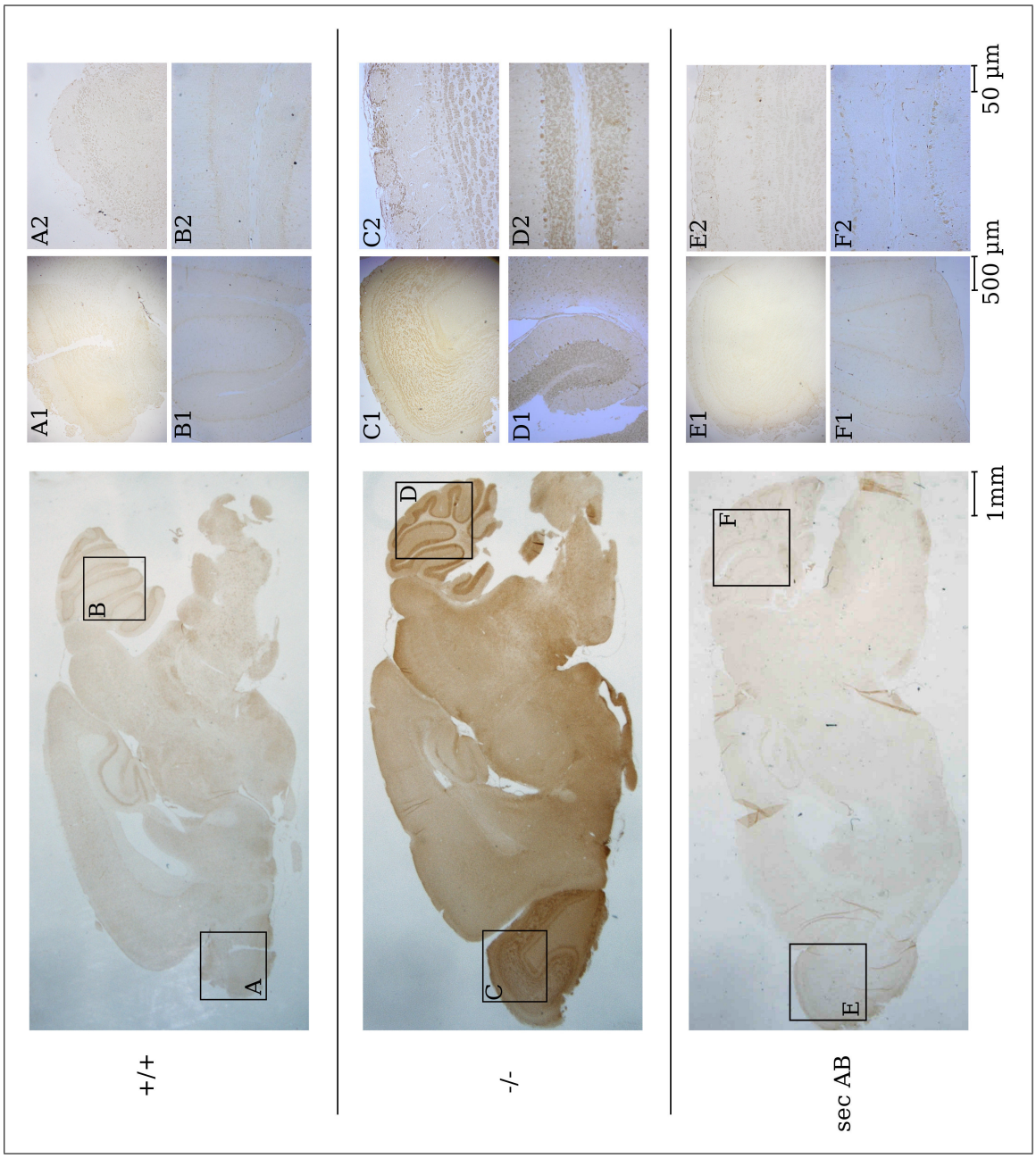

Figure 4.20 – **Immunohistochemistry of the brain** An overview over the complete brains of wild type and heterozygous mice, as well as the secondary antibody control, stained against GFP, are shown here. Different magnifications of the olfactory bulb (A1, C1 and E1 are 200 times magnified, A2, C2 and E2 are 400 times magnified) and the cerebellum (B1, D1 and F1 are 200 times magnified, B2, D2, and F2 are 400 times magnified) are depicted on the right.

4.7 Verification of the Reporter Gene

4.7.1 Native eGFP Fluorescence

Since immunohistochemistry of eGFP was not satisfying, the native eGFP expression was analysed in collaboration with Prof. Wolfgang Voos of the Institut für Biochemie und Molekularbiologie. A Fujifilm FLA-5100 fluorescent image analyser was used to verify reporter gene expression. Therefore, a wild type and a heterozygous mouse, each two-weeks-old, were euthanised and the brains isolated quickly. They were placed in ice-cold PBS and directly scanned on the fluorescence scanner from above and below. Then, the hemispheres were cut to attain a sagittal scan. An excitation at 495 nm and an emission at 519 nm was used together with the filter LPB.

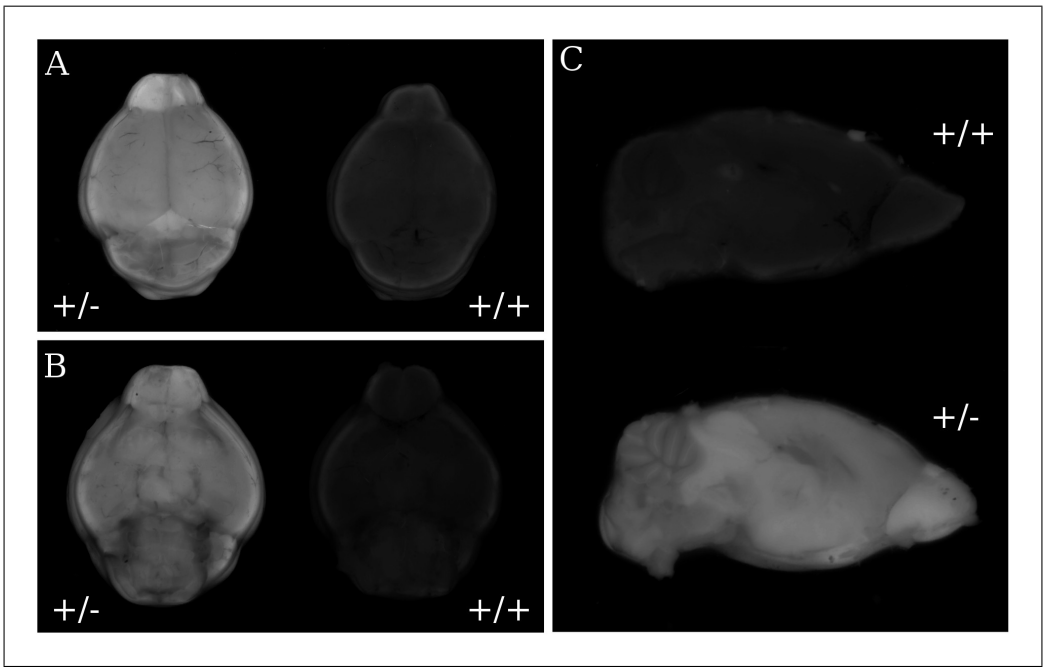

Figure 4.21 – eGFP-fluorescence of an HRP-3 heterozygous brain. An HRP-3 wild type and heterozygous brain from two-weeks-old mice were scanned using the Fujifilm FLA-5100 fluorescence imager. (A) shows the brains from above and (B) from below. Afterwards, they were cut for a sagittal scan, shown in (C).

Picture 4.21 shows the result of the fluorescent imager. In (A), the brains are scanned from above. The heterozygous brain shows a clear fluorescence signal, whereas the

wild type brain is only visible through background fluorescence. The olfactory bulb shows a stronger signal than the rest of the brain. (B) shows the brains scanned from the bottom. The same pattern is visible here, only background for the wild type brain, but a visible fluorescence for the heterozygous brain. In (C), the hemispheres were cut apart to get a sagittal view into the brain. The cerebellum is clearly visible showing a signal in the grey matter, whereas the white matter remains dark. The olfactory bulb again shows a stronger signal than the rest of the brain.

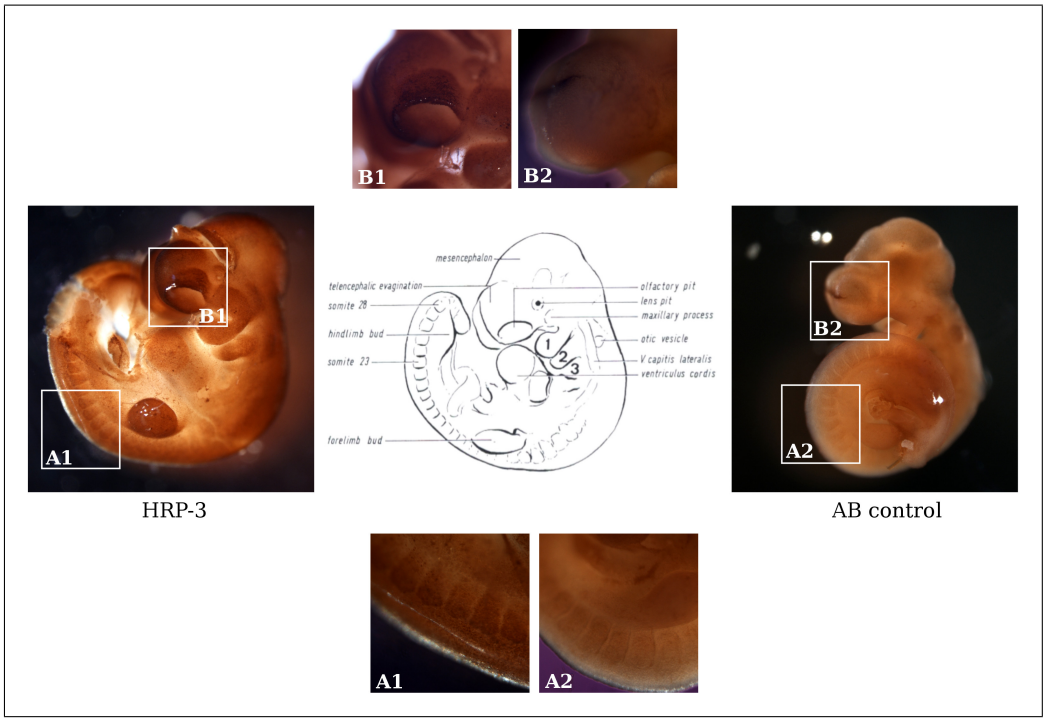

Figure 4.22 – Whole mount HRP-3-staining of wild type embryos E11.5 Wild type embryos were fixed with PFA, and stained uncut against HRP-3. The secondary antibody control on the right shows a minimal background staining, whereas in the HRP-3 stained embryo, many structures are clearly positive. Among them, the developing olfactory pit (compare pictures B1 and B2), extremities and the somites (compare pictures A1 and A2). Other features, e.g. the developing heart, show a weaker signal.

4.8 Expression during Embryonic Development

A whole mount staining of E.11.5 wild type embryos was performed to analyse the HRP-3 expression during embryonic development. The procedure is described in

3.6.3. Pictures were taken with a binocular and are shown in 4.22. The HRP-3-stained embryo is depicted on the left, the secondary antibody control on the right. Many features are clearly stained for HRP-3. The nasal placode, more specifically the developing olfactory pit, depicted in B1, shows a clear, dark staining at the rim. The developing extremities, e.g. the forelimb bud and the hindlimb bud, as well as the branchial archs (1 and 2) show a strong signal. In the enlargement A1, staining of the somites is visibly stronger than the background of the secondary antibody control. The developing heart (ventriculus cordis) is slightly stained.
EGFP expression of heterozygous embryos was analysed with a GFP binocular in cooperation with Dr. Bernhard Fuss from the Department of Molecular Developmental Biology. Some features of the embryo are prominently positive for eGFP, as for example the extremities and the ear placode. Less structures can be identified as in the whole mount staining.

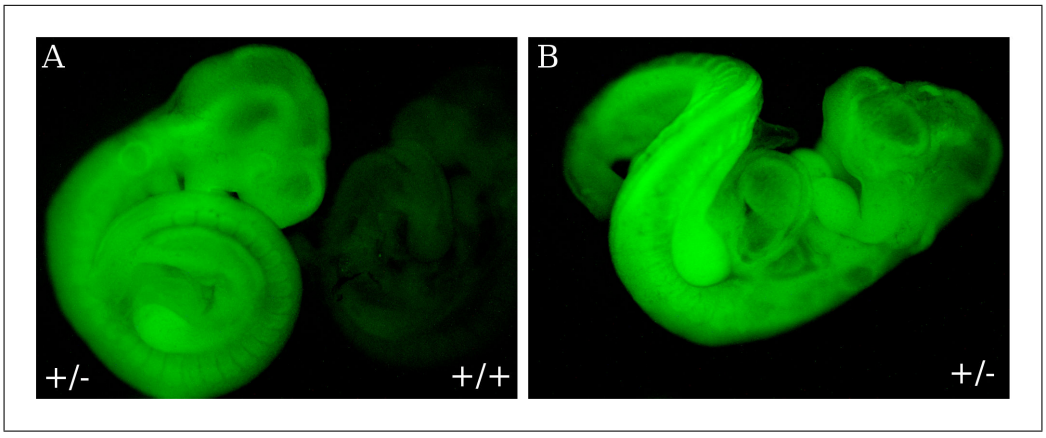

Figure 4.23 – Native eGFP fluorescence of HRP-3 heterozygous embryos. E10.5 embryos were extracted and placed on ice-cold PBS for the analysis with a fluorescent binocular. Picture A shows an heterozygous and a wild type embryo. Picture B the heterozygous embryo from a different angle.

4.9 HRP-3 Expression in Other Tissues than the Brain

4.9.1 Western Blot Analysis of Different Tissues

Reverse transcription of wild type RNA showed weak signals for different tissues than the brain, namely, liver, heart and lung (see image 4.11). Also, HRP-3 expression during embryonic development gave signals other than those present in the brain (see image 4.22). Furthermore, it has been shown that HRP-3 is expressed in granule cells of the cerebellum, which has been confirmed by a deficiency of that staining in knockout cerebellum. Western blot analysis of all major organs of an adult mouse was thus performed to check for expression in a wide variety of tissues.

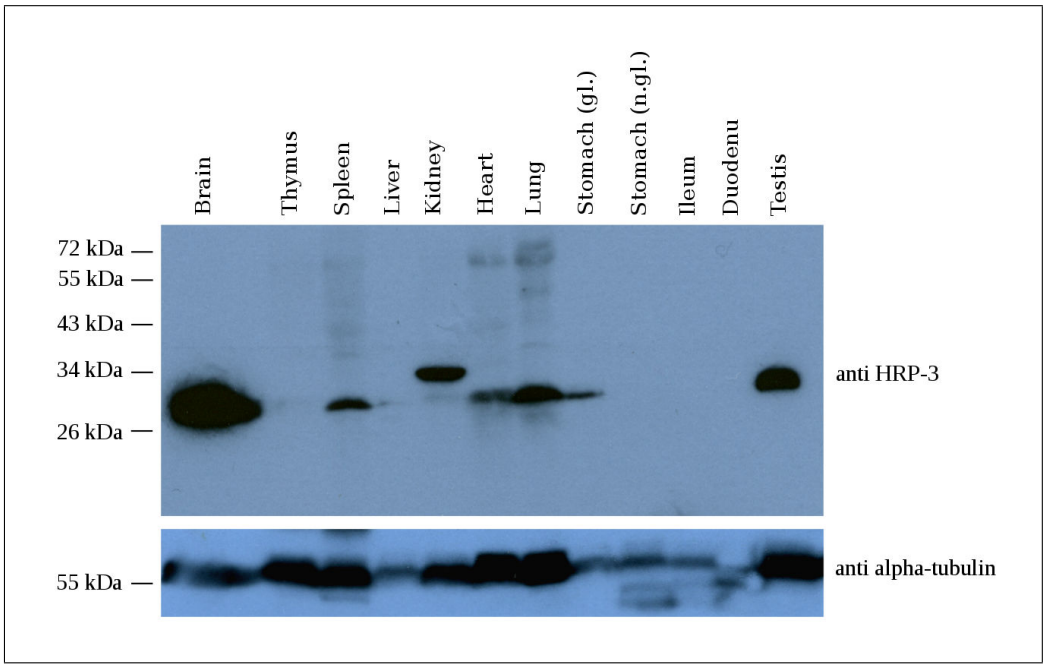

Figure 4.24 – Western blot analysis of HRP-3 in tissues of an adult wild type mouse. A six-month-old wild type mouse was dissected, its organs shock frosted in liquid nitrogen, and prepared for Western blot analysis. 100 µg of protein were loaded onto an SDS-gel, separated and blotted onto nitrocellulose membrane. The membrane was incubated with rabbit anti HRP-3 as a primary antibody and peroxidase coupled goat anti rabbit as a secondary antibody. Mouse anti α-tubulin was used as a loading control.

The western blot analysis depicted in figure 4.24 presents the expression of HRP-3 in tissues of a six-month-old male C57Bl/6N mouse. By far the strongest signal at the size of about 30 kDa can be seen in the brain. Due to running anomalies, HRP-3 has an apparent molecular weight of about 30 kDa in SDS-Page. The second highest expression level can be observed in testis. Medium expression levels can be detected in spleen, lung and the heart. Weak signals can be detected in thymus and liver. Surprisingly, HRP-3 is expressed in the glandular part of the stomach, but not in the non glandular part, or in other parts of the digestive system. Furthermore, the kidney is the only tissue in which a clear signal at 34 kDa is visible. α-tubulin was used as an internal marker on the same gel, showing that every sample contained protein. The tubulin signal in the liver is quite weak, an higher amount of protein might have led an higher HRP-3 expression level.
Due to the expression data that were shown in Western blot analysis, selected organs were also analysed via immunohistochemistry to confirm these results and to analyse the expression on the cellular level. The heart, kidney and stomach were chosen for that analysis and results are presented in the following section.

4.9.2 The Heart

Image 4.25 shows 4 µm thick paraffin sections of the heart of wild type and knockout mice. Wild type sections were also used as a secondary antibody control. Images A, D and G show the signals arising from the primary rabbit anti HRP-3 antibody that was detected with a secondary goat anti rabbit C3 antibody. In images B, E and H the nuclei are stained with DAPI. Merged images are depicted in C, F and I. A signal for HRP-3 that colocalises with DAPI can be detected in wild type hearts (A), but not in knockout (D) or the secondary antibody control (G). The nuclear signal can be accounted to the nuclei of the heart muscle cells. Cross striations of the muscle cells are clearly visible.
A diffuse background autofluorescence is observed in knockout and secondary antibody control. Furthermore, fluorescent erythrocytes can be seen in wild type,

knockout and antibody control.

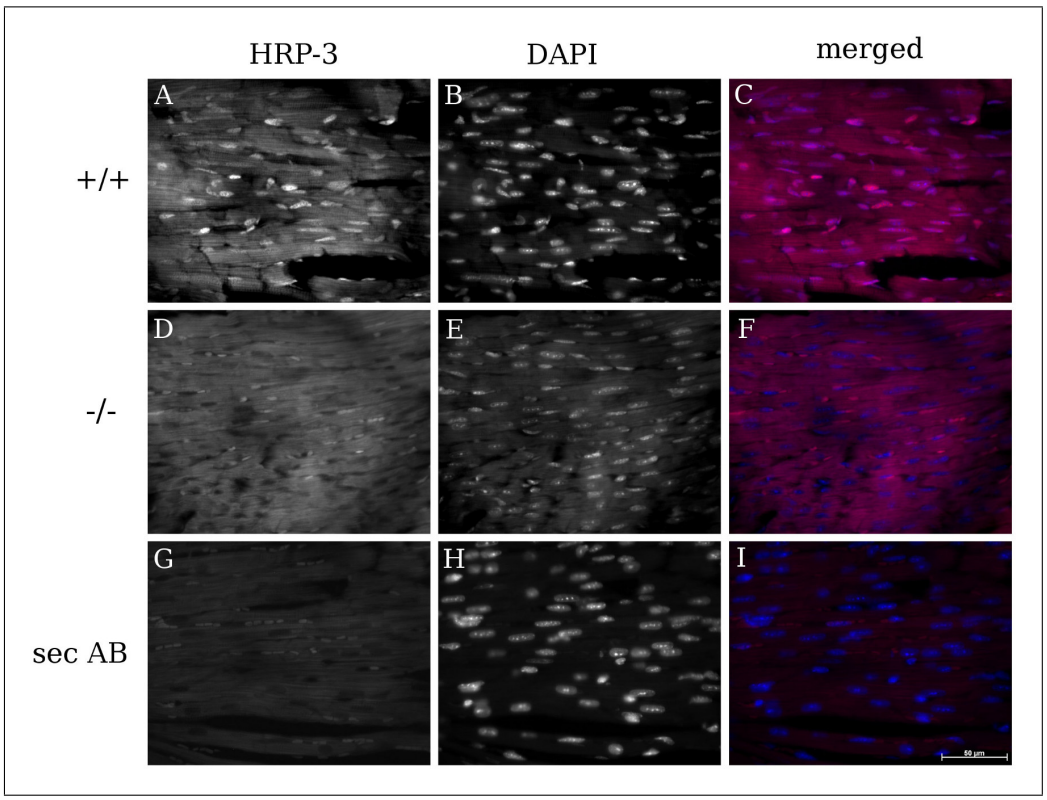

Figure 4.25 – Immunohistochemistry of the heart Paraffin sections of hearts from wild type and knockout mice were sectioned and stained using the rabbit anti HRP-3 antibody. Fluorescent goat anti rabbit C3 was used as a secondary antibody. Secondary antibody control was not incubated with a primary antibody. Nuclei were counterstained with DAPI. The scale bar designates 50 µm.

4.9.3 The Kidney

Image 4.26 depicts the immunohistological staining of paraffin sections of the kidney from wild type and knockout mice. Wild type kidney was also used as a secondary antibody control. The primary rabbit anti HRP-3 antibody was detected with a biotinylated goat anti rabbit secondary antibody. Development of the chromogenic signal was performed as described in 3.6.2 with the Vectastain ABC kit. Different magnifications, 200 times and 400 times, are shown. Nuclei were stained with hema-

toxilin and show a clear blue colour.
The glomeruli, round structures with cells inside, were photographed in all images. They perform the first filtering step from blood to urine in the kidney. In wild type kidneys, these glomeruli contain nuclei that are positive for HRP-3 (images A and D), most likely the podocytes. The same nuclei do not show a signal in knockout sections or in the secondary antibody control. Structures around the glomeruli, the renale tubules, show a strong brown background staining in wild type, knockout and secondary antibody control.

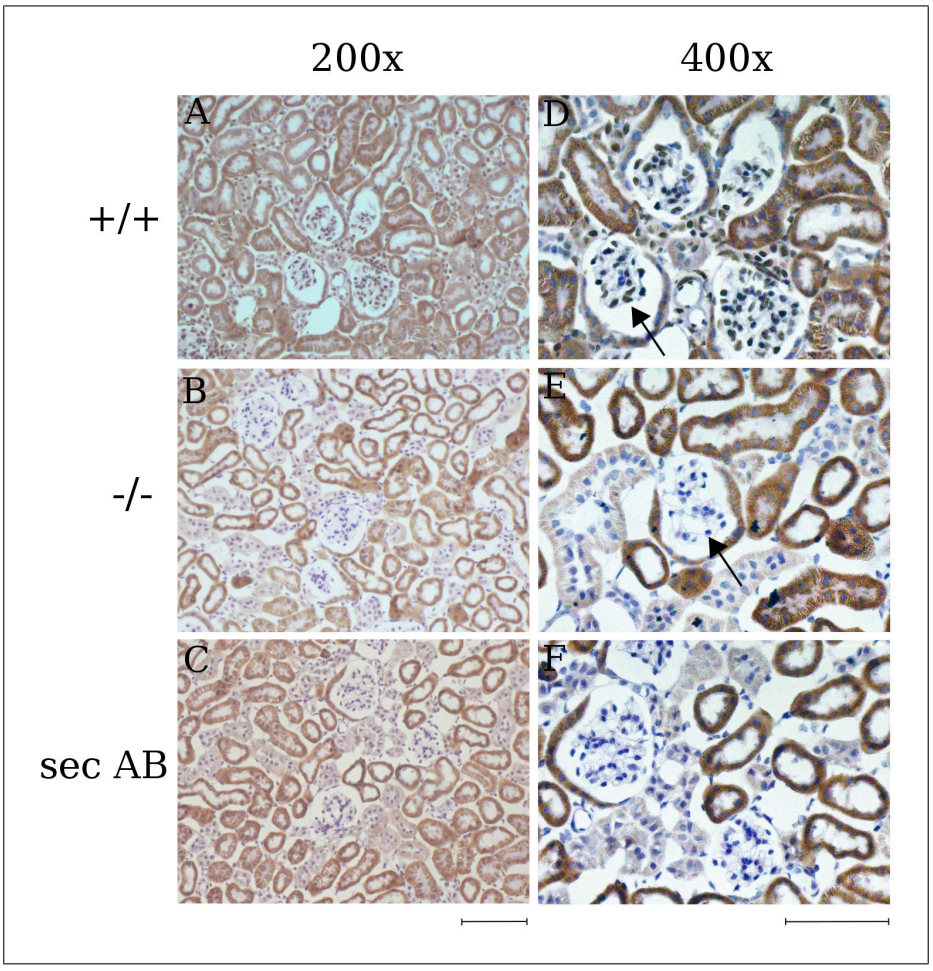

Figure 4.26 – Immunohistochemistry of the kidney Paraffin sections of wild type (A and D) and knockout (B and E) kidney were stained with a rabbit anti HRP-3 antibody. The primary antibody was detected with a biotinylated secondary, followed detection with the ABC kit from Vectastain as described in section 3.6.2. Sections from images C and F were not incubated with a primary antibody. Nuclei in all sections were counterstained with hematoxilin. The scale bars mark 50 µm.

4.9.4 The Stomach

An unusual observation was made in the stomach of HRP-3-deficient mice. A hyperplasia of the stomach's mucosa and submucosa led to the development of strong foldings in the non-glandular part of the stomach. No other pathological abnormalities were detected. Occurrence of these foldings was not age related.

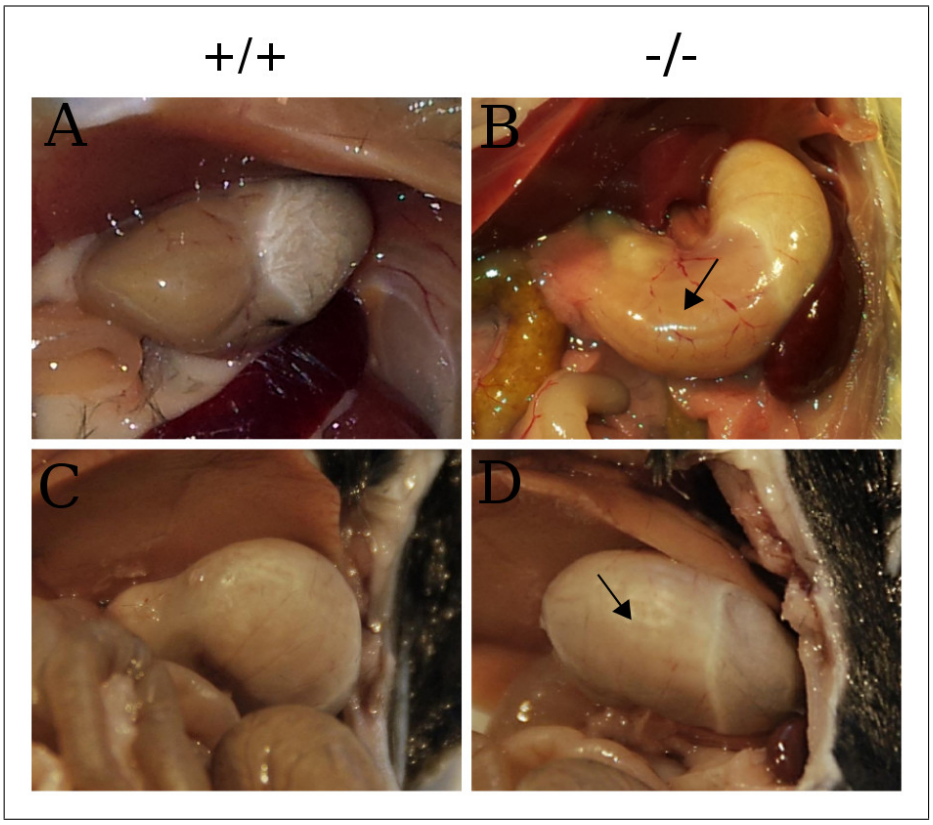

Figure 4.27 – Hyperplasia of stomach foldings. Images of wild type (A and C) and knockout (B and D) mice stomachs were taken. A and B are from unperfused six-month-old animals, while C and D were taken from nine-month-old animals after intracardial perfusion with 4 % PFA. Arrows mark the unusual foldings that can be seen from the outside. Images C and D were taken by Prof. Hartmann, Institut für Anatomie, Bonn

Figures 4.27 and 4.28 show examples of these stomach foldings. Photos in figure 4.27, A and C were taken of stomachs of wild type mice, B and D of the corresponding knockouts. Arrows mark the areas where the horizontal foldings can be seen clearly. Figure 4.28 shows stomachs from four other mice, cut open and emptied. While the inside of wild type mice stomachs is relatively smooth, distinct foldings

and more tissue can be detected in the respective knockouts.

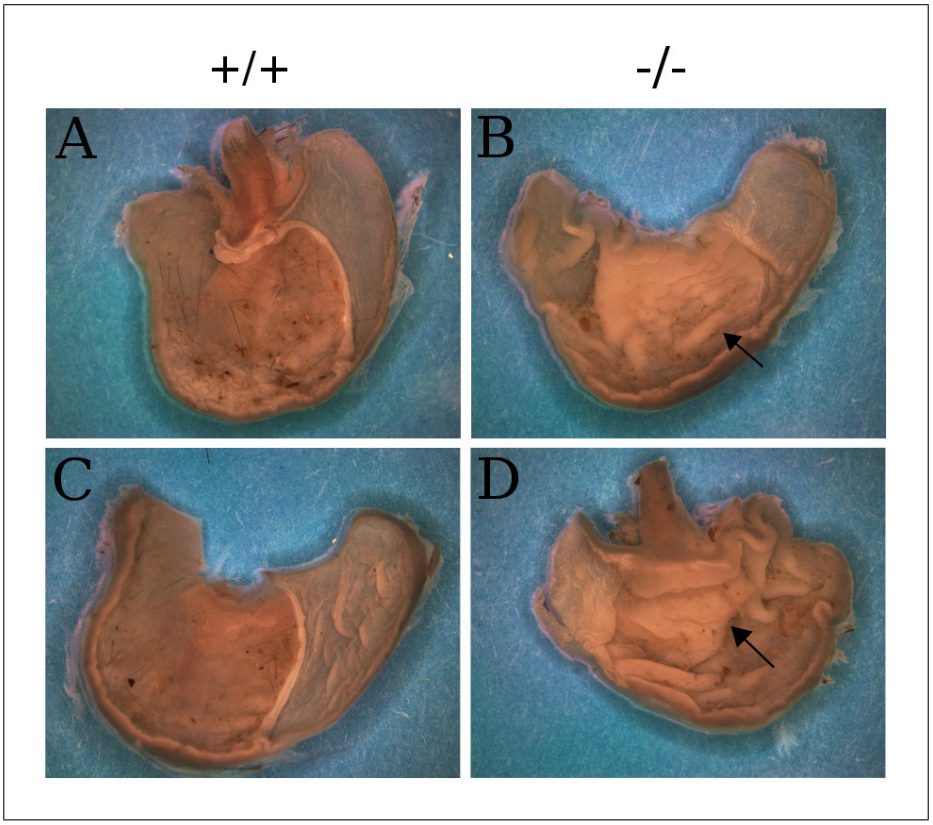

Figure 4.28 – Hyperplasia of stomach foldings. Images of wild type (A and C) and knockout (B and D) mice stomachs were taken. Stomachs were dissected from nine-month-old mice, cut open and their contents flushed out. Foldings are marked with arrows. Images were taken by Prof. Hartmann, Institut für Anatomie, Bonn.

Figure 4.29 shows a histological staining of stomachs of wild type and HRP-3-deficient mice. HRP-3 expression in the stomach of the wild type mouse is clearly nuclear in several types of cells, which can be attributed to parietal cells, chief cells and cells located beneath the mucous neck cells. Additionally, parietal cells show a weak cytosolic signal (4.29, A). No clear staining is detectable in the knockout (B) nor in the secondary antibody control (C). An abnormal cellular distribution was detected in a stomach of another HRP-3-deficient mouse (D). Parietal cells are localised in the fundus of the stomach, where normally chief cells are located.

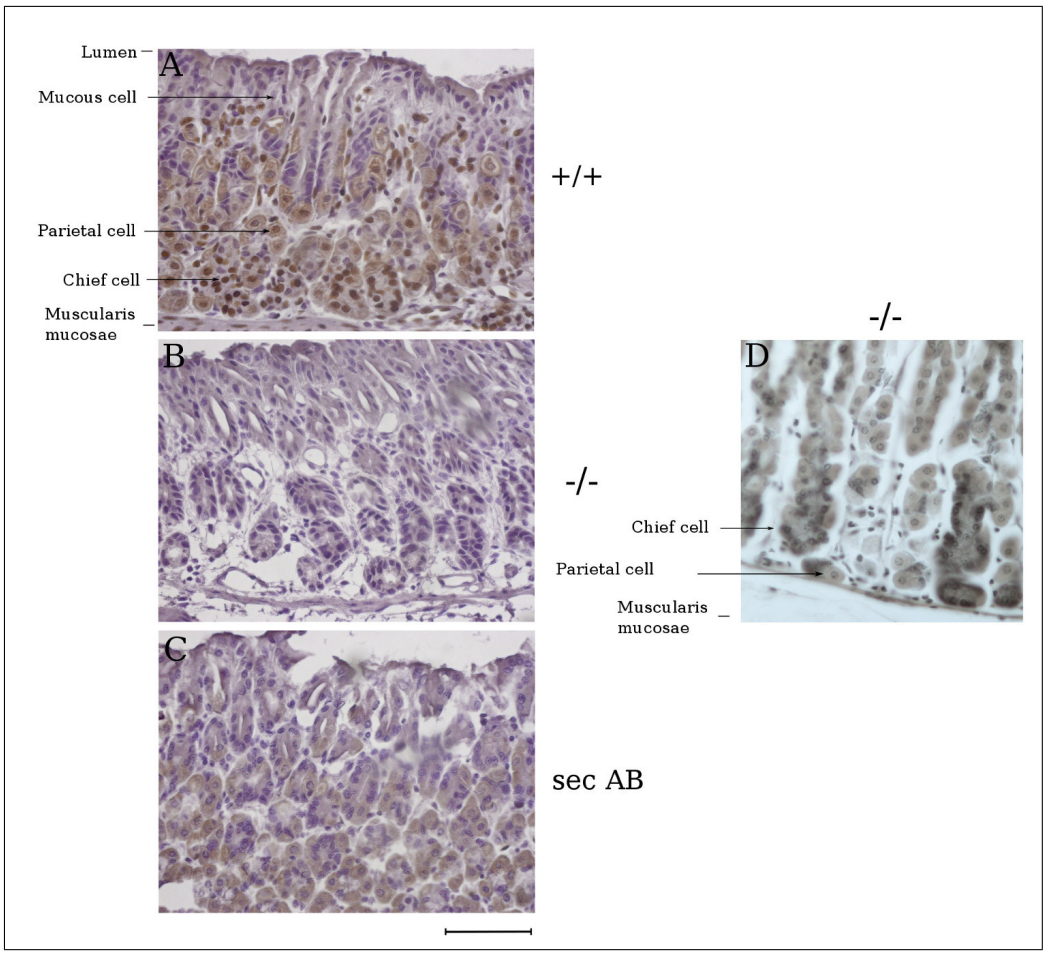

Figure 4.29 – Immunohistochemistry of the glandular stomach. Paraffin sections of the stomach of wild type and HRP-3-deficient mice were stained against HRP-3. The staining was detected with a biotinylated secondary antibody, followed by development with the ABC kit from Vectastain. Image A shows the glandular stomach of a wild type mouse, images B and D were taken of the stomachs of deficient animals. In image C, no abnormalities regarding the cellular distribution can be detected. In image D on the other hand, parietal cells are visible at the stomach fundus, where normally chief cells are located. Image C shows the secondary antibody control. Nuclei of all sections were counterstained with hematoxylin. The scale bar designated 50 µm. Image D taken by Prof. Hartmann, Institut für Anatomie, Bonn

4.10 Neuronal Cultures

Abouzied et al. [2010] reported that primary cultures of cortical neurons reacted to knockdown of HRP-3 via siRNA with shortened neurite length.

To evaluate whether neurons from HRP-3 knockout mice show shortened neurites,

primary cultures from wild type and deficient E14.5 were isolated as described in 3.3.4. Cells were seeded on poly-l-lysine-coated glass coverslips in 24-well plates with a concentration of 80,000 cells per well. The cells were cultivated for exactly 24 hours before they were fixed with 4 % PFA and stained against beta-III-tubulin as described in chapter 3.6.1.

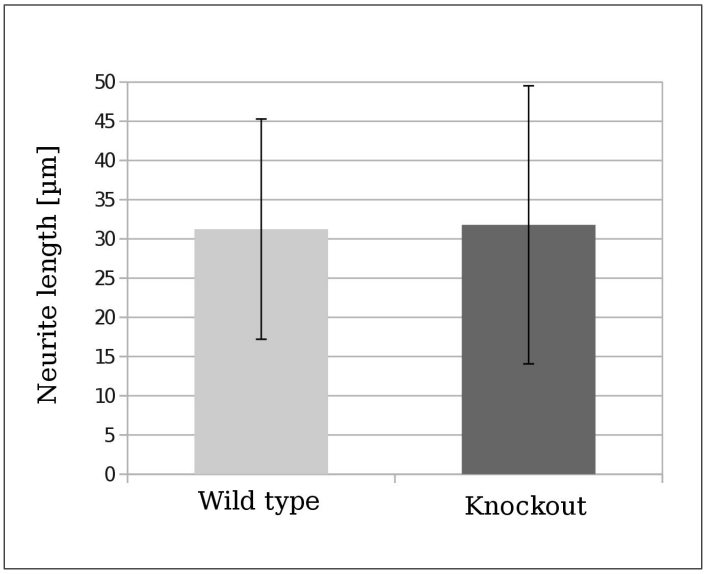

Figure 4.30 – Neurite length of wild type and knockout primary cortical neurons Primary cortical neurons were cultivated for 24 hours and the length of the longest neurite was determined using the software ImageJ with the plugin NeuronJ. N = 135 wild type cells and n= 163 knockout cells were blindly analysed. Mean neurite length for knockout cells was 31.79 µm and 31.24 µm for wild type cells.

Coverslips were evaluated randomised single-blinded. Five photos of each coverslip were taken with the Axiovert 100M in areas with 5-15 neurons per visual field. Neurite lengths and the amount of neurites were determined with the software ImageJ (Meijering et al. [2004]). For each analysed neuron, the longest neurite was measured to determine the neurite length and the amount of neurites were counted. N=135 knockout cells and n=163 wild type cells were analysed. The result is depicted in diagram 4.30. The neurite lengths varied strongly, since the cultures were very diversified. But the mean length was 31.79 µm for the knockout cells and 31.24 µm for the wild type cells. Standard deviation for knockout cells was 17.73 µm and 14.04 µm, therefore there is no difference in the neurite length of wild type and HRP-3 deficient primary cortical neurons.

5 Discussion

The hepatoma-derived growth factor-related protein-3 (HDGFRP-3 or HRP-3) is a secreted growth factor and a member of the HDGF protein family. In contrast to other members of this family, which are expressed in a wide range of different tissues, HRP-3 is predominantly expressed in the brain and exhibits several characteristics that suggest a function during embryonic brain development. More specifically, expression of HRP-3 varies quantitatively during brain development. It is strongly expressed in the embryonic brain, with elevated levels at the time of birth. In the postnatal brain, the amount of protein is reduced, whereas in the adult brain stronger expression levels are again reached (Abouzied et al. [2004]).

Like other members of the HDGF protein family, HRP-3 possesses a bipartite nuclear localisation signal, which is accountable for its nuclear expression in postmitotic neurons of the adult brain. Surprisingly, a solely cytosolic signal for HRP-3 can be attained via immunochemistry in embryonic brain sections or freshly isolated cortical neurons. A translocation from the cytosol to the nucleus occurs in the early postnatal brain for currently unknown reasons (El-Tahir et al. [2009]). According to Xiao et al. [2012], a translocation from the nucleus to the cytosol in HRP-3-transfected cells can be obtained by stimulation with epidermal growth factor (EGF).

Furthermore, HRP-3 possesses neurotrophic abilities on primary cortical neurons and is able to keep these cells alive when added recombinantly as a sole supplemental factor to the culture medium. Moreover, primary neurons are able to attach and present full neurite outgrowth when plated on HRP-3-coated cell culture dishes. In contrast, neither HDGF itself nor β-galactosidase as a recombinant control protein exhibited these or similar effects when used as a coating reagent (Abouzied et al. [2010]).

The described effects are manifested by cells when HRP-3 is provided extracellularly. In contrast, intracellular HRP-3 interacts with the cytoskeleton and influences neurite outgrowth. It was shown that HRP-3 binds to tubulin and is thus able to

stabilise microtubules. Additionally, the reduction of HRP-3 in primary neurons via siRNA led to a significant reduction in neurite length and a reduced number of neurites per cell (El-Tahir et al. [2009]).
Even though the characteristics described above give a few indications, the specific function of HRP-3 is currently unknown. These indications, however, may suggest that a loss-of-function mutation of HRP-3 has a drastic impact on the development of neuronal cells and the brain in total.
HRP-3 is a neurotrophic factor and in general, neurotrophic factors are survival-promoting agents for neurons whose imbalance in the brain is observed as part of neurodegenerative diseases (Peng et al. [2005], Zuccato and Cattaneo [2009]). In rodent models of neurodegenerative diseases, administration of neurotrophic factors has been successfully examined as a therapeutic treatment, e.g. NGF for cholinergic neurons in Alzheimer's disease, BDNF for dopaminergic neurons in Parkinson's disease (PD), CTNF in motorneuron diseases (Lindsay [1994]).
Fundamental research is needed to reach a deeper understanding of neurotrophic factors and their potential as therapeutic options. Thus, this dissertation describes the generation of an HRP-3-deficient mouse model with the objective to further characterise HRP-3 function. HRP-3 is a relatively unknown neurotrophic factor, thus, information provided by this mouse model should give new insights. Below, the generation of the knockout construct and the mouse model itself will be discussed, followed by a characterisation of the HRP-3-deficient mouse and its phenotype.

5.1 Gene Targeting and Generation of Mice

The genomic information for *Hrp-3* is located on mouse chromosome 7 (human chromosome 15). It is composed of six exons, with a 30 kb gap between the first two exons. This made exon 1 an appealing target for previous gene targeting experiments. Although different approaches and constructs have been tried, these experiments were unsuccessful for several years. Therefore, a new construct was to be designed and cloned that should implement a different targeting approach for the homologous recombination. The new targeting strategy included several characteristics:

- The construct was planned to be plain and without extensive features. Targeting experiments with conditional knockout constructs have been unsuccessful before, so a traditional knockout was therefore intended.

- Longer homologous arms increase the probability of a successful targeting experiment (Deng and Capecchi [1992]). Therefore a 10.6 kp long region of homology was used as 3' arm for the targeting construct. The other region of homology is only 1.4 long, to ensure a fast PCR-based screening.

- A Diphteria toxin-A (DT-A) cassette for negative selection gives a tenfold higher chance of a homologous recombination event (Yagi et al. [1990]).

The successful homologous recombination event is depicted in figure 4.5. The start codon and exon 1 of the *Hrp-3* gene are left intact. Since the splice acceptor site of exon 2 is integrated in frame with the eGFP reporter gene in the targeting vector, a fusion protein is expressed. The 31 kDa sized exon-1-eGFP-fusion protein is thus expressed under the endogenous *Hrp-3* promoter.
The hypoxanthine phosphoribosyltransferase (HPRT) minigene was used for positive selection. Since HM-1 cells are deficient for the HRPT-gene, this allowed a selection for cell clones with successful integration of the minigene, using medium supplemented with hypoxanthine, aminopterin and thymidin (HAT-supplement).
The targeting vector was constructed in three steps (see figures 4.1, 4.2 and 4.3): a DT-A cassette was subcloned into an older version of an exon 2 targeting construct, generated by Rainer Gallitzendörfer. A PCR-amplified 10.6 kb long homologous region was then added as a long homologous arm. The resulting plasmid, HRP-3-Exon2KO6.1 was then control digested (see figure 4.4) and partially sequenced (sequencing results can be found in the supplementals).
1344 embryonic stem (ES-) cell clones were picked in the targeting experiment that led to the isolation of positive clone number 9.45. Four copies of all 96-well plates were produced. The cell clones were genotyped via Southern blot and PCR analysis, although not all of them were successfully genotyped for different reasons. Not all cell clones grew confluent enough to isolate DNA for Southern blot analysis. PCR analysis led to the identification of false positive clones, so that a new genotyping PCR had to be established during mid-screening. DNA digestion for Southern blot analysis in 96-well plates had to be modified slightly due to insufficient results. The targeting experiment was repeated while clone # 9.45 was injected, and led to the identification of another positive ES-cell clone out of 480 clones in total. In the meantime, the male chimera, resulting from the injection of clone # 9.45, produced heterozygous offspring, so the other clone was not used for blastocyst injection.

The targeting frequency depends on several different factors, e.g. the length of homologous regions or the use of isogenic DNA. It is also locus dependent (Hasty et al. [1991], Müller [1999]). Due to the previous negative results, and considering these facts, the long homologous region was cloned from an isogenic BAC clone. Still, the targeting frequency for *Hrp-3* was extraordinary low with around 1/500 to 1/750. In contrast, the targeting frequency for HDGF has been 4 positive clones from 144 analysed (Gallitzendoerfer et al. [2008]). However, HRP-3-Exon2KO6.1 was the first targeting vector to successfully undergo homologous recombination in ES cells and the positive clone was confirmed via Southern blotting (see figure 4.6) and PCR genotyping (see figure 4.7).
Morula injection was performed at the Haus für experimentelle Therapie, Bonn. From the two resulting highly chimeric mice (see photo 4.8), one led to the founding of the HPR-3-deficient mouse line. As expected, 50 % of the resulting offspring with a brown coat were heterozygous for the inserted mutation, thus successfully giving rise to the mutant mouse line.
In addition to Southern blot and PCR analysis, the expected deletion of *Hrp-3* was further confirmed in mutant mice at protein level by Western blot analysis (see figure 4.10). The amount of protein was shown to be reduced in heterozygous animals and no signal was detectable in homozygous animals. The same result was confirmed at RNA level (see figure 4.11).

5.2 Coat Colour

One of the first observations regarding the HRP-3-deficient mouse line was that mice homozygous for the mutation were prevalently white and had bright red / pink eyes (see photo 4.9). No animal that was heterozygous or wild type for the *Hrp-3* locus was ever born with a white coat colour. This indicates that the white coat colour is recessive and does not originate from the mixed genetic background of the mice (129ola and C57Bl/6).
A reasonable explanation for the white coat is a genetic linkage of the mutant *Hrp-3* locus with a mutation in a locus responsible for coat colour. Two loci or a combination of both are possible candidates here. The first, tyrosinase (*tyr*), is a locus encoding for the key enzyme in the synthesis of the pigment melanin, converting L-tyrosine to 3,4-dihydroxyphenylalanine-(DOPA-)quinone. Mutations in the *tyr*

locus that interrupt the melanin synthesis lead to an absence of the pigment (Saran et al. [2004]). This would explain the observed coat colour and the non-pigmented eyes.

The tyrosinase locus is linked with the *p* locus, this linkage on chromosome 7 is the first linkage described in literature (Brilliant et al. [1997]). The *p* locus encodes for the p protein, also named oca-2 or pink-eyed dilution, because mutations in this locus lead to oculocutaneous albinism form II in humans. In mice, different spontaneously occurring mutations are known that cause hypopigmented eyes and fur, leading a dilution of the original coat colour (Brilliant [2002]). The p protein is probably needed for the transport of tyrosinase into melanosomes (Toyofuku et al. [2002]). P-deficient mice have melanosomes that are smaller than usual and contain only a little amount of pigment (Brilliant [2002]). Since these animals are still pigmented, no bright white-coated mice would result from these mutations, therefore a linkage to this locus alone would not explain the coat colour.

According to the Mouse Genome Database (MGD, http://www.informatics.jax.org), *Hrp-3* is located on chromosome 7, position 89026137 - 89079359 bp (45.71 cM). The tyrosinase gene is located on the same chromosome, position 94575915 - 94641921 bp (49.01 cM) and the *p* locus on position 63495130 - 63791887 bp (33.44 cM). The genetic distance between *Hrp-3*and *tyr* is thus only 3.3 cM. One centimorgan equals a 1 % chance of two genes getting separated during meiosis and does not always relate to their distance on the chromosome. Since the white coat colour is a recessive phenotype, the number of heterozygous animals with the genetic linkage on one allele is not known. Theoretically, in a homozygous animal there should be a 6.6 % chance (3.3 % for each allele) of a separation of the two loci. Since the event of a double recombination is not distinguishable from no recombination event, the number might even be lower. In this thesis, 21 homozygous mice originated from heterozygous matings, a 6.6 % chance of separation would result in 1.4 non-white animals. In reality, 3 of 21 were grey or black, indicating a successful separation of the loci, which is a higher number than expected.

It is possible that the HM-1 cells themselves already have the mutations on chromosome 7 necessary to create the white coat colour heterozygously. In that case, the mutant chromosome was targeted and the linkage not separated. Another possibility is that the mutation was acquired in the ES-cells or during the first matings of the mouse line.

The same phenomenon of a white fur colour linked to the genotype has been reported for Bax-deficient mice (http://jaxmice.jax.org/faq/bulletin/bulletin02.html, and Hamann et al. [2009]). Bax is a tumorsupressor, its genetic information is located on chromosome 7 at 29.32 cM and is linked to *tyr* and p. According to the Jackson Laboratory, it was not possible to separate the loci even after 8 generations of breeding with C57Bl/6 mice. Furthermore, some mutations in *tyr* and *p* are linked to several defects, for example neurological disorders, decreased viability and fertility (Brilliant [2002]). This was the reason why non-white homozygous mice were mated with C57Bl/6 wild type mice or heterozygous animals, leading to white and non-white offspring. Still, most homozygous mutants analysed in this thesis were white.

5.3 Expression Analysis of HRP-3

Up to now, HRP-3 protein has only been detected in the brain and testis (Abouzied et al. [2004]). Northern blotting analysis of human RNA indicated further HRP-3 expressing tissues, as the heart, kidney, lung, liver and pancreas (Ikegame et al. [1999], Xiao et al. [2012]). As a reason for this unclear expression data, Abouzied et al. [2004] discussed differences between human and mouse HRP-3 and a protein level that is too low to detect in Western blotting. An N-terminally histidine-tagged, shortened form of HRP-3, lacking the first 100 amino acids, was used to immunise rabbits for antibody production as described in Abouzied et al. [2004]. The reason why a shortened form was used is in the high level of homology in the HATH (Homologous to the Amino Terminus of HDGF)-domain between the HDGF family members, which might lead to a cross reaction of the antibodies with different family members. The antibodies were then purified from the rabbit antiserum by immunoaffinity chromatography using glutathione S-transferase (GST)-tagged recombinant HRP-3.

For the experiments described in this thesis, new antiserum had to be produced. This time, a full length N-terminal histidin-tagged form of HRP-3 was used to immunise rabbits (immunisation by Pineda, Berlin, Germany). After affinity purification against GST-tagged HRP-3, the resulting antibody was tested. It was shown to recognise HDGF as well as HRP-3 in Western blot analyses. Affinity purification was then performed with the shortened form of HRP-3, lacking the HATH-region,

so that only antibodies binding to the non-HATH part of HRP-3 would be purified. The resulting antibody did not show any further cross reaction with HDGF and gave extraordinarily good signals for HRP-3 in Western blotting and immunocyto- and immunohistochemistry.

This antibody was used to perform a Western blot analysis on different wild type mouse tissues to address the question of HRP-3 expression (see figure 4.24). With this antibody, HRP-3 is detectable not only in the brain, but also several other tissues. Namely, the thymus, spleen, liver, kidney, heart, lung, and the glandular part of the stomach; however, not the non-glandular part. These results were also confirmed in RT-PCR (figure 4.11) where HRP-3-specific primers detected a signal of the correct size in the liver, heart and lung of wild type and heterozygous, but not homozygous animals, indicating a specific signal. RT-PCR with eGFP-specific primers on the other hand did not lead to any signals in wild type tissues, but in heterozygous and knockout brain, heart, lung and liver, where the expression of the HRP-3-exon1-eGFP fusion protein under the endogenous HRP-3 promoter indicates the expression of HRP-3.

This new expression data was supported by immunohistochemistry. Figures 4.12, 4.13, 4.14 and 4.15 present an analysis of several brain regions, where HRP-3 expression has been reported before (Abouzied et al. [2004]). The signals in wild type brain are not detectable in knockout tissue or in the secondary antibody control. The same was shown in other tissues beside the brain, namely, the heart, the kidney and the stomach (compare figures 4.25, 4.26 and 4.29). HRP-3 expression in these organs is confined to the nucleus of heart muscle cells, podocytes in the kidney and parietal cells of the stomach. The relatively small amount of HRP-3 in contrast to the volume of the whole organ explains the low level of expression and why these signals have not been detected before. The other organs (the thymus, spleen, liver and the lung) have not yet been analysed for their subcellular HRP-3 expression.

One additional, as yet unknown, locus of expression of HRP-3 was found in the granule cells in the cerebellum. This was a surprising result, since no staining in granule cells has been detected before, not even in low amounts (Abouzied et al. [2004]). Compared to the Purkinje neurons, the staining of granule cells is somewhat weaker, but still clearly visible. It resembles the pattern that is shown when brain sections are stained with an antibody against HDGF (El-Tahir et al. [2006]). But the affinity purification against the shortened form of HRP-3 without the HATH-

region diminishes the detection of other family members, particularly HDGF. Also, no signal was retained in HRP-3 knockout cerebellum (figure 4.15, picture E). The staining was confirmed by using a different antibody against HRP-3 (mouse anti HRP-3 by Santa Cruz, see table 2.12). This antibody detected the same signal in granule cells, which was diminished in knockout brain and the secondary antibody control.

In Western blot analyses of wild type tissues, it was further confirmed that no other polypeptides were detected except the 30 kDa sized protein that resembles HRP-3 (see figure (4.24). The possibility of a cross reaction of the antibody with other HDGF family members was thus excluded.

The results presented here show new expression loci for HRP-3 that include not only further tissues than the brain, but also different cell types within the brain. Since all expression levels are much lower in all other tissues beside the brain, a possible explanation is that the antibody has a higher sensitivity and thus already detects a lesser amount of protein. But this does not explain the staining of granule cells of the cerebellum in immunohistochemistry. For these cells, at least a low signal should have been detected in earlier stainings, but this was not the case.

Since a polyclonal antibody is a mixture of antibodies binding to several different epitopes on the same protein, it is possible that the antibody used here has other epitopes than the one published in Abouzied et al. [2004]. Immunisation of the rabbit was performed with the full length protein, a mixture of recombinant bacterial and eukaryotic HRP-3 produced in HEK-cells. Since eukaryotic proteins are post-translationally modified, these modifications might be possible epitopes that are not recognised by the previous antibody.

It is likely that the full length protein has a different tertiary structure than the non-HATH region alone. Thakar et al. [2010] showed that the N-terminal part of HDGF interacts with the C-terminal part. The same might be the case for HRP-3, thus presenting different regions of the protein for antibody production. These regions might lead to a higher immunological response. Also, the use of a larger protein might lead to a higher response of the immune system.

It is possible that the antibody detects postranslational modifications of HRP-3. But it is also possible that two different isoforms of HRP-3 were detected here. According to the Ensembl database (http://www.ensembl.org), three transcripts for HRP-3 exist, two of which are transcribed into proteins. The first transcript codes

for a protein of 202 amino acids and represents the sequence which is commonly known as HRP-3. The second protein is produced by alternative splicing without the sixth exon and has a size of 205 amino acids. The small difference between these two isoforms makes it hard to distinguish them on the protein level.
Figure 4.10 shows an HRP-3 Western blot result where the exposure time was much shorter as in 4.24. It can be seen here that there is not only one, but two bands for HRP-3 which are running very close together, indicating only a small difference in their apparent size. The same phenomenon was shown for HDGF (Abouzied et al. [2004]).
In contrast to the protein size, the mRNA size of these potential isoforms varies strongly (5887 bp in contrast to 2865 bp), so a Northern blot analysis would provide insights into whether different isoforms exist in different organs or even within the brain. Additionally, in-situ-hybridisation with specific probes against the different isoforms, would indicate whether the expression in granule cells is derived from a different HRP-3 isoform.
It can be concluded that HRP-3 is not only expressed in the brain and testis as was shown by [Abouzied et al., 2004]. In fact, the substantiated expression shown here, fits with the results of the Northern blot analysis performed on human RNA by Ikegame et al. [1999] and Xiao et al. [2012]. The restricted expression of HRP-3 in contrast to the other HDGF family members was always seen as a unique characteristic for its neuronal function. The data presented here requires that the functional analysis of HRP-3 is expanded further beyond its function in the nervous system.
Excluding the kidney, all polypeptides detected with the HRP-3 antibody in immunoblot analyses 4.24 have the same molecular weight. In the kidney, a signal is detected, corresponding to an approximate size of 32-34 kDa, 2-4 kDa bigger than the usual HRP-3 signal. This is only an estimation, since HRP-3 has a size of 23 kDa, but appears at 30 kDa in SDS-Page due to running anomalies (Abouzied et al. [2004]). If a modification has an influence on these running anomalies, the kidney variant of HRP-3 might be more than just 2-4 kDa bigger. Posttranslational modifications of HRP-3 might be a reason for the increased size of the protein in the kidney.

5.4 Expression of eGFP and Possible Secretion

Immunohistochemical detection of eGFP is a standard technique and many companies offer specific antibodies. It was thus surprising that even in areas with a high expression level of HRP-3, as the olfactory bulb or the cerebellum, no optimal staining was achieved. Different antibodies against eGFP and different methods of antigen retrieval were tried. With one of the GFP antibodies and a prolonged incubation time of all reagents, poor signals were finally derived (see figure 4.18). A positive control (pax-2 knockout/GFP knockin mouse brain sections, kindly provided by Sabine Topka, Institut für Anatomie, Bonn) was stained together with HRP-3-deficient sections and showed satisfactory results, indicating that the staining protocol was not the problem (see image 4.19).
Signals on HRP-3-deficient brain sections were only marginally stronger than background staining in the wild type brain and the secondary antibody control. But, cells that were stained visibly (granule cells of the cerebellum and the olfactory bulb, images 4.20, C2, D2) were specific compared to the HRP-3 staining in wild type brains (image 4.15, 4.12). No staining of neurites was detected though, which is not surprising due to the weak signal strength.
A GFP signal was expected to be cytosolic in contrast to wild type HRP-3, since no nuclear localisation signal is left in the HRP-1-exon1-eGFP fusion protein. It was not possible to show this, since co-staining with hematoxylin masked the weak brown GFP-derived staining completely.
Surprisingly, native eGFP fluorescence, as shown with a fluorescent scanner in heterozygous brains (image 4.21), was relatively strong. The native fluorescence in E10.5 embryos (image 4.23) was clearly detectable. Immunohistochemistry with chromogenic substances is highly sensitive and should lead to an increase of the signal.
A discrepancy exists in the detection of GFP: it is easily detectable in Western blot analysis of whole brain lysates (image 4.10, RT-PCR (image 4.11) and with a fluorescence scanner or binocular (images 4.23 and 4.21), but not in immunohistochemistry. Of course, processing of paraffin sections for staining takes a long time and GFP is not bound in the cell since it has no intracellular binding partners. Due to its solubility it might be washed out during processing. It is more probable though, that GFP is secreted from the cells and then washed out from the tissue

during the processing steps. Thakar et al. [2010] describe that HDGF is secreted via a non-classical secretion pathway that is mediated via the N-terminus of the protein. When they attached the first ten amino acids of HDGF to GFP or SNAP, they were able to shuffle these out of the cells into the supernatant; the phosphorylation at serine 165 is a prerequisite for this secretion process. As all family members, HRP-3 shares the HATH (homologous to the amino terminus of HDGF)-domain with HDGF. It is thus not unlikely that HRP-3 is secreted via the same mechanism. Since exon 1 of HRP-3 is still expressed and localised N-terminally of eGFP, the same secretion mechanism probably takes place. As Thakar et al. [2010] showed, GFP becomes a secretory protein when fused to the N-Terminus of HDGF. The N-termini of HDGF and HRP-3 are not identical (HDGF: methionine, serine, arginine, serine, asparagine, arginine, glutamine, lysine, glutamic acid, tyrosine; HRP-3: methionine, alanine, arginine, proline, arginine, proline, arginine, glutamic acid, tyrosine, lysine) but both contain a high amount of basic amino acids. A comparison of both protein sequences is depicted in figure 5.1.

Figure 5.1 – Alignment of the protein sequence of HDGF and HRP-3. The protein sequences of HDGF and HRP-3 have been compared using the software CloneManager. Amino acids 1-100 share a high degree of identity, the so called HATH-domain. The serine/proline motif at position 165 of HDGF has an equivalent at position 162 at HRP-3.

The high degree of identity in the HATH region is clearly visible. Also, the serine 165 phosphorylation site in HDGF has an equivalent in HRP-3, a serine at posi-

tion 162 (both marked with red circles in figure 5.1. Both are followed by proline, which is discussed by Thakar et al. [2010] to undergo a cis/trans transformation when phosphorylated. It is known that HRP-3 is secreted in primary cortical neurons (Abouzied et al. [2010]). Since eGFP can be secreted by the amino terminus of HDGF, it is likely that the same is possible with the amino terminus of HRP-3. Most of the secreted protein would thus be outside of the cells and get washed out during tissue processing. That would explain the rare and weak signals in immunohistochemistry in contrast to the strong signals in other detection methods. Unfortunately, characterisation of the reporter gene activity in HRP-3-deficient mice on the cellular level is thus not possible by immunohistochemistry. On the other hand, analysis via in-situ-hybridisation at RNA level should allow confirmation of the expression of GFP in the correct localisation and could thus give valuable information about the secretion mechanism of HRP-3 and HDGF.

5.5 Hyperplasia of Mucosa and Submucosa of the Stomach

A unexpected observation in HRP-3-deficient mice was a strong folding of the stomach's mucosa and submucosa, but without any other pathological changes (fig. 4.27, 4.28). Since the breed was still on a mixed genetic background of 129/ola mice and C57BL/6, weighting of the animals was not performed. However, HRP-3-deficient animals did not show signs of obesity or undernourishment. HRP-3 is expressed in the glandular part of the stomach, but not the non-glandular part (see figure 4.24). On the cellular level, HPR-3 is expressed in the parietal cells of the stomach.
The stomach mucosa is innervated by extrinsic and intrinsic nerves and especially parietal cells are described to be highly dependent on nervous stimuli (Ekblad et al. [2000]). The parietal cells are necessary for the production of hydrochloric acid, a process which is induced by the release of different stimuli. Histamine, gastrin and acetylcholine operate via endocrine, paracrine and neurocrine pathways on parietal cells. Several growth factors play a role in the growth and differentiation of the stomach. For example, gastrin upregulates the epidermal growth factor (EGF), the transforming growth factor α (TGFα), and the heparin-binding EGF-like growth

factor (HB-EGF) (Friis-Hansen [2007]). Also, basic fibroblast growth factor, a neurotrophic factor, was shown to be trophic for gastric nerves (Ekblad et al. [2000]). Another neurotrophic factor, namely BDNF, influences innervation of the stomach and mechanoreceptors there. These receptors, intraganglionic laminar endings (IGLE) and intramuscular arrays, connect the gastrointestinal muscles with the vagus nerve. The vagus nerve is important for the connection of inner organs, such as the heart or the digestive system, with the central nervous system. In the stomach it is, amongst others, important for the intake of food and its digestion. BDNF knockout mice show a 50 % reduction of intraganglionic laminar endings in the stomach of newborn mice, while myenteric neurons (their target cells) were unaffected. Three days after birth, the number of IGLEs is back to wild type level (Murphy and Fox [2010]). This indicates that other trophic factors are able to substitute for the loss of BDNF.

These results show that neurotrophic factors also act in the stomach, which could be possible for HRP-3 as well. It is not clear though, whether the enlarged gastric folds stand in connection with its neurotrophic activity or general growth factor activity. Ménétrier disease is a rare human disorder that partially resembles the phenotype seen in HRP-3-deficient animals. A strong hyperplasia of stomach foldings is characteristic for this disease and is also accompanied by a reduction of parietal and chief cells. As an origin for Ménétrier disease, an increased stimulation of the epidermal growth factor receptor (EGFR) is being discussed. The stimulation is induced by a local overproduction of the EGFR ligand TGFα, which is expressed in parietal and mucous cells (Coffey et al. [2007]). Mice that overexpress TGFα in the stomach develop a phenotype that resembles Ménétrier disease. But how exactly the disease develops is not yet known (Takagi and Jhappan [1992]).

Ogawa et al. [2003] show that histamine H2-receptor-deficient mice exhibit the same phenotype. The histamine H2 receptor is located on parietal cells and when activated by histamine, stimulates secretion of hydrochloric acid. Mutant mice older than sixth months develop a phenotype that resembles Ménétrier disease, including a local overexpression of TGFα.

Whether or not HRP-3 plays a role in the abnormal signalling that leads to Ménétrier disease, can not be concluded from the data presented here. Further characterisations of the enlarged stomach foldings are necessary. On a cellular level, the number of parietal and chief cells have to be estimated, since these are reduced in the hu-

man disease. Immunohistochemistry and Western blot analysis of TGFα in HRP-3-deficient stomachs would reveal an upregulation and thus an increased stimulation of EGFR.

5.6 Neuronal Development and Cortical Lesions

HRP-3-deficient mice developed normally and did not show any deficits. No histological abnormalities were detected in the brains of deficient two to six-weeks-old mice compared to wild type mice. Isolated primary cortical neurons of mutant mice did not show a shortened neurite length compared to wild type neurons (see figure 4.30). It was thus concluded that HRP-3 is replaceable in embryonic brain development. Since HRP-3 is highly expressed in the adult mouse brain (Abouzied et al. [2004]), a function in the aged brain, as well as a function in the response to injuries is possible. Emphasis was thus put on the analysis of adult mice. The animals examined in this thesis were between four weeks and six months old because no older animals were available. However, it should be kept in mind that older animals also have to be analysed to gain a complete overview of the effect of HRP-3-deficiency on the brain.

In the brain of a six-month-old mouse, small lesions within the cerebral cortex were detected. In these lesions, degenerating neurons and a few activated astrocytes were found. Unfortunately, time did not permit further analysis of aged HRP-3-deficient animals. Thus, whether or not HRP-3-deficient mice are prone to such lesions or even neurodegeneration, cannot be concluded yet and will have to be shown in future experiments. However, a few possible approaches will be discussed in the following. Examples in the literature show that, ideally, aged animals between one or two years should be analysed. For example, Capsoni et al. [2000] created a transgenic mouse model, expressing an antibody against NGF and thus reducing the amount of NGF by at least 50 %. These mice exhibited an age-dependent neurodegenerative disease comparable to Alzheimer's disease. Mice at the age of 15-17 months showed neuronal loss in the cortex, cholinergic deficits, amyloid plaques and neurofibrillary tangles.

Mice transgenic for a dominant-negative form of mitochondrial aldehyde dehydrogenase 2 (ALDH2), an enzyme necessary to detoxify toxic aldehydes, are histologically inconspicuous and show no behavioural deficits at the age of sixth months or earlier.

By contrast, mice at the age of 12 and 18 month, show age-dependent neurodegeneration and memory loss (Ohsawa et al. [2008]). These publications place an emphasis on the importance of the analysis of older animals when searching for neurodegeneration.

Degeneration of synapses is one of the earliest signs of neurodegeneration, even before other markers are detectable. Whether the synaptic dysfunction is a reason for neurodegeneration or a side effect, is not yet known (Perry and O'Connor [2010], Milnerwood and Raymond [2010]). It would thus be useful to stain HRP-3-deficient brain sections with antibodies against synaptical markers. Perry and O'Connor [2010] found that the first synpaptic markers to be reduced are the vesicle-associated membrane protein-2 (VAMP-2), cysteine string protein (CSP) and synaptophysin. It would thus be reasonable to analyse HRP-3-deficient brains with these markers. Furthermore, the demise of synapses is accompanied by a loss of mitochondrial function but not a reduction in their number. Cytochrome c oxidase activity is reduced and the mitochondria undergo morphological abnormalities (Perry and O'Connor [2010]). Mitochondria are also discussed as a cause for the onset of neurodegenerative diseases (Johri and Beal [2012]). Analysis of mitochondrial markers should thus be performed.

Fluoro-Jade B (Millipore) is described to specifically stain degenerating neurons and activated astroglia, although the reason for the binding is not known (Schmued and Hopkins [2000]). Paraffin sections of two five-month-old knockout and respective wild type brains were stained with Fluoro-Jade B, yielding no differences compared to wild type sections. This is not surprising, since paraffin sections with a thickness of 4 µm are too thin to make out small areas of degeneration. To screen for such areas, a complete brain should be cut into 50 - 100 µm thick sections using a vibratome and then the sections should be stained with Fluoro-Jade B. Due to the low number of animals at the right age, this was not possible as part of this thesis.

In later stages of a neurodegenerative disease, cells undergo apoptosis, necrosis and / or autophagic cell death. Staining with apoptotic marker, e.g. activated caspase-3, will indicate if apoptosis is taking place in the brain.

5.7 Comparison with Other Loss-of-Function Mutations

Loss-of-function mouse models of other neurotrophic factors show strongly varying phenotypes, depending on which specific factor (or its corresponding receptor) is deleted. Some show drastic phenotypes, as for example the neurotrophin-3 (NT-3)-deficient mouse model. Mice have huge deficits in neuronal development of sensory neurons, which occur before and during target innervation. Homozygous mutants die within 48 hours after birth (Tessarollo et al. [1994], Ernfors et al. [1995]). Interestingly, trkC-deficient mice (trkC is the main receptor for NT-3) develop normally until postnatal day two and live about 30 days. This phenotype is a milder version of the NT-3-deficiency, since NT-3 is still able to use trkA and trkB as receptors (Tessarollo et al. [1994]).
Conover et al. [1995] created BDNF and neurotrophin-4/5 (NT-4)-deficient mice, as well as double knockout mice. BDNF-deficient mice show immense neurological deficits, coordination problems and die usually within three weeks after birth. Mice that are heterozygous for the deficiency still exhibit aggressiveness between males, increased eating habits and weight gain. They also show a degeneration of serotonergic neurons, for which BDNF is a trophic factor. Human psychiatric diseases such as obsessive compulsive disorder (obsession for hand washing etc.), bulimia and others are also linked with an imbalance of the serotonin level and are treated with drugs that enhance the serotonin level (Lyons et al. [1999]).
A better comparison for the HRP-3-deficient mouse model are mice with a homozygous deletion for the NT-4 gene. These mice are viable and fertile and show no obvious neurological deficits up to the age of ten months, which is comparable to HRP-3-deficiency. Conover et al. [1995] assumed that NT-4/5 activity is important during responses to injury or aged nervous system. Interestingly, Fox et al. [2001] show that the amount of vagal sensory neurons is reduced by more than the half in NT-4-deficient mice, whereas other neuronal cell types are not affected. Deficient mice show a huge decrease (80.9 %) of mechanoreceptors in the small intestine. These receptors (intraganglionic laminar endings and intramuscular arrays) connect the gastrointestinal muscles with the vagus nerve. In contrast, mechanoreceptors in the stomach are unchanged compared to the wild type control. As a result, mice showed a changed eating habit, with a 76 % longer duration of meals. Body weight

and total food intake was not affected due a reduced amount of meals compared to the wild type control. This is a rather mild phenotype and shows that loss of neurotrophic factors does not always cause massive deficits, but can also be supplemented within the body. Deficits in the number of mechanoreceptors do not inhibit normal life or changes the behaviour of mice and is therefore a phenotype which is hard to detect. Also, the HRP-3 mouse model might exhibit such inconspicuous abnormalities, especially since it is now known that it is expressed not only in the brain but in a number of different organs. Further, and more detailed analyses are necessary here.

5.8 Functional Replacement of HRP-3 in Knockout Mice?

Wat et al. [2010] discuss that human patients with microdeletions on chromosome 15.q25.2, which includes the genomic locus of *Hrp-3*, are susceptible for congenital diaphragmic hernia (CDH). The authors hold the loss of HRP-3 responsible for the cognitive deficits arising in this disease. No hernia was detected in HRP-3-deficient mice, but conclusions cannot be drawn about cognitive deficits since no behavioural analyses were performed. Unexpectedly, brain development of HRP-3-deficient mice is not disturbed. It was presumed that HRP-3 plays a role during brain development, for example by establishing neuronal polarity or neurogenesis. A reduction of HRP-3 via siRNA led to significantly shortened neurites in primary cortical neurons (El-Tahir et al. [2009]). However, the complete deficiency of HRP-3 shows no effect in primary cortical neurons that have never produced HRP-3. It is possible that the function of HRP-3 is replaced by other proteins in vivo.
The same was shown for HDGF itself in deficient mice. No phenotype differing from wild type mice was detectable. Although an upregulation of other proteins was discussed by Gallitzendoerfer et al. [2008], none of the other family members were found to be upregulated. It was assumed that in HRP-3-deficient mice no upregulation in other family members would happen either. HDGF expression was therefore analysed via immunoblotting, which confirmed this assumption (compare figure 4.10). Further analyses of other family members and growth factors still would have to be performed.

A substitution of HRP-3 protein function is not restricted to HDGF-family members. Since HRP-3 is predominantly expressed in the brain, other neurotrophic factors could intervene to fulfil the missing function. It would be interesting to analyse expression patterns of different neurotrophic factors in HRP-3-deficient brains.
According to D. Sanes, A. Thomas [2006] central neurons, in contrast to peripheral neurons, have multiple targets and to decrease neuronal survival, two or more growth factors have to be disrupted. Even though that is not the case for most of the members of the neurotrophin family, it might be the case for HRP-3 and HDGF. Many growth factors are needed in emergencies, e.g. in case of injury, as for example the platelet-derived growth factor (Werner and Grose [2003]). It is possible that HRP-3 has a similar function. Eltahir [2009] showed in nerve crush experiments that HRP-3 is downregulated and translocates into the cytoplasma after nerve injury. The effect of HRP-3 on injury could be analysed in vivo and in vitro. For example, injury can be induced chemically in cell culture by the activation of the NMDA or AMPA/kainate receptors (Carriedo et al. [1996]).
If two or more trophic factors share the same receptor, the same signalling cascade can still be induced and the phenotype rescued. For example, the fact that trkB-deficient mice die within 24-48 hours after birth was not reproduceable in BDNF/NT-4 double knockouts. TrkB receptor knockout mice have a decrease of motorneurons in the facial nucleus, a trait which double knockout mice do not exhibit. Therefore, it was correctly assumed that trkB acts as a receptor for another neurotrophin (compare figure 1.2, Conover et al. [1995]). To date, no receptor for HRP-3 is known. It can only be speculated whether stronger deficits are rescued in this mouse model by other growth factors.

5.9 HRP-3-deficient Mouse Model as a Tool for Further Analyses

The HRP-3-deficient mouse model is a versatile tool and can be used for further analyses on HRP-3 protein functions.
Since eGFP is probably secreted out of the cells by the use of the first ten amino acids of HRP-3, this permits study of the secretion mechanism. Using antibodies against GFP, the exon 1-eGFP fusion protein could be purified from brain lysates.

With the help of mass spectrometry, interaction partners could be identified and thus elucidate the secretion mechanism of HDGF and HRP-3. Classical secretion can be blocked by the inhibitor brefeldin A (Nickel [2010]), which should not influence secretion of HRP-3 / GFP. Primary neuronal cultures can be a useful cell culture model here, because it is known that they secrete HRP-3.
Furthermore, the question remains, how HRP-3 is internalised by cells. Primary neuronal cultures might also be used here. These cultures do not show any differences to wild type cultures in growth and neurite lengths. Using recombinant HRP-3, the cultures can be fed and checked via immunocytochemistry for internalised HRP-3. The blockage of receptors with different inhibitors then allows an investigation of possible receptors of HRP-3. On the other hand, an internalisation via macropinocytosis with the involvement of heparane sulfates and activation of map kinase downstream signalling was shown for HDGF and the HATH domain (Wang et al. [2011]). The blockage of macropinocytosis with the inhibitor amiloride should diminish the uptake of HRP-3, if it happens via this mechanism.
In the same cell culture model, it can be examined whether the neurotrophic and neurite-outgrowth abilities of extracellular HRP-3 also leads to the intracellular effects of HRP-3 (stabilisation of microtubules). One possibility for further studies is the quantitative analysis of acetylated tubulin after cells have been fed with recombinant HRP-3. This could be a way to show the direct uptake of HRP-3 and a subsequent modulation of the cytoskeleton.
The literature discusses that, like HDGF, HRP-3 is a protein overexpressed in tumours. Ortega-Paino et al. [2008] described the overexpression of HRP-3 in mantle cell lymphoma, Xiao et al. [2012] in hepatocellular carcinomas. Although the reduction of HDGF in tumours via siRNA leads to enhanced apoptosis, necrosis and reduced blood vessel formation (Zhang et al. [2006], Liao et al. [2010]), it is not classified as an oncogene and is described as a factor for non-oncogene addiction. Proteins of this category are not oncogenes, but are upregulated in tumours; tumour growth and progression depends on them (Sedlmaier et al. [2011]). It is likely that the same concept is valid for HRP-3. In this case, HRP-3 might serve as a prognostic marker or even as a target in cancer therapy. Further validation is needed here.

5.10 Outlook

Unfortunately, the mouse model generated did not allow to draw a specific conclusion regarding the function of HRP-3 within the scope of this thesis. However, a foundation for further analyses of HRP-3 was laid.
Most importantly, the existence of lesions within the cerebral cortex has to be confirmed or disproven. Mice should be analysed via vibratome sectioning of the brain including evaluation of neurodegenerative, apoptotic and inflammatory markers; the animals should be as old as possible.
In this thesis, the analysis of HRP-3-deficient mice was predominantly focussed on the brain. The new expression data described here demands further histological analyses of all new HRP-3 expression loci in wild type mice and a comparison to the corresponding knockout tissue. The hyperplasia in the stomach of HRP-3-deficient mice strongly indicates that a phenotype differing from wild type does not have to be restricted to the brain.
For histological analyses, the likely secretion of eGFP in these mice is unfortunate, but it might proof useful for an investigation of the non-classical secretion mechanism of HRP-3.

Summary

This dissertation describes the generation of a mutant mouse model and its initial analysis. The hepatoma-derived growth factor-related protein-3 (HRP-3) is a growth factor of the HDGF protein family with neurotrophic activity. Predominantly expressed in the brain, it was shown to bind and stabilise microtubules and a function during brain development is speculated in the literature.

Although multiple targeting experiments with different vectors were tried, targeting of the HRP-3 locus has been hitherto unsuccessful. The targeting strategy used in this thesis was thus modified to target exon 2 with a classic non-conditional knockout. Even though the targeting frequency was clearly below average, the mutant mouse line was finally created.

It was discovered that HRP-3, in contrast to findings in contemporary literature, is indeed predominantly expressed in the brain, but also to lesser extent in a range of other tissues and specific cell types. These include podocytes in the kidney or heart muscle cells. It can thus be supposed that the function of HRP-3 is not only confined to the brain, but also extends to other organs. Additionally, it was also shown that expression of HRP-3 within the brain extends to more cell types than previously reported.

It is highly probable that the reporter gene eGFP is secreted due to a secretion mechanism supported by the first ten amino acids of HRP-3. To analyse this non-classical secretion pathway, this might prove useful.

Mice were viable and fertile and lived up to the age of ten months without any obvious abnormalities. A single case of a six-month-old mouse with small lesions in the cerebral cortex was found, but due to time constraints and the absence of older animals, these results were not reproduced.

Furthermore, some HRP-3-deficient animals exhibited a hyperplasia of stomach mucosa and submucosa, resulting in extreme stomach folds. Since it was shown that HRP-3 is expressed in the parietal cells of the stomach, a phenotype is conceivable. The mutant mouse model might prove useful as a model for human Ménétrier disease, but this has to be further researched.

Due to these unanswered questions and the fact that the mouse model at hand warrants more a extensive analysis, it might provide interesting possibilities for further studies of HRP-3.

6 Supplemental Data

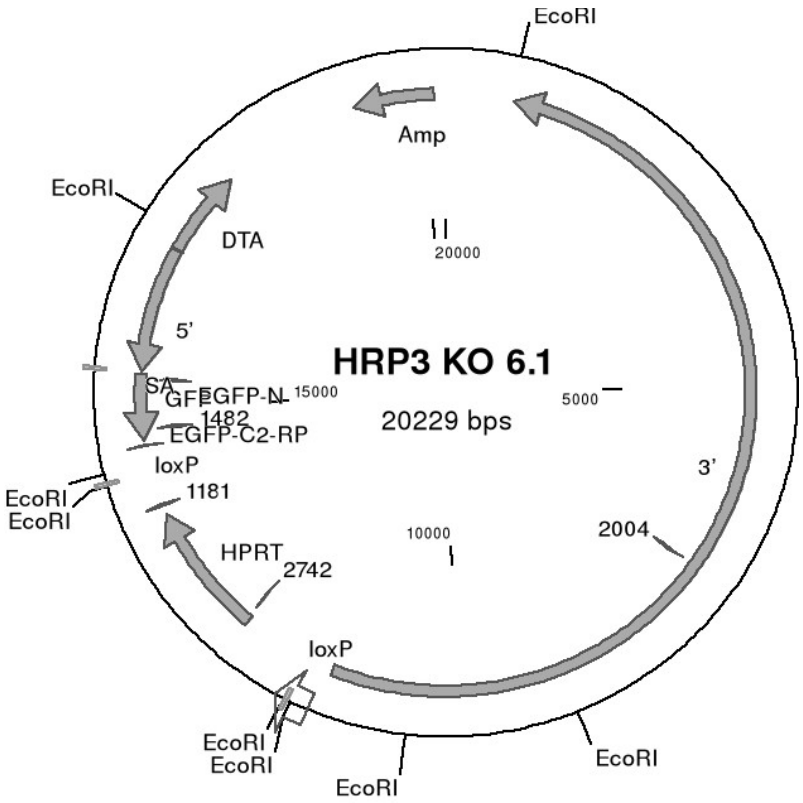

Figure 6.1 – Plasmid map of the targeting vector. A map of the targeting vector, HRP3-Exon2KO6.1, including selected enzyme cutting sites, is shown here. PmeI was used to linearise the plasmid before electroporation, EcoRI and SmaI were used for control digestions. Abbreviations: Amp (ampicillin resistance), 3' and 5' (3' and 5' homologous arms), loxP (locus of X over P1, allows site-specific recombination with Cre-recombinase), HPRT (hypoxanthine phosphoribosyltransferase, positive selection), GFP (enhanced green fluorescent protein), SA (splice acceptor site of exon 2), DTA (diphteria toxin fragment-A, negative selection cassette), 1482 and 1181 are the primers necessary for the mouse genotyping PCR. 2004, 2742, EGFP-C2-RP and EGFP-N are primers that were used for partial sequencing of the targeting vector.

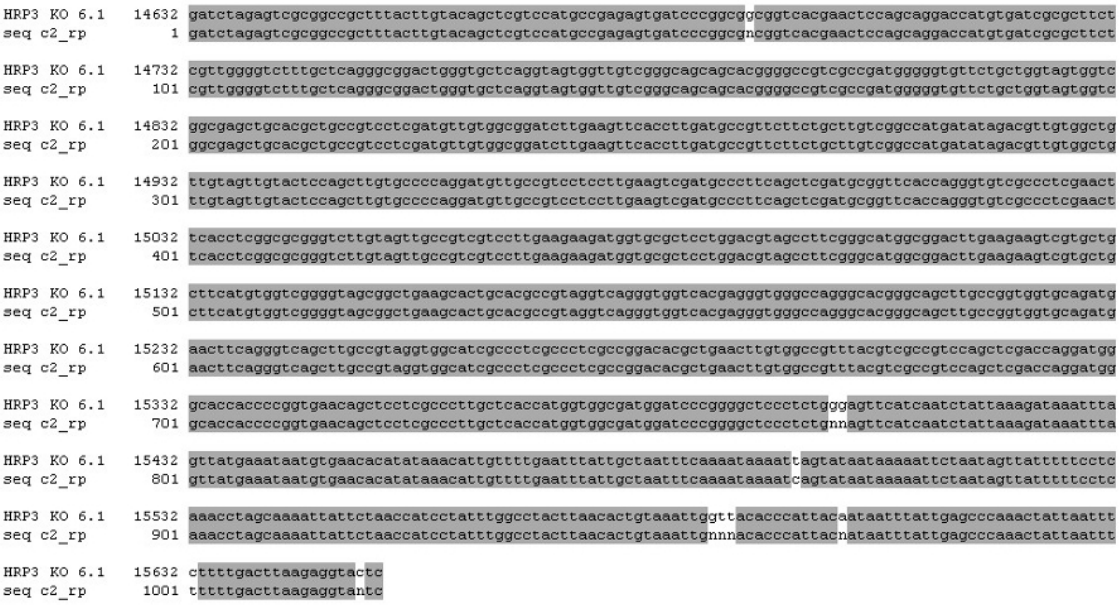

Figure 6.2 – Sequencing result with primer pEGFP-C2-RP. Sequencing with primer number pEGFP-C2-RP (GATC standardprimer, sequence: GATCACATGGTCCTGCTG) led to a sequence of the GFP cassette. Sequencing was performed by GATC Biotech, Koblenz.

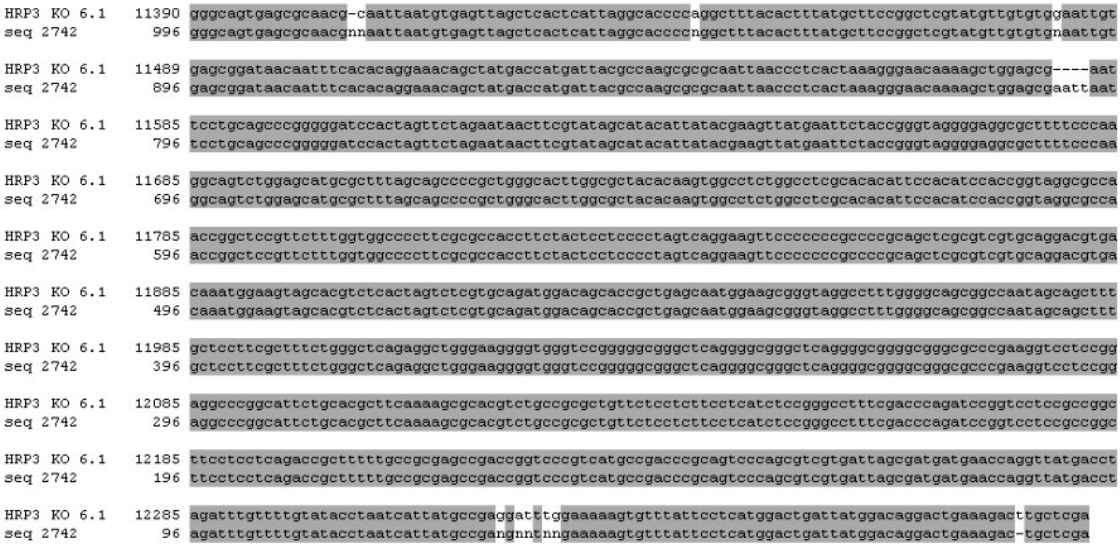

Figure 6.3 – Sequencing result with primer 2742. Sequencing with primer number 2742 (sequence: CACAGAGGGCCACAATG) led to a sequence of part between the HPRT cassette and the 3' homologous arm. Sequencing was performed by GATC Biotech, Koblenz.

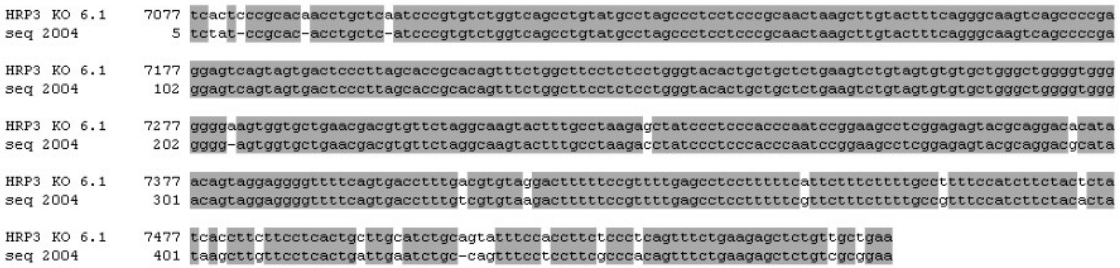

Figure 6.4 – Sequencing result with primer 2004. Sequencing with primer number 2004 (sequence: TCTCCCCTCTCCTTTTCCAT) led to a partial sequence of the 3' homologous arm. Sequencing was performed by GATC Biotech, Koblenz.

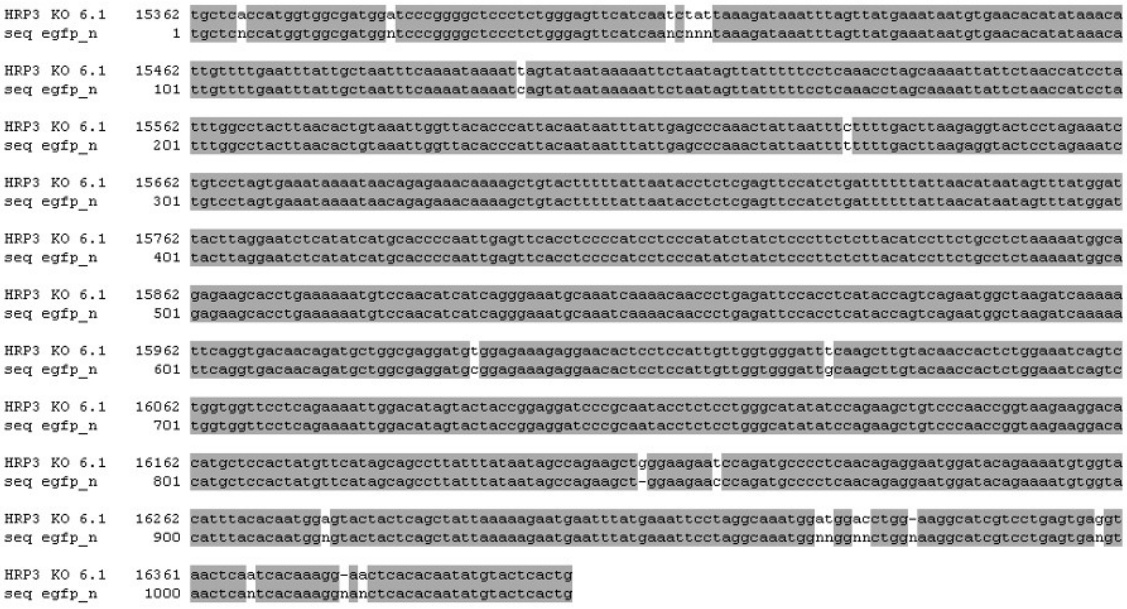

Figure 6.5 – Sequencing result with primer EGFP-N. Sequencing with primer number EGFP-N (GATC standardprimer, sequence: CCGTCCAGCTCGACCAG) led to a sequence of the GFP cassette and the 5' homologous arm. Sequencing was performed by GATC Biotech, Koblenz.

Bibliography

M. M. Abouzied, S. L. Baader, F. Dietz, J. Kappler, V. Gieselmann, and S. Franken. Expression patterns and different subcellular localization of the growth factors HDGF (hepatoma-derived growth factor) and HRP-3 (HDGF-related protein-3) suggest functions in addition to their mitogenic activity. *The Biochemical journal*, 378(Pt 1):169–76, Feb. 2004. ISSN 1470-8728. doi: 10.1042/BJ20030916. URL http://www.pubmedcentral.nih.gov/articlerender.fcgi?artid=1223924&tool=pmcentrez&rendertype=abstracthttp://dx.doi.org/10.1042/BJ20030916.

M. M. Abouzied, H. M. El-Tahir, V. Gieselmann, and S. Franken. Hepatoma-derived growth factor-related protein-3: a new neurotrophic and neurite outgrowth-promoting factor for cortical neurons. *Journal of neuroscience research*, 88(16):3610–20, Dec. 2010. ISSN 1097-4547. doi: 10.1002/jnr.22507. URL http://www.ncbi.nlm.nih.gov/pubmed/20890995.

F. C. Alsina, F. Ledda, and G. Paratcha. New insights into the control of neurotrophic growth factor receptor signaling: implications for nervous system development and repair. *Journal of neurochemistry*, 123(5):652–61, Dec. 2012. ISSN 1471-4159. doi: 10.1111/jnc.12021. URL http://www.ncbi.nlm.nih.gov/pubmed/22994539.

K. Bernard, E. Litman, J. L. Fitzpatrick, Y. G. Shellman, G. Argast, K. Polvinen, A. D. Everett, K. Fukasawa, D. A. Norris, N. G. Ahn, and K. A. Resing. Functional proteomic analysis of melanoma progression. *Cancer Res*, 63(20):6716–6725, Oct. 2003.

H. C. Birnboim and J. Doly. A rapid alkaline extraction procedure for screening recombinant plasmid DNA. *Nucleic acids research*, 7(6):1513–23, Nov. 1979. ISSN 0305-1048. URL http://www.pubmedcentral.nih.gov/articlerender.fcgi?artid=342324&tool=pmcentrez&rendertype=abstract.

V. Bocchini and P. U. Angeletti. The nerve growth factor: purification as a 30,000-molecular-weight protein. *Proceedings of the National Academy of Sciences of the United States of America*, 64(2):787–94, Oct. 1969. ISSN 0027-8424. URL http://www.pubmedcentral.nih.gov/articlerender.fcgi?artid=223412&tool=pmcentrez&rendertype=abstract.

R. Brandt. Cytoskeletal mechanisms of neuronal degeneration. *Cell and Tissue Research*, 305(2):255–265, Aug. 2001. ISSN 0302-766X. doi: 10.1007/s004410000334. URL http://www.springerlink.com/openurl.asp?genre=article&id=doi:10.1007/s004410000334.

M. Brilliant. The mouse p (pink-eyed dilution) and human P genes, oculocutaneous albinism type 2 (OCA2), and melanosomal pH. *Pigment Cell Research*, pages 86–93, 2002. URL http://onlinelibrary.wiley.com/doi/10.1034/j.1600-0749.2001.140203.x/full.

M. H. Brilliant, R. W. Williams, B. C. Holdener, J. M. Angel, M. Stern, and K. Hunter. Mouse chromosome 7. *Mammalian genome : official journal of the International Mammalian Genome Society*, 7 Spec No:S121–42, Jan. 1997. ISSN 0938-8990. URL http://www.ncbi.nlm.nih.gov/pubmed/9233390.

P. Calissano, G. Amadoro, C. Matrone, S. Ciafrè, R. Marolda, V. Corsetti, M. T. Ciotti, D. Mercanti, a. Di Luzio, C. Severini, C. Provenzano, and N. Canu. Does the term 'trophic' actually mean anti-amyloidogenic? The case of NGF. *Cell death and differentiation*, 17(7):1126–33, July 2010. ISSN 1476-5403. doi: 10.1038/cdd.2010.38. URL http://www.ncbi.nlm.nih.gov/pubmed/20395961.

S. Capsoni, G. Ugolini, a. Comparini, F. Ruberti, N. Berardi, and a. Cattaneo. Alzheimer-like neurodegeneration in aged antinerve growth factor transgenic mice. *Proceedings of the National Academy of Sciences of the United States of America*, 97(12):6826–31, June 2000. ISSN 0027-8424. URL http://www.pubmedcentral.nih.gov/articlerender.fcgi?artid=18754&tool=pmcentrez&rendertype=abstract.

S. G. Carriedo, H. Z. Yin, and J. H. Weiss. Motor neurons are selectively vulnerable to AMPA/kainate receptor-mediated injury in vitro. *The Journal of neuroscience : the official journal of the Society for Neuroscience*, 16 (13):4069–79, July 1996. ISSN 0270-6474. URL http://www.ncbi.nlm.nih.gov/pubmed/8753869.

S.-C. Chen, M.-L. Kung, T.-H. Hu, H.-Y. Chen, J.-C. Wu, H.-M. Kuo, H.-E. Tsai, Y.-W. Lin, Z.-H. Wen, J.-K. Liu, M.-H. Yeh, and M.-H. Tai. Hepatoma-Derived Growth Factor Regulates breast cancer cell invasion by Modulating Epithelial Mesenchymal Transition. *The Journal of pathology*, Jan. 2012. ISSN 1096-9896. doi: 10.1002/path.3988. URL http://www.ncbi.nlm.nih.gov/pubmed/22247069.

P. Chomczynski and N. Sacchi. Single-step method of RNA isolation by acid guanidinium thiocyanate-phenol-chloroform extraction. *Analytical biochemistry*, 162(1):156–9, Apr. 1987. ISSN 0003-2697. doi: 10.1006/abio.1987.9999. URL http://www.ncbi.nlm.nih.gov/pubmed/2440339.

R. J. Coffey, M. K. Washington, C. L. Corless, and M. C. Heinrich. Ménétrier disease and gastrointestinal stromal tumors: hyperproliferative disorders of the stomach. *The Journal of clinical investigation*, 117(1):70–80, Jan. 2007. ISSN 0021-9738. doi: 10.1172/JCI30491. URL http://www.pubmedcentral.nih.gov/articlerender.fcgi?artid=1716220&tool=pmcentrez&rendertype=abstract.

C. Conde and A. Cáceres. Microtubule assembly, organization and dynamics in axons and dendrites. *Nature reviews. Neuroscience*, 10(5):319–32, May 2009. ISSN 1471-0048. doi: 10.1038/nrn2631. URL http://www.ncbi.nlm.nih.gov/pubmed/19377501.

J. C. Conover, J. T. Erickson, D. M. Katz, L. M. Bianchi, W. T. Poueymirou, J. McClain, L. Pan, M. Helgren, N. Y. Ip, and P. Boland. Neuronal deficits, not involving motor neurons, in mice lacking BDNF and/or NT4. *Nature*, 375(6528):235–8, May 1995. ISSN 0028-0836. doi: 10.1038/375235a0. URL http://www.ncbi.nlm.nih.gov/pubmed/7746324.

J. D. Cooper, a. Salehi, J. D. Delcroix, C. L. Howe, P. V. Belichenko, J. Chua-Couzens, J. F. Kilbridge, E. J. Carlson, C. J. Epstein, and W. C. Mobley. Failed retrograde transport of NGF in a mouse model of Down's syndrome: reversal of cholinergic neurodegenerative phenotypes following NGF infusion. *Proceedings of the National Academy of Sciences of the United States of America*, 98(18):10439–44, Aug. 2001. ISSN 0027-8424. doi: 10.1073/pnas.181219298. URL http://www.pubmedcentral.nih.gov/articlerender.fcgi?artid=56979&tool=pmcentrez&rendertype=abstract.

R. J. Crowder and R. S. Freeman. Phosphatidylinositol 3-kinase and Akt protein kinase are necessary and sufficient for the survival of nerve growth factor-dependent sympathetic neurons. *The Journal of neuroscience : the official journal of the Society for Neuroscience*, 18(8):2933–43, May 1998. ISSN 0270-6474. URL http://www.ncbi.nlm.nih.gov/pubmed/9526010.

W. D. Sanes, A. Thomas. *Development of the Nervous System, Second Edition.* Boston: Academic Press, 2006.

D. Dawbarn and S. J. Allen. Neurotrophins and neurodegeneration. *Neuropathology and applied neurobiology*, 29 (3):211–30, June 2003. ISSN 0305-1846. URL http://www.ncbi.nlm.nih.gov/pubmed/12787319.

E. J. de la Rosa and F. de Pablo. Cell death in early neural development: beyond the neurotrophic theory. *Trends in neurosciences*, 23(10):454–8, Oct. 2000. ISSN 0166-2236. URL http://www.ncbi.nlm.nih.gov/pubmed/11006461.

C. Deng and M. R. Capecchi. Reexamination of gene targeting frequency as a function of the extent of homology between the targeting vector and the target locus. *Molecular and cellular biology*, 12(8):3365–71, Aug. 1992. ISSN 0270-7306. URL http://www.pubmedcentral.nih.gov/articlerender.fcgi?artid=364584&tool=pmcentrez&rendertype=abstract.

E. Ekblad, Q. Mei, and F. Sundler. Innervation of the gastric mucosa. *Microscopy research and technique*, 48(5):241–57, Mar. 2000. ISSN 1059-910X. doi: 10.1002/(SICI)1097-0029(20000301)48:5<241::AID-JEMT2>3.0.CO;2-2. URL http://www.ncbi.nlm.nih.gov/pubmed/23339174.

H. M. El-Tahir, F. Dietz, R. Dringen, K. Schwabe, K. Strenge, S. S. r. Kelm, M. M. Abouzied, V. Gieselmann, and S. Franken. Expression of hepatoma-derived growth factor family members in the adult central nervous system. *BMC Neurosci*, 7:6, Jan. 2006. ISSN 1471-2202. doi: 10.1186/1471-2202-7-6. URL http://dx.doi.org/10.1186/1471-2202-7-6http://www.pubmedcentral.nih.gov/articlerender.fcgi?artid=1363353&tool=pmcentrez&rendertype=abstract.

H. M. El-Tahir, M. M. Abouzied, R. Gallitzendoerfer, V. Gieselmann, and S. Franken. Hepatoma-derived growth factor-related protein-3 interacts with microtubules and promotes neurite outgrowth in mouse cortical neurons. *The Journal of biological chemistry*, 284(17):11637–51, Apr. 2009. ISSN 0021-9258. doi: 10.1074/jbc.M901101200. URL http://www.pubmedcentral.nih.gov/articlerender.fcgi?artid=2670168&tool=pmcentrez&rendertype=abstract.

H. Eltahir. Developmentally-regulated localization and possible functions of HRP-3 in the murine nervous tissue. *hss.ulb.uni-bonn.de*, 2009. URL http://hss.ulb.uni-bonn.de:90/2010/2165/2165.pdf.

P. Ernfors, J. Kucera, K. F. Lee, J. Loring, and R. Jaenisch. Studies on the physiological role of brain-derived neurotrophic factor and neurotrophin-3 in knockout mice. *The International journal of developmental biology*, 39(5):799–807, Oct. 1995. ISSN 0214-6282. URL http://www.ncbi.nlm.nih.gov/pubmed/8645564.

A. D. Everett, D. R. Lobe, M. E. Matsumura, H. Nakamura, and C. a. McNamara. Hepatoma-derived growth factor stimulates smooth muscle cell growth and is expressed in vascular development. *The Journal of clinical investigation*, 105(5):567–75, Mar. 2000. ISSN 0021-9738. doi: 10.1172/JCI7497. URL http://www.pubmedcentral.nih.gov/articlerender.fcgi?artid=289171&tool=pmcentrez&rendertype=abstract.

M. Fahnestock, B. Michalski, B. Xu, and M. D. Coughlin. The precursor pro-nerve growth factor is the predominant form of nerve growth factor in brain and is increased in Alzheimer's disease. *Molecular and cellular neurosciences*, 18(2):210–20, Aug. 2001. ISSN 1044-7431. doi: 10.1006/mcne.2001.1016. URL http://www.ncbi.nlm.nih.gov/pubmed/11520181.

H. F. Farhadi, S. J. Mowla, K. Petrecca, S. J. Morris, N. G. Seidah, and R. a. Murphy. Neurotrophin-3 sorts to the constitutive secretory pathway of hippocampal neurons and is diverted to the regulated secretory pathway by coexpression with brain-derived neurotrophic factor. *The Journal of neuroscience : the official journal of the Society for Neuroscience*, 20(11):4059–68, June 2000. ISSN 1529-2401. URL http://www.ncbi.nlm.nih.gov/pubmed/10818141.

D. A. Fletcher and R. D. Mullins. Cell mechanics and the cytoskeleton. *Nature*, 463(7280):485–92, Jan. 2010. ISSN 1476-4687. doi: 10.1038/nature08908. URL http://www.pubmedcentral.nih.gov/articlerender.fcgi?artid=2851742&tool=pmcentrez&rendertype=abstract.

E. A. Fox, R. J. Phillips, E. A. Baronowsky, M. S. Byerly, S. Jones, and T. L. Powley. Neurotrophin-4 deficient mice have a loss of vagal intraganglionic mechanoreceptors from the small intestine and a disruption of short-term satiety. *The Journal of neuroscience : the official journal of the Society for Neuroscience*, 21(21):8602–15, Nov. 2001. ISSN 1529-2401. URL http://www.ncbi.nlm.nih.gov/pubmed/11606648.

W. Friedman. Proneurotrophins, seizures, and neuronal apoptosis. *The Neuroscientist*, 16(3):244–252, 2010. doi: 10.1177/1073858409349903.Proneurotrophins. URL http://nro.sagepub.com/content/16/3/244.short.

L. Friis-Hansen. Lessons from the gastrin knockout mice. *Regulatory peptides*, 139(1-3):5–22, Mar. 2007. ISSN 0167-0115. doi: 10.1016/j.regpep.2006.12.008. URL http://www.ncbi.nlm.nih.gov/pubmed/17234279.

R. Gallitzendoerfer, M. M. Abouzied, D. Hartmann, R. Dobrowolski, V. Gieselmann, and S. Franken. Hepatoma-derived growth factor (HDGF) is dispensable for normal mouse development. *Developmental dynamics : an official publication of the American Association of Anatomists*, 237(7):1875–1885, July 2008. ISSN 1058-8388. doi: 10.1002/dvdy.21589. URL http://www.ncbi.nlm.nih.gov/pubmed/18570251.

S. S. Gill, N. K. Patel, G. R. Hotton, K. O'Sullivan, R. McCarter, M. Bunnage, D. J. Brooks, C. N. Svendsen, and P. Heywood. Direct brain infusion of glial cell line-derived neurotrophic factor in Parkinson disease. *Nature medicine*, 9(5):589–95, May 2003. ISSN 1078-8956. doi: 10.1038/nm850. URL http://www.ncbi.nlm.nih.gov/pubmed/12669033.

S. Hamann, D. F. Schorderet, and S. Cottet. Bax-induced apoptosis in Leber's congenital amaurosis: a dual role in rod and cone degeneration. *PloS one*, 4(8):e6616, Jan. 2009. ISSN 1932-6203. doi: 10.1371/journal.pone.0006616. URL http://www.pubmedcentral.nih.gov/articlerender.fcgi?artid=2720534&tool=pmcentrez&rendertype=abstract.

J. Hardy and D. J. Selkoe. The amyloid hypothesis of Alzheimer's disease: progress and problems on the road to therapeutics. *Science (New York, N.Y.)*, 297(5580):353–6, July 2002. ISSN 1095-9203. doi: 10.1126/science.1072994. URL http://www.ncbi.nlm.nih.gov/pubmed/12130773.

P. Hasty, J. Rivera-Pérez, and A. Bradley. The length of homology required for gene targeting in embryonic stem cells. *Molecular and cellular biology*, 11(11):5586–91, Nov. 1991. ISSN 0270-7306. URL http://www.pubmedcentral.nih.gov/articlerender.fcgi?artid=361929&tool=pmcentrez&rendertype=abstract.

S.-S. Hsu, C.-H. Chen, G.-S. Liu, M.-H. Tai, J.-S. Wang, J.-C. Wu, M.-L. Kung, E. C. Chan, and L.-F. Liu. Tumorigenesis and prognostic role of hepatoma-derived growth factor in human gliomas. *Journal of neuro-oncology*, Oct. 2011. ISSN 1573-7373. doi: 10.1007/s11060-011-0733-z. URL http://www.ncbi.nlm.nih.gov/pubmed/22037800.

T.-H. Hu, C.-C. Huang, L.-F. Liu, P.-R. Lin, S.-Y. Liu, H.-W. Chang, C.-S. Changchien, C.-M. Lee, J.-H. Chuang, and M. H. Tai. Expression of hepatoma-derived growth factor in hepatocellular carcinoma. *Cancer*, 98(7):1444–1456, Oct. 2003. doi: 10.1002/cncr.11653. URL http://dx.doi.org/10.1002/cncr.11653.

K. Ikegame, M. Yamamoto, Y. Kishima, H. Enomoto, K. Yoshida, M. Suemura, T. Kishimoto, and H. Nakamura. A new member of a hepatoma-derived growth factor gene family can translocate to the nucleus. *Biochem Biophys Res Commun*, 266(1):81–87, Dec. 1999. doi: 10.1006/bbrc.1999.1733. URL http://dx.doi.org/10.1006/bbrc.1999.1733.

T. Iwasaki, K. Nakagawa, H. Nakamura, Y. Takada, K. Matsui, and K. Kawahara. Hepatoma-derived growth factor as a prognostic marker in completely resected non-small-cell lung cancer. *Oncol Rep*, 13(6):1075–1080, June 2005.

A. Johri and M. F. Beal. Mitochondrial dysfunction in neurodegenerative diseases. *The Journal of pharmacology and experimental therapeutics*, 342(3):619–30, Sept. 2012. ISSN 1521-0103. doi: 10.1124/jpet.112.192138. URL http://www.ncbi.nlm.nih.gov/pubmed/22700435.

K. Kuida, T. S. Zheng, S. Na, C. Kuan, D. Yang, H. Karasuyama, P. Rakic, and R. A. Flavell. Decreased apoptosis in the brain and premature lethality in CPP32-deficient mice. *Nature*, 384(6607):368–72, Nov. 1996. ISSN 0028-0836. doi: 10.1038/384368a0. URL http://www.ncbi.nlm.nih.gov/pubmed/8934524.

K. Kuida, T. F. Haydar, C. Y. Kuan, Y. Gu, C. Taya, H. Karasuyama, M. S. Su, P. Rakic, and R. A. Flavell. Reduced apoptosis and cytochrome c-mediated caspase activation in mice lacking caspase 9. *Cell*, 94(3):325–37, Aug. 1998. ISSN 0092-8674. URL http://www.ncbi.nlm.nih.gov/pubmed/9708735.

R. Lee, P. Kermani, K. K. Teng, and B. L. Hempstead. Regulation of cell survival by secreted proneurotrophins. *Science (New York, N.Y.)*, 294(5548):1945–8, Nov. 2001. ISSN 0036-8075. doi: 10.1126/science.1065057. URL http://www.ncbi.nlm.nih.gov/pubmed/11729324.

R. Levi-Montalcini. Effects of Mouse Tumor Transplantation on the Nervous System. *Annals New York Academy of Sciences*, (1), 1952.

R. Levi-Montalcini and P. Calissano. The nerve-growth factor. *Scientific American*, 240(6):68–77, June 1979. ISSN 0036-8733. URL http://www.ncbi.nlm.nih.gov/pubmed/472707.

F. Liao, W. Dong, and L. Fan. Apoptosis of human colorectal carcinoma cells is induced by blocking hepatoma-derived growth factor. *Medical oncology (Northwood, London, England)*, 27(4):1219–26, Dec. 2010. ISSN 1559-131X. doi: 10.1007/s12032-009-9362-1. URL http://www.ncbi.nlm.nih.gov/pubmed/19924574.

R. M. Lindsay. Neurotrophic growth factors and neurodegenerative diseases: therapeutic potential of the neurotrophins and ciliary neurotrophic factor. *Neurobiology of aging*, 15(2):249–51, 1994. ISSN 0197-4580. URL http://www.ncbi.nlm.nih.gov/pubmed/7838303.

L. A. Lowery and D. Van Vactor. The trip of the tip: understanding the growth cone machinery. *Nature reviews. Molecular cell biology*, 10(5):332–43, May 2009. ISSN 1471-0080. doi: 10.1038/nrm2679. URL http://www.pubmedcentral.nih.gov/articlerender.fcgi?artid=2714171&tool=pmcentrez&rendertype=abstract.

O. H. Lowry, N. J. Rosebrough, A. L. Farr, and R. J. Randall. Protein measurement with the Folin phenol reagent. *The Journal of biological chemistry*, 193(1):265–75, Nov. 1951. ISSN 0021-9258. URL http://www.ncbi.nlm.nih.gov/pubmed/14907713.

W. E. Lyons, L. a. Mamounas, G. a. Ricaurte, V. Coppola, S. W. Reid, S. H. Bora, C. Wihler, V. E. Koliatsos, and L. Tessarollo. Brain-derived neurotrophic factor-deficient mice develop aggressiveness and hyperphagia in conjunction with brain serotonergic abnormalities. *Proceedings of the National Academy of Sciences of the United States of America*, 96(26):15239–44, Dec. 1999. ISSN 0027-8424. URL http://www.pubmedcentral.nih.gov/articlerender.fcgi?artid=24804&tool=pmcentrez&rendertype=abstract.

T. M. Magin, J. McWhir, and D. W. Melton. A new mouse embryonic stem cell line with good germ line contribution and gene targeting frequency. *Nucleic acids research*, 20(14):3795, July 1992. ISSN 0305-1048. URL http://www.pubmedcentral.nih.gov/articlerender.fcgi?artid=334045&tool=pmcentrez&rendertype=abstract.

A. Markus, T. D. Patel, and W. D. Snider. Neurotrophic factors and axonal growth. *Current opinion in neurobiology*, 12(5):523–31, Oct. 2002. ISSN 0959-4388. URL http://www.ncbi.nlm.nih.gov/pubmed/12367631.

C. T. McMurray. Neurodegeneration: diseases of the cytoskeleton? *Cell death and differentiation*, 7(10):861–5, Oct. 2000. ISSN 1350-9047. doi: 10.1038/sj.cdd.4400764. URL http://www.ncbi.nlm.nih.gov/pubmed/11279530.

E. Meijering, M. Jacob, J.-C. F. Sarria, P. Steiner, H. Hirling, and M. Unser. Design and validation of a tool for neurite tracing and analysis in fluorescence microscopy images. *Cytometry. Part A : the journal of the International Society for Analytical Cytology*, 58(2):167–76, Apr. 2004. ISSN 1552-4922. doi: 10.1002/cyto.a.20022. URL http://www.ncbi.nlm.nih.gov/pubmed/15057970.

A. Meyer-Franke, M. R. Kaplan, F. W. Pfrieger, and B. a. Barres. Characterization of the signaling interactions that promote the survival and growth of developing retinal ganglion cells in culture. *Neuron*, 15(4):805–19, Oct. 1995. ISSN 0896-6273. URL http://www.ncbi.nlm.nih.gov/pubmed/7576630.

D. L. Miller, S. Ortega, O. Bashayan, R. Basch, and C. Basilico. Compensation by fibroblast growth factor 1 (FGF1) does not account for the mild phenotypic defects observed in FGF2 null mice. *Molecular and cellular biology*, 20(6):2260–8, Mar. 2000. ISSN 0270-7306. URL http://www.pubmedcentral.nih.gov/articlerender.fcgi?artid=110842&tool=pmcentrez&rendertype=abstract.

A. J. Milnerwood and L. a. Raymond. Early synaptic pathophysiology in neurodegeneration: insights from Huntington's disease. *Trends in neurosciences*, 33(11):513–23, Nov. 2010. ISSN 1878-108X. doi: 10.1016/j.tins.2010.08.002. URL http://www.ncbi.nlm.nih.gov/pubmed/20850189.

U. Müller. Ten years of gene targeting: targeted mouse mutants, from vector design to phenotype analysis. *Mechanisms of development*, 82(1-2):3–21, Apr. 1999. ISSN 0925-4773. URL http://www.ncbi.nlm.nih.gov/pubmed/10354467.

M. Murphy and E. Fox. Mice deficient in brain-derived neurotrophic factor have altered development of gastric vagal sensory innervation. *The Journal of comparative neurology*, 518(15):2934–2951, 2010. doi: 10.1002/cne.22372.Mice. URL http://onlinelibrary.wiley.com/doi/10.1002/cne.22372/full.

H. Nakamura, Y. Izumoto, H. Kambe, T. Kuroda, T. Mori, K. Kawamura, H. Yamamoto, T. Kishimoto, K. Kawamuran, H. Yamamotos, and T. Kishimotos. Molecular Cloning of Complementary DNA for a Novel Human Hepatoma-derived Growth Factor. *The Journal of biological chemistry*, 269(40):25143–25149, 1994.

W. Nickel. Pathways of unconventional protein secretion. *Current opinion in biotechnology*, 21(5):621–6, Oct. 2010. ISSN 1879-0429. doi: 10.1016/j.copbio.2010.06.004. URL http://www.ncbi.nlm.nih.gov/pubmed/20637599.

T. Ogawa, K. Maeda, S. Tonai, and T. Kobayashi. Utilization of Knockout Mice to Examine the Potential Role of Gastric Histamine H 2 -Receptors in Menetrier's Disease. 70:61–70, 2003.

I. Ohsawa, K. Nishimaki, Y. Murakami, Y. Suzuki, M. Ishikawa, and S. Ohta. Age-dependent neurodegeneration accompanying memory loss in transgenic mice defective in mitochondrial aldehyde dehydrogenase 2 activity. *The Journal of neuroscience : the official journal of the Society for Neuroscience*, 28(24):6239–49, June 2008. ISSN 1529-2401. doi: 10.1523/JNEUROSCI.4956-07.2008. URL http://www.ncbi.nlm.nih.gov/pubmed/18550766.

J. A. Oliver and Q. Al-Awqati. An endothelial growth factor involved in rat renal development. *The Journal of clinical investigation*, 102(6):1208–19, Sept. 1998. ISSN 0021-9738. doi: 10.1172/JCI785. URL http://www.pubmedcentral.nih.gov/articlerender.fcgi?artid=509104&tool=pmcentrez&rendertype=abstract.

R. Oppenheim. Cell Death During Development Of The Nervous System. *Annual Review of Neuroscience*, 14(1):453–501, Jan. 1991. ISSN 0147006X. doi: 10.1146/annurev.neuro.14.1.453. URL http://neuro.annualreviews.org/cgi/doi/10.1146/annurev.neuro.14.1.453.

R. W. Oppenheim. The neurotrophic theory and naturally occurring motoneuron death. *Trends in neurosciences*, 12(7):252–5, July 1989. ISSN 0166-2236. URL http://www.ncbi.nlm.nih.gov/pubmed/2475935.

E. Ortega-Paino, J. Fransson, S. Ek, and C. a. K. Borrebaeck. Functionally associated targets in mantle cell lymphoma as defined by DNA microarrays and RNA interference. *Blood*, 111(3):1617–24, Mar. 2008. ISSN 0006-4971. doi: 10.1182/blood-2007-02-068791. URL http://www.ncbi.nlm.nih.gov/pubmed/18024791.

S. Peng, J. Wuu, E. J. Mufson, and M. Fahnestock. Precursor form of brain-derived neurotrophic factor and mature brain-derived neurotrophic factor are decreased in the pre-clinical stages of Alzheimer's disease. *Journal of neurochemistry*, 93(6):1412–21, June 2005. ISSN 0022-3042. doi: 10.1111/j.1471-4159.2005.03135.x. URL http://www.ncbi.nlm.nih.gov/pubmed/15935057.

V. H. Perry and V. O'Connor. The role of microglia in synaptic stripping and synaptic degeneration: a revised perspective. *ASN neuro*, 2(5):e00047, Jan. 2010. ISSN 1759-0914. doi: 10.1042/AN20100024. URL http://www.pubmedcentral.nih.gov/articlerender.fcgi?artid=2954441&tool=pmcentrez&rendertype=abstract.

L. F. Reichardt. Neurotrophin-regulated signalling pathways. *Philosophical transactions of the Royal Society of London. Series B, Biological sciences*, 361(1473):1545–64, Sept. 2006. ISSN 0962-8436. doi: 10.1098/rstb.2006.1894. URL http://www.pubmedcentral.nih.gov/articlerender.fcgi?artid=1664664&tool=pmcentrez&rendertype=abstract.

A. Saran, M. Spinola, S. Pazzaglia, B. Peissel, C. Tiveron, L. Tatangelo, M. Mancuso, V. Covelli, L. Giovannelli, V. Pitozzi, C. Pignatiello, S. Milani, P. Dolara, and T. a. Dragani. Loss of tyrosinase activity confers increased skin tumor susceptibility in mice. *Oncogene*, 23(23):4130–5, May 2004. ISSN 0950-9232. doi: 10.1038/sj.onc.1207565. URL http://www.ncbi.nlm.nih.gov/pubmed/15007389.

L. C. Schmued and K. J. Hopkins. Fluoro-Jade B: a high affinity fluorescent marker for the localization of neuronal degeneration. *Brain research*, 874(2):123–30, Aug. 2000. ISSN 0006-8993. URL http://www.ncbi.nlm.nih.gov/pubmed/10960596.

A. Sedlmaier, N. Wernert, R. Gallitzendörfer, M. M. Abouzied, V. Gieselmann, and S. Franken. Overexpression of hepatoma-derived growth factor in melanocytes does not lead to oncogenic transformation. *BMC cancer*, 11(1): 457, Jan. 2011. ISSN 1471-2407. doi: 10.1186/1471-2407-11-457. URL http://www.pubmedcentral.nih.gov/articlerender.fcgi?artid=3213223&tool=pmcentrez&rendertype=abstract.

D. M. Skovronsky, V. M.-Y. Lee, and J. Q. Trojanowski. Neurodegenerative diseases: new concepts of pathogenesis and their therapeutic implications. *Annual review of pathology*, 1:151–70, Jan. 2006. ISSN 1553-4006. doi: 10.1146/annurev.pathol.1.110304.100113. URL http://www.ncbi.nlm.nih.gov/pubmed/18039111.

A. G. Smith, J. K. Heath, D. D. Donaldson, G. G. Wong, J. Moreau, M. Stahl, and D. Rogers. Inhibition of pluripotential embryonic stem cell differentiation by purified polypeptides. *Nature*, 336(6200):688–90, Dec. 1988. ISSN 0028-0836. doi: 10.1038/336688a0. URL http://www.ncbi.nlm.nih.gov/pubmed/3143917.

H. Takagi and C. Jhappan. Hypertrophic gastropathy resembling Ménétrier's disease in transgenic mice overexpressing transforming growth factor alpha in the stomach. *Journal of Clinical . . .*, pages 1161–1167, 1992. URL http://www.ncbi.nlm.nih.gov/pmc/articles/PMC329980/.

L. Tessarollo, K. S. Vogel, M. E. Palko, S. W. Reid, and L. F. Parada. Targeted mutation in the neurotrophin-3 gene results in loss of muscle sensory neurons. *Proceedings of the National Academy of Sciences of the United States of America*, 91(25):11844–8, Dec. 1994. ISSN 0027-8424. URL http://www.pubmedcentral.nih.gov/articlerender.fcgi?artid=45332&tool=pmcentrez&rendertype=abstract.

K. Thakar, T. Kröcher, S. Savant, D. Gollnast, S. r. Kelm, and F. Dietz. Secretion of hepatoma-derived growth factor is regulated by N-terminal processing. *Biological chemistry*, 391(12):1401–10, Dec. 2010. ISSN 1437-4315. doi: 10.1515/BC.2010.147. URL http://www.ncbi.nlm.nih.gov/pubmed/21087088.

K. Toyofuku, J. C. Valencia, T. Kushimoto, G.-E. Costin, V. M. Virador, W. D. Vieira, V. J. Ferrans, and V. J. Hearing. The etiology of oculocutaneous albinism (OCA) type II: the pink protein modulates the processing and transport of tyrosinase. *Pigment cell research / sponsored by the European Society for Pigment Cell Research and the International Pigment Cell Society*, 15(3):217–24, June 2002. ISSN 0893-5785. URL http://www.ncbi.nlm.nih.gov/pubmed/12028586.

C.-H. Wang, F. Davamani, S.-C. Sue, S.-C. Lee, P.-l. Wu, F.-M. Tang, C. Shih, T.-h. Huang, and W.-g. Wu. Cell surface heparan sulfates mediate internalization of the PWWP/HATH domain of HDGF via macropinocytosis to fine-tune cell signalling processes involved in fibroblast cell migration. *The Biochemical journal*, 433(1):127–38, Jan. 2011. ISSN 1470-8728. doi: 10.1042/BJ20100589. URL http://www.ncbi.nlm.nih.gov/pubmed/20964630.

M. J. Wat, V. B. Enciso, W. Wiszniewski, T. Resnick, P. Bader, E. R. Roeder, D. Freedenberg, C. Brown, P. Stankiewicz, S.-W. Cheung, and D. A. Scott. Recurrent microdeletions of 15q25.2 are associated with increased risk of congenital diaphragmatic hernia, cognitive deficits and possibly Diamond–Blackfan anaemia.

Journal of medical genetics, 47(11):777–81, Nov. 2010. ISSN 1468-6244. doi: 10.1136/jmg.2009.075903. URL http://www.ncbi.nlm.nih.gov/pubmed/20921022.

G. Watts. Rita Levi-Montalcini. *Nature*, 381(9863):288, Jan. 2013. ISSN 01406736. doi: 10.1016/S0140-6736(13)60124-5. URL http://linkinghub.elsevier.com/retrieve/pii/S0140673613601245.

I. B. Weinstein. Cancer. Addiction to oncogenes–the Achilles heal of cancer. *Science (New York, N.Y.)*, 297(5578):63–4, July 2002. ISSN 1095-9203. doi: 10.1126/science.1073096. URL http://www.ncbi.nlm.nih.gov/pubmed/12098689.

S. Werner and R. Grose. Regulation of wound healing by growth factors and cytokines. *Physiological reviews*, 83(3):835–70, July 2003. ISSN 0031-9333. doi: 10.1152/physrev.00031.2002. URL http://www.ncbi.nlm.nih.gov/pubmed/12843410.

Q. Xiao, K. Qu, C. Wang, Y. Kong, C. Liu, D. Jiang, H. Saiyin, F. Jia, C. Ni, T. Chen, Y. Zhang, P. Zhang, W. Qin, Q. Sun, H. Wang, Q. Yi, J. Liu, H. Huang, and L. Yu. HDGF-related protein-3 is required for anchorage-independent survival and chemoresistance in hepatocellular carcinomas. *Gut*, pages 1–14, Apr. 2012. ISSN 1468-3288. doi: 10.1136/gutjnl-2011-300781. URL http://www.ncbi.nlm.nih.gov/pubmed/22490522.

T. Yagi, Y. Ikawa, K. Yoshida, Y. Shigetani, N. Takeda, I. Mabuchi, T. Yamamoto, and S. Aizawa. Homologous recombination at c-fyn locus of mouse embryonic stem cells with use of diphtheria toxin A-fragment gene in negative selection. *Proceedings of the National Academy of Sciences of the United States of America*, 87(24):9918–22, Dec. 1990. ISSN 0027-8424. URL http://www.pubmedcentral.nih.gov/articlerender.fcgi?artid=55285&tool=pmcentrez&rendertype=abstract.

T. Yamashita, K. L. Tucker, and Y. a. Barde. Neurotrophin binding to the p75 receptor modulates Rho activity and axonal outgrowth. *Neuron*, 24(3):585–93, Nov. 1999. ISSN 0896-6273. URL http://www.ncbi.nlm.nih.gov/pubmed/10595511.

E. C. Yuen, C. L. Howe, Y. Li, D. M. Holtzman, and W. C. Mobley. Nerve growth factor and the neurotrophic factor hypothesis. *Brain & development*, 18(5):362–8, 1996. ISSN 0387-7604. URL http://www.ncbi.nlm.nih.gov/pubmed/8891230.

J. Zhang, H. Ren, P. Yuan, W. Lang, L. Zhang, and L. Mao. Down-regulation of hepatoma-derived growth factor inhibits anchorage-independent growth and invasion of non-small cell lung cancer cells. *Cancer research*, 66(1):18–23, Jan. 2006. ISSN 0008-5472. doi: 10.1158/0008-5472.CAN-04-3905. URL http://www.ncbi.nlm.nih.gov/pubmed/16397209.

F.-Q. Zhou, J. Zhou, S. Dedhar, Y.-h. Wu, W. D. Snider, C. Hill, and N. Carolina. NGF-induced axon growth is mediated by localized inactivation of GSK-3beta and functions of the microtubule plus end binding protein APC. *Neuron*, 42(6):897–912, June 2004. ISSN 0896-6273. doi: 10.1016/j.neuron.2004.05.011. URL http://www.ncbi.nlm.nih.gov/pubmed/15207235.

C. Zuccato and E. Cattaneo. Brain-derived neurotrophic factor in neurodegenerative diseases. *Nature reviews. Neurology*, 5(6):311–22, June 2009. ISSN 1759-4766. doi: 10.1038/nrneurol.2009.54. URL http://www.ncbi.nlm.nih.gov/pubmed/19498435.

Erklärung

Hiermit versichere ich, Katharina M. Klein, dass ich die hier vorliegende Arbeit selbständig angefertigt und keine anderen, als die angegebenen Hilfsmittel und Quellen benutzt habe. Ferner erkläre ich, die vorliegende Arbeit an keiner anderen Hochschule als Dissertation eingereicht zu haben.

Bonn, März 2013,

Katharina M. Klein